

# INVESTIGATING THE ROLE OF APOPTOSIS IN CALCIFICATION OF THE AORTIC VALVULAR INTERSTITIAL CELLS

---

A Dissertation Submitted to the Faculty of  
WORCESTER POLYTECHNIC INSTITUTE  
in Partial Fulfillment of the Requirements for the Degree of  
DOCTOR OF PHILOSOPHY  
in Biomedical Engineering  
27 October 2022

By:

---

Mahvash Jebeli

Approved by:

---

Kristen L. Billiar, PhD  
Dissertation Advisor  
Professor & Department Head  
Biomedical Engineering  
Worcester Polytechnic Institute

---

Marsha Rolle, PhD  
Professor  
Biomedical Engineering  
Worcester Polytechnic Institute

---

Catherine Whittington, PhD  
Assistant Professor  
Biomedical Engineering  
Worcester Polytechnic Institute

---

Qi Wen, PhD  
Associate Professor  
Physics  
Worcester Polytechnic Institute

---

Lauren Black III, PhD  
Associate Professor  
Biomedical Engineering  
Tufts University

To Roya,

My sister, my role model, my love...

Who could not survive 2020...

## Acknowledgments

This thesis could never be finished without the outstanding help of many people who showed their support and encouragement throughout the last three and a half years of my Ph.D. journey. First, I want to thank my advisor, Prof. Kristen Billiar, who believed in me and pushed me to be a better version of myself. He gave invaluable emotional support during days that were unimaginable for many, but I could keep going on with his support. My warmest gratitude goes to my committee members, Dr. Catherine Whittington, Dr. Marsha Rolle, Dr. Qi Wen, and Dr. Lauren Black, for their expertise, insight, and time.

I would like to sincerely thank the past members of the Billiar lab who paved the road for my project and also the current members of it who helped me in every way possible. Special thanks to Dr. Zachary Goldblatt, whom I have always gone to for my many questions, some not very smart! My biggest thanks to Samantha Lopez, indeed a gem, my undergraduate student, who worked by my side throughout this project. This work could not have been completed without her insights and passion for science. I enjoyed our time, and mentoring [and working with] her was one of my most precious experiences.

I also would like to thank the fantastic graduate students at Gateway Park I, who were always there for me no matter what. During a Ph.D., all students need such support, and I was blessed to have it. Among many, I would like to mention soon-to-be Dr. Sabine Hahn for her unconditional support.

Last but one of the most important ones, I would like to thank my family, who are suffering from the distance between us but going through with it only for my success. I miss you all very much.

# Table of Contents

Acknowledgments.....	3
Table of Contents.....	4
List of Abbreviations and Symbols.....	7
Abstract.....	8
Chapter I: Introduction.....	9
1.1    References.....	12
Chapter II: Background.....	15
2.1    Overview.....	15
2.2    Calcification in body.....	15
2.3    The aortic valve and valvular interstitial cells .....	18
2.4    Potential mechanisms of CAVD.....	20
2.4.1    Putative role of mechanical environment on CAVD .....	20
2.4.2    VICs differentiate into osteoblast-like type .....	21
2.4.3    VICs differentiating into myofibroblasts .....	22
2.4.4    Inflammation.....	22
2.4.5    Membrane-enclosed vesicles .....	23
2.5    Sex-related differences in CAVD .....	23
2.5.1    Apoptosis-mediated .....	24
2.6    The potential mechanism linking apoptosis and calcification .....	26
2.7    Summary.....	28
2.8    References.....	28
Chapter III: Multicellular Aligned Bands Disrupt Global Collective Cell Behavior.....	40
3.1    Abstract.....	41
3.2    Introduction.....	42
3.3    Methods .....	44
3.3.1    Substrate preparation .....	44
3.3.2    Traction force microscopy .....	45
3.3.3    Dynamic stretching .....	45
3.3.4    Cell culture and media .....	46
3.3.5    Stable YAP-VIC cell line.....	46
3.3.6    Imaging and immunohistochemistry.....	47
3.3.7    Quantification of confluency level, cell density, and cell alignment.....	48

3.3.8	Statistical Analysis.....	49
3.4	Results.....	50
3.4.1	Aggregates have variable rates of progression towards confluency .....	50
3.4.2	Local hyperconfluency occurs following band formation .....	53
3.4.3	Banding occurs regardless of aggregate size .....	55
3.4.4	Cells migrate to connect with bands and then move in coordination.....	56
3.4.5	Local hyperconfluency is inhibited by depleting calcium .....	57
3.4.6	Hyperconfluent bands increase local traction stresses .....	59
3.4.7	Cytosolic YAP indicates low tension in hyperconfluent bands .....	60
3.4.8	Cells in bands reorient towards stretch but not completely .....	63
3.4.9	Proliferation occurs throughout aggregates but decreases in hyperconfluent regions 65	
3.4.10	Apoptosis increases in high density regions in a YAP-dependent manner.....	66
3.5	Discussion .....	68
3.6	Conclusion .....	74
3.7	Acknowledgment .....	75
3.8	Appendix 1.....	75
3.9	Appendix 2.....	77
3.10	Supplemental Figures.....	78
3.11	Appendix 3.....	88
3.11.1	Movie 1:.....	88
3.11.2	Movie 3 .....	94
3.12	References.....	97
<b>Chapter IV: Phosphatidylserine Correlates with in vitro Calcification of Valvular Interstitial Cells</b>		
	Cells .....	104
4.1	Introduction.....	104
4.2	Methods .....	105
4.2.1	Substrate preparation .....	105
4.2.2	Cells and media.....	106
4.2.3	Immunohistochemistry and imaging.....	107
4.2.4	Uniform confluency was targeted for the aggregates to study.....	108
4.2.5	Image Analysis in MATLAB.....	108
4.2.6	Quantification of Annexin V tagged PtdSer .....	109
4.2.7	Statistical analysis.....	109
4.3	Results.....	110

4.3.1	Calcification increases with the addition of PtdSer in inhibited apoptosis treatments as well as the not-treated cells.....	110
4.3.2	Heterogeneity observed in reported data.....	111
4.3.3	Limiting the confluency of the analyzed aggregates further removes heterogeneity in response to exogenous PtdSer.....	111
4.3.4	Exogenous PtdSer enters as lipid vesicles into the media and incorporates into the cell membrane.....	113
4.3.5	Exogeneous PtdSer affects female cells more than male cells .....	114
4.4	Discussion.....	115
4.5	Appendix 1: Additional Experiments to Examine Further the Mechanisms of PtdSer-Induced Calcification.....	118
4.5.1	Future work 1:.....	118
4.5.2	Future work 2:.....	122
4.6	Supplemental material .....	124
4.7	References.....	124
Chapter V: Conclusions, Limitations, and Future Work .....		129
5.1	Conclusions.....	129
5.1.1	Conclusions: Aim 1.....	130
5.1.2	Conclusions: Aim 2.....	131
5.2	Experimental limitations and next steps .....	132
5.2.1	Study limitations: Aim 1 .....	132
5.2.2	Study limitations: Aim 2.....	134
5.3	Long-term future work for the field.....	135
5.3.1	Future work: Aim 1.....	135
5.3.2	Future work: Aim 2.....	137
5.4	References.....	138

## List of Abbreviations and Symbols

<b>AFM</b>	Atomic force microscopy
<b>CAVD</b>	Calcific aortic valvular disease
<b>ECM</b>	Extracellular matrix
<b>PA</b>	Polyacrylamide
<b>PDMS</b>	Polydimethylsiloxane
<b>PtdSer</b>	Phosphatidylserine
<b>TFM</b>	Traction force microscopy
<b>VIC</b>	Valvular interstitial cell
<b>YAP</b>	Yes-associated protein

## Abstract

Calcification of the aortic valve is a significant source of mortality in the elderly in the US. Even as a serious disease, calcification does not have any permanent therapeutics. Valvular interstitial cells, fibroblastic in nature and located in the middle layer of the aortic valve, are mainly involved in the pathology of this disease.

Apoptosis, i.e., programmed cell death, is a crucial phenomenon in the body to maintain homeostasis. Apoptosis is a biological phenomenon that is affected by the collective behavior of the cells, as cells' behavior defers in the proximity of others. In the early stages of apoptosis, the phosphate head of phosphatidylserine, a phospholipid in the cell membrane, translocates to the outside of the cell. Although a correlation between calcification and apoptosis is shown, no definite reason behind this correlation has been introduced so far.

Here, we show how the collective behavior develops, as multicellular bands, in aggregates of valvular interstitial cells and how it leads to changes in mechanical states of the cells demonstrated by the biological markers of low-stress environments such as higher apoptosis. Then, we examine the effect of phosphatidylserine on calcification, indicating the possible role of phosphatidylserine exposure during the early stages of apoptosis in the initiation of calcification.

The knowledge obtained from this thesis expands our understanding of fibroblastic collective behavior that leads to different biological phenomena, such as the development of higher apoptosis rates. Further, the results from this research could assist in further investigations on phosphatidylserine's role in calcification. Also, the results of this study could be applied to other fibroblasts, such as human dermal fibroblasts, and similar diseases, such as atherosclerosis.

## Chapter I: Introduction

Calcific Aortic Valve Disease (CAVD) is the third most common heart disease in the US (Pibarot et al. 2007) and is the second leading cause of heart surgery (Yutzey et al. 2014). CAVD is a progressive disease that ranges from aortic sclerosis, mild valve thickening without the obstruction of blood flow, fibrosis, and early calcification, to aortic stenosis, severe calcification with impaired leaflet motion (Freeman Rosario et al. 2005, Gharacholou et al. 2011, Rajamannan et al. 2011). This process causes nodules to form on the valve and inhibit its normal function (Yutzey et al. 2014). Aortic stenosis is the second most frequent heart disease after coronary artery disease and systemic arterial hypertension in individuals over 65 years old (Lindman et al. 2016). Although it is a significant problem, the only therapy remains surgical or transcatheter aortic valve replacement (Leopold 2012). However, calcification is the major reason for failure in such treatments as well (Schoen et al. 2005). The importance of this issue inspires us to investigate the mechanisms of CAVD further to develop efficient therapies.

The binding between phospholipids and calcium could play a role in calcification; as one of the phospholipids in the cell membrane, phosphatidylserine (PtdSer), has a high binding affinity for  $Ca^{2+}$  (Boyan et al. 1989). One of the first main changes during apoptosis, programmed cell death, is a disruption in the asymmetry of the cell membrane. During apoptosis, which is a vital procedure to maintain the cells' homeostasis, repair, and growth, PtdSer flips to be exposed to the extracellular matrix - (Birge et al. 2016, Fadok et al. 1998, Mariño et al. 2013). Apoptotic cells, although variable in size and content, have phospholipid-rich membranes and concentrated calcium that may initiate mineralization (Giachelli 2004, Leopold 2015, Proudfoot et al. 2000). If these apoptotic cells are not adequately cleared by immune cells, they may serve as nucleation sites for calcification (Jian et al. 2003, Kim 1995).

Many biological conditions may affect apoptosis, such as the mechanical state of the cells (Chen et al. 1997, Kaiser et al. 1997, Mih et al. 2011, Wang et al. 2000, Zazzeroni et al. 2018, Zhang et al. 2011). The mechanical state is determined by different factors such as ECM stiffness, the forces applied by neighboring cells, and dynamic

cyclic loading. It has been shown that the cells in low-stress environments, i.e., ECM with low stiffness, hyperconfluent regions, and static loading, experience higher apoptosis rates. As cells collectively behave differently compared to single cells, and the changes the cellular collective behavior may induce on the mechanical state of the cells, it is crucial to study the effects of collective behaviors on apoptosis that may lead to calcification.

In this project, we will study the collective behavior of cells and how it affects their mechanical state and apoptosis signal that has been shown to correlate with calcification. We will explore the effects of exogenous PtdSer addition on calcification as we hypothesize with this addition, even with inhibition of apoptosis, we will observe more calcification. The motivation for this project is raised from the lack of treatment for CAVD, a deadly disease, and the lack of knowledge of the causes of the correlation between apoptosis and calcification. The proposed research offers an addition to our understanding of how the valvular interstitial cells (VICs) behave collectively, how it leads to apoptosis, and which component of apoptosis may have a role in the initiation of calcification. The most common method for studying calcification in 2D models are monolayers left to rip from the dish and from nodules to study the multicellular behavior. As they become more confluent, cells induce higher tensions leading to ripping into aggregates. Here, we utilize microcontact printed aggregates to have a well-controlled model of aggregates, as we can print different sizes and shapes of collagen island to seed cells (Cirka et al. 2017). Two aims have been established to explore the proposed research. In the first aim, we investigate the collective behavior of VICs and how it affects apoptosis. In the second aim, we determine the role of PtdSer in the initiation of classification.

In Chapter Two, we provide a literature review on calcification, its potential mechanisms, and the possible role of apoptosis in its initiation. In detail, we provide recaps on calcification in different parts of the body, such as the aortic valve, cardiovascular system, other soft tissues, and examples of similar diseases. As potential mechanisms, we lay out mechanical environment, VICs differentiating into osteoblast-like type, or myofibroblasts, membrane-enclosed vesicles, and apoptosis. Further, we

discuss apoptosis, the structural changes of the cells that it causes, and its relationship with the collective behavior of VICs. Ultimately, we provide more evidence on how PtdSer, an important part of apoptosis, can be related to calcification.

The first aim is delineated in Chapter 3, where we investigate the local collective behavior of VICs in printed circular aggregates and subsequent apoptosis. Previously, we have studied the aggregates with snapshots and observed heterogeneity in different biological markers. As we improved our model to track individual aggregates over a time span of days, we observed local collective behaviors develop. The cells formed a band spanning the aggregate's diameter leading to resultant heterogeneity in different signals, such as apoptosis. We hypothesize local cell collective behavior interacts with and often supersedes collective behavior guided by global stimuli and constraints. We characterize different collective behaviors that affect global collective behavior induced by global constraints. In both hours and days' time-course experiments, we study cell-cell interactions in microcontact printed multicellular aggregates of valvular interstitial cells. We examine proliferation, cell mobility, YAP exclusion from nuclei, apoptosis, and traction forces applied to the substrate to study the mechanical states of the cells under the influence of collective behaviors. Additionally, we explore the effects of uniaxial dynamic loading on cell behaviors as we change the mechanical state of the cells with an implication of such loading. This aim is essential as it expands our knowledge on the evolution of behavior of cells in our 2D aggregates, how the cells interact collectively, and how it leads to apoptosis that correlates with calcification.

The second aim is addressed in Chapter 4, where we investigate the effects of PtdSer in initiating calcification in VICs in multicellular aggregates. We postulate that the exposure of PtdSer at the beginning of apoptosis correlates with the initiation of calcification. We utilize our 2D microcontact printed aggregates to study the effect of PtdSer addition on resultant calcification. We investigate the mechanism of how exogenous PtdSer will be incorporated into the cell membrane. We also measure the amount of PtdSer on the cell membrane exposed to the extracellular environment after its artificial addition. This aim is significant as it demonstrates the role of PtdSer as a potential mechanism of calcification in VICs. With the knowledge obtained from this

aim, the particular component of apoptosis that plays a role in the initiation of calcification will be clarified, and its mediation could lead to therapeutic solutions.

The conclusions, limitations, and future directions of this project are discussed in Chapter 5. More investigation on cell-cell forces is critical to understand how the cells behave collectively in a certain location inside of 2D aggregates. Further research on the different behavior of different sexes of cells is needed. Also, an extension of the current model by coculturing macrophages and VICs could expand our knowledge on immune deficiencies that lead to excess apoptosis bodies on the aortic valve that may lead to calcification.

The result of this project is significant as it is the first to examine the role of PtdSer in the initiation of calcification in valvular interstitial cells (VICs) and also the first to track the individual multicellular aggregates over days that help us to understand VICs' collective behavior. The results assist us in the identification of possible causes of CAVD that could result in the development of new therapeutic solutions.

## 1.1 References

Birge, R. B., S. Boeltz, S. Kumar, J. Carlson, J. Wanderley, D. Calianese, M. Barcinski, R. A. Brekken, X. Huang, J. T. Hutchins, B. Freimark, C. Empig, J. Mercer, A. J. Schroit, G. Schett and M. Herrmann (2016). "Phosphatidylserine Is a Global Immunosuppressive Signal in Efferocytosis, Infectious Disease, and Cancer." Cell Death And Differentiation **23**: 962.

Boyan, B. D., Z. Schwartz, L. D. Swain and A. Khare (1989). "Role of Lipids in Calcification of Cartilage." the Anatomical Record **224**(2): 211-219.

Chen, C. S., M. Mrksich, S. Huang, G. M. Whitesides and D. E. Ingber (1997). "Geometric Control of Cell Life and Death." Science **276**(5317): 1425-1428.

Cirka, H. A., J. Uribe, V. Liang, F. J. Schoen and K. L. Billiar (2017). "Reproducible in Vitro Model for Dystrophic Calcification of Cardiac Valvular Interstitial Cells: Insights into the Mechanisms of Calcific Aortic Valvular Disease." Lab Chip **17**(5): 814-829.

Fadok, V. A., D. L. Bratton, S. C. Frasch, M. L. Warner and P. M. Henson (1998). "The Role of Phosphatidylserine in Recognition of Apoptotic Cells by Phagocytes." Cell Death And Differentiation **5**(7): 551-562.

Freeman Rosario, V. and M. Otto Catherine (2005). "Spectrum of Calcific Aortic Valve Disease." Circulation **111**(24): 3316-3326.

Gharacholou, S. M., B. L. Karon, C. Shub and P. A. Pellikka (2011). "Aortic Valve Sclerosis and Clinical Outcomes: Moving toward a Definition." The American Journal of Medicine **124**(2): 103-110.

Giachelli, C. M. (2004). "Vascular Calcification Mechanisms." Journal of the American Society of Nephrology **15**(12): 2959-2964.

Jian, B., N. Narula, Q.-y. Li, E. R. Mohler and R. J. Levy (2003). "Progression of Aortic Valve Stenosis: Tgf-B1 Is Present in Calcified Aortic Valve Cusps and Promotes Aortic Valve Interstitial Cell Calcification Via Apoptosis." The Annals of thoracic surgery **75**(2): 457-465.

Kaiser, D., M.-A. Freyberg and P. Friedl (1997). "Lack of Hemodynamic Forces Triggers Apoptosis in Vascular Endothelial Cells." Biochemical and biophysical research communications **231**(3): 586-590.

Kim, K. M. (1995). "Apoptosis and Calcification." Scanning Microscopy **9**(4): 1137-1175; discussion 1175-1138.

Leopold, J. A. (2012). "Cellular Mechanisms of Aortic Valve Calcification." Circulation. Cardiovascular interventions **5**(4): 605-614.

Leopold, J. A. (2015). "Vascular Calcification: Mechanisms of Vascular Smooth Muscle Cell Calcification." Trends in Cardiovascular Medicine **25**(4): 267-274.

Lindman, B. R., M.-A. Clavel, P. Mathieu, B. Iung, P. Lancellotti, C. M. Otto and P. Pibarot (2016). "Calcific Aortic Stenosis." Nature reviews. Disease primers **2**: 16006-16006.

Mariño, G. and G. Kroemer (2013). "Mechanisms of Apoptotic Phosphatidylserine Exposure." Cell research **23**(11): 1247-1248.

Mih, J., F. Liu, D. Tschumperlin and A. Marinković (2011). "Transitions in Matrix Stiffness Uncouple Lung Fibroblast Proliferative and Morphological Responses from Cytoskeletal Tension." Am J Respir Crit Care Med **183**: A3562.

Pibarot, P. and J. G. Dumesnil (2007). "New Concepts in Valvular Hemodynamics: Implications for Diagnosis and Treatment of Aortic Stenosis." The Canadian journal of cardiology **23 Suppl B**(Suppl B): 40B-47B.

Proudfoot, D., J. N. Skepper, L. Hegyi, M. R. Bennett, C. M. Shanahan and P. L. Weissberg (2000). "Apoptosis Regulates Human Vascular Calcification in Vitro." Circulation research **87**(11): 1055-1062.

Rajamannan, N. M., F. J. Evans, E. Aikawa, K. J. Grande-Allen, L. L. Demer, D. D. Heistad, C. A. Simmons, K. S. Masters, P. Mathieu, K. D. O'Brien, F. J. Schoen, D. A. Towler, A. P. Yoganathan and C. M. Otto (2011). "Calcific Aortic Valve Disease: Not Simply a Degenerative Process: A Review and Agenda for Research from the National Heart and Lung and Blood Institute Aortic Stenosis Working Group. Executive Summary: Calcific Aortic Valve Disease-2011 Update." Circulation **124**(16): 1783-1791.

Schoen, F. J. and R. J. Levy (2005). "Calcification of Tissue Heart Valve Substitutes: Progress toward Understanding and Prevention." The Annals of thoracic surgery **79**(3): 1072-1080.

Wang, H.-B., M. Dembo and Y.-L. Wang (2000). "Substrate Flexibility Regulates Growth and Apoptosis of Normal but Not Transformed Cells." American Journal of Physiology-Cell Physiology **279**(5): C1345-C1350.

Yutzey, K. E., L. L. Demer, S. C. Body, G. S. Huggins, D. A. Towler, C. M. Giachelli, M. A. Hofmann-Bowman, D. P. Mortlock, M. B. Rogers, M. M. Sadeghi and E. Aikawa (2014). "Calcific Aortic Valve Disease: A Consensus Summary from the Alliance of Investigators on Calcific Aortic Valve Disease." Arteriosclerosis, thrombosis, and vascular biology **34**(11): 2387-2393.

Zazzeroni, L., G. Faggioli and G. Pasquinelli (2018). "Mechanisms of Arterial Calcification: The Role of Matrix Vesicles." European Journal of Vascular and Endovascular Surgery **55**(3): 425-432.

Zhang, Y.-H., C.-Q. Zhao, L.-S. Jiang and L.-Y. Dai (2011). "Substrate Stiffness Regulates Apoptosis and the Mrna Expression of Extracellular Matrix Regulatory Genes in the Rat Annular Cells." Matrix Biology **30**(2): 135-144.

## Chapter II: Background

### 2.1 Overview

In this chapter, we review the literature on calcification of VICs with a focus on the role of apoptosis in its initiation, as apoptosis precedes calcification in multicellular aggregates and dense mineralized particles are observed. We briefly introduce different kinds of calcification, aortic valve, valvular interstitial cells, and current knowledge on the correlation between apoptosis and calcification. Additionally, we review the literature on the influence of collective behavior on apoptosis, as it has been shown apoptosis is correlated with calcification (Giachelli 2004, Leopold 2015, Proudfoot et al. 2000). Then, we explore the literature on the different mechanisms involved in calcification and specially PtdSer exposure, a potential mechanism relating apoptosis to calcification. The goal of this chapter is to summarize current knowledge of the correlation between apoptosis and calcification, in addition to the effects of collective behaviors of cells on apoptosis.

The gap in our knowledge about how calcification could proceed after apoptosis is significant, especially since the mechanistic link between them has not been investigated sufficiently and remains unclear (Leopold 2012). There are numerous open questions on how ectopic calcification, unwanted mineralization that happens in soft tissues typically consisting of calcium phosphate salts (Giachelli 1999), is related to apoptosis and whether these could lead to therapeutic targets.

### 2.2 Calcification in body

Even though calcium is a necessary component to life, its accumulation on tissues could lead to major health issues and diseases, such as in cardiovascular tissues (Mundy et al. 1993), especially in calcification of the aortic valve (Freeman Rosario et al. 2005), nephrocalcinosis in the kidney (Mizobuchi et al. 2009), genitourinary schistosomiasis in the bladder (Lee et al. 2018), and cranial calcification in brain tissue (Oliveira et al.

2016). The calcium accumulation, calcification, in tissues interrupts their homeostasis and results in their malfunction (Freeman Rosario et al. 2005).

Different types of calcification occur in the body, such as ectopic, which is generally termed dystrophic (Giachelli 1999), metastatic, idiopathic, iatrogenic, calciphylaxis (Le et al. 2021 Jul 17), and osteogenic (Chen et al.). Among those mentioned, ectopic calcification contributes more to the progression of CAVD compared to osteogenic calcification (Chen et al. 2015).

Calcification of the aortic valve is the most frequent disorder in heart valves (Alushi et al. 2020). This slowly progressive disease ranges from aortic sclerosis, mild valve thickening, to aortic stenosis, severe calcification, where calcification obstructs blood flow (Freeman Rosario et al. 2005). This matrix stiffness increase results in reduced flexibility of the valve due to excessive collagen (Rajamannan et al. 2011) and calcium deposition. CAVD is recognizable by thickening of the valve, formation of fibrosis and the calcified matrix also new vascularization in its structure (Freeman Rosario et al. 2005, Leopold 2012, Miller et al. 2011, Rajamannan et al. 2011). In this process, the valve remodels over the years resulting in its malfunction or impairment (Lindman et al. 2016).

Many factors are known to play a role in CAVD, such as genetics, chronic inflammation, and mineralization (Alushi et al. 2020, Demer et al. 2014). Other diseases such as hypertension (Lindroos et al. 1994) and malfunctioned mineral metabolism (Chen et al. 2019), as well as age, body mass index (Lindroos et al. 1994), sex (Summerhill et al. 2020), and lifestyle like smoking (Chen et al. 2019) are risk factors in developing CAVD.

In CAVD, tissue alteration is evident and recognizable by different types of cell death, such as apoptosis (Bonetti et al. 2019). It appears that apoptotic and necrotic VICs and their remnants remain uncleared by macrophages (Bonetti et al. 2019, Schrijvers Dorien et al. 2005, Yurdagul et al. 2018) and proceed to calcification (Proudfoot et al. 2000). This mainly happens when VICs in mechanical environment of AV is injured and cannot heal.

Calcification in the cardiovascular system is not restricted to valves, as in major arteries; it is present in most individuals over 60 years old (Allison Matthew et al. 2004). Calcification in such tissues changes the elastance of arteries which causes considerable morbidity (Arad et al. 2000, Keelan Paul et al. 2001, Wayhs et al. 2002). In the cardiovascular system, coronary artery calcification is predictive of upcoming cardiovascular events (Shekar et al. 2018).

Investigating the similarities and differences of calcification in other parts of the cardiovascular system is of importance. Even though there is growing evidence that CAVD is unique from other vascular diseases, as valve structure and function are distinct from blood vessels, there are some similarities with the etiology of the diseases that may shed insight into CAVD, especially on how mechanics and apoptosis contribute to calcification in blood vessels.

As an example of such similarities, coronary artery calcification that can lead to atherosclerosis shares pathological features and histopathology (Mohler et al. 1991, Nasir et al. 2010) and clinical risk factors (Lee et al. 2021) with calcification of the aortic valve. The association and similarities assist the surgeons in evaluating patients presurgery by imaging coronary atherosclerosis as a negative predictor of CAVD (Lee et al. 2021). Also, as an example of the differences between these diseases, the CAVD progression is only associated with the calcified plaque volume in coronary atherosclerosis and not the noncalcified plaque volume (Lee et al. 2021).

Ectopic calcification in the body is not restricted to the cardiovascular system, and it can happen throughout the body; it is observed mainly in the skin, also in renal cells (Mezzabotta et al. 2015), tubules of kidneys (Cliff 1970, Klotz 1905, Rockley 1965), and articular cartilage (Hashimoto et al. 1998). The nodules are hydroxyapatite, calcium phosphate salt, that usually does not precipitate in the body (Giachelli 1999).

The calcified tissues, including the calcified aortic valve, show alteration in tissue and apoptosis/necrosis (Giachelli 1999), demonstrating a correlation between apoptosis/necrosis with calcification. For example, calcification in cardiovascular tissues,

in addition to the aortic valve and tubules of kidneys, has followed necrosis (Cliff 1970, Klotz 1905, Rockley 1965), as the calcium and phosphate deposition in the HK-2 cells were visible only in or near areas where apoptotic cells were present (Priante et al. 2019). Also, apoptosis activation was reported in calcifying cartilage (Bonetti et al. 2019), and the chondrocyte-derived apoptotic bodies have been discussed as a cause (Hashimoto et al. 1998). This correlation is not limited to the unwanted calcification that leads to diseases and even in required calcification in the body, such as near growth plates calcification happens near apoptotic chondrocytes (Fujita et al. 2014).

### 2.3 The aortic valve and valvular interstitial cells

While calcification occurs in different parts of the body, this thesis focuses on calcification in the aortic valve (AV) and VICs that are mainly involved in the pathology of the disease. AV is a trileaflet structure that acts as a check valve between the left ventricle and the aorta (Leopold 2012). It consists of three different extracellular matrices (ECM) layers: fibrosa, spongiosa, and ventricularis (Hinton et al. 2011). The unique ECM structure of AV provides its macroscopic mechanical properties to sustain the condition of its mechanical environment (Wang et al. 2014). In addition to its ECM structure, AV is populated by specialized cells participating in its vitality. Valvular endothelial cells line both the surfaces exposed to blood flow, and valvular interstitial cells (VICs) are found throughout the ECM layers.

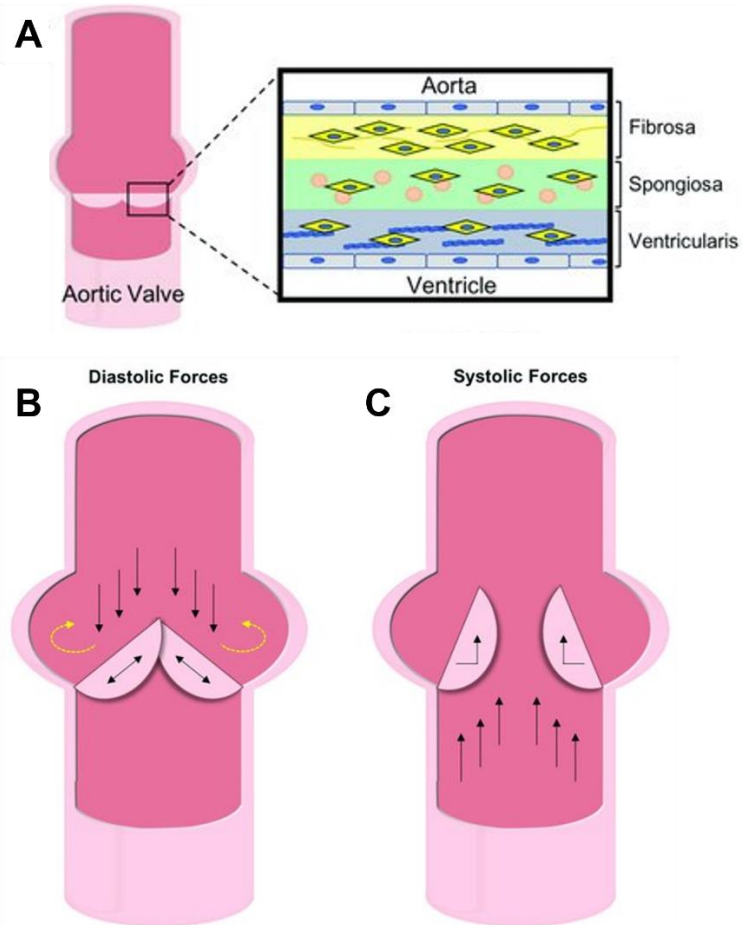


Figure 2-1. ECM composition of the aortic leaflet and the forces on it. A) Its structure consists of three layers: fibrosa, spongiosa, and ventricularis. B) Diastolic forces on the aortic valve when it is closed. C) Systolic forces on the valve when opened—adapted from (Gomel et al. 2019) via license: [CC BY 4.0](https://creativecommons.org/licenses/by/4.0/).

Although it has been thought that CAVD is a degenerative disease, due to the time span it takes to develop, and calcium deposition present in the diseased tissue, the evidence of osteoblast activity in addition to lipoprotein deposition and chronic inflammation demonstrates an active process (Lerman et al. 2015). The active nature of this disease makes the study of VICs essential to understanding the progression of calcification, as these cells can differentiate into other phenotypes in different conditions.

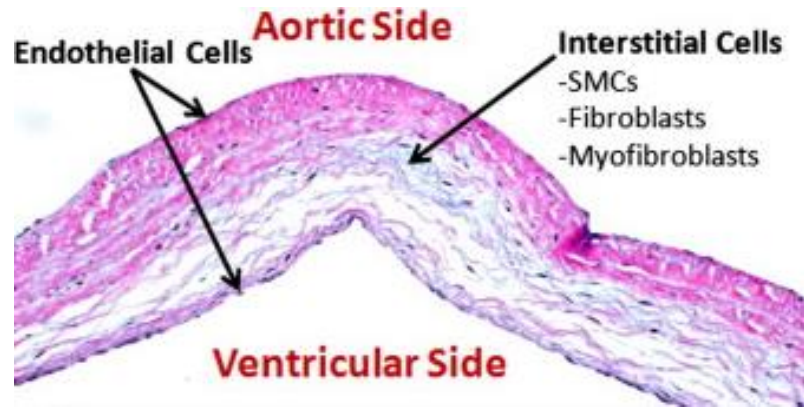


Figure 2-2. Histological section of the aortic valve structure showing its cellular distribution. Endothelial cells on both sides of the valve tissue and interstitial cells in the middle of the tissue. From (El-Hamamsy et al. 2010) via a Creative Commons [license](#).

## 2.4 Potential mechanisms of CAVD

Calcification can occur via multiple passive and active processes, including bone formation (Thompson et al. 2012), mechanical environment (Merryman et al. 2013), valvular interstitial cells (VICs) differentiating into osteoblast-like phenotype, and myofibroblast (Wang et al. 2014), membrane-enclosed vesicles (Proudfoot et al. 2001), and apoptosis-mediated dystrophic calcification (Jian et al. 2003, Yip et al. 2009). Some of these potential mechanisms are discussed in turn below.

### 2.4.1 Putative role of mechanical environment on CAVD

Cells can "sense" the mechanical properties of their extracellular matrix (Yip et al. 2009). Stiffness of the extracellular matrix is known to regulate motility, proliferation, and differentiation in cells (Yip et al. 2009). In VICs, mechanobiology of the cell's environment, such as matrix stiffness, plays a crucial role in activating the differentiation into myofibroblast cells (Wang et al. 2014), regulating the apoptosis of fibroblasts (Liu et al. 2010, Wang et al. 2000, Zhang et al. 2011), and regulating the calcific nodule formation (Yip et al. 2009). The elasticity modulus of the valve ranges from 0.1 kPa to 2 MPa (Gould Sarah et al. 2013, Krishnamurthy et al. 2011, Sewell-Loftin et al. 2012, Stella et al. 2007, Zhao et al. 2011). It has been shown that with the manipulation of the stiffness of the substrate ranging gradually from 7 to 32 kPa, the porcine aortic VICs

differentiated significantly more near the stiffer region (Jenkins 2008, Quinlan et al. 2012).

The calcific nodules and lesions start at the fibrosa layer and extend to the aortic side of the valve (Caira et al. 2006). It has been shown in an *ex vivo* study that calcification follows the pattern of the valve stress and stretch (Weiler et al. 2011) in the base and coaptation line of the aortic valve (Thubrikar M Fau - Piepgrass et al. 1979). Also, in *in vitro* models, the implication of dynamic cyclic loading calcification was probably elevated due to increased matrix remodeling enzyme expression, pro-inflammatory proteins (Balachandran et al. 2010), or osteogenic differentiation of VICs (Bogdanova et al. 2018).

#### 2.4.2 VICs differentiate into osteoblast-like type

The differentiation of the cells in the structure of the aortic valve, such as the quiescent cells differentiating into osteoblasts, is one of the potential mechanisms contributing to calcification. In general, there are five different phenotypes of VICs in the aortic valve environment (Liu et al. 2007). Among these phenotypes, myofibroblast and osteoblast-like ones are more associated with CAVD (Wang et al. 2014). In the progression of the calcification, quiescent VICs differentiate into osteoblast-like phenotypes, which are amenable to bone morphogenic proteins (BMPs) (Leopold 2012). The BMPs, a member of the TGF- $\beta$  superfamily, make osteoblasts that initiate bone formation by inducing the expression of Runx2, an osteoblast transcription factor reviewed in (Boström et al. 2011). After the expression of Runx2, the osteoblast-like cells upregulate the expression of osteopontin and osteocalcin, which are proteins responsible for the calcification process (Johnson Rebecca et al. 2006). The differentiation to osteoblast-like cells has been shown in human VICs *in vitro* to be achieved with applied cyclic stretch or other mechanical changes (Alexopoulos et al. 2010, Miller et al. 2010) by measuring Runx2, Osterix, or APS (the osteoblast gene markers).

### 2.4.3 VICs differentiating into myofibroblasts

In cases of injury, VICs are activated to the myofibroblast phenotype to remodel the surrounding ECM, which could result in disease progression (Rajamannan et al. 2011). Myofibroblasts phenotype (Egan et al. 2011, Gössl et al. 2012, Paranya et al. 2001, Pho et al. 2008, Walker Gennyne et al. 2004), as well as osteoblast-like cells (Bischoff et al. 2011, Chen et al. 2009, Egan et al. 2011, Gössl et al. 2012, Wang et al. 2013), are the result of differentiation of VICs and VECs in the diseased valve, as the microenvironmental cues such as matrix stiffness and TGF- $\beta$ 1 level. TGF- $\beta$ 1 initiates the myofibroblast activation of VICs, which affects collagen deposition (Hinz et al. 2012, Walker Gennyne et al. 2004) and could enhance apoptosis-associated calcification (Jian et al. 2003). The differentiation to myofibroblast phenotype has been shown to be reversible in VICs in vitro; myofibroblasts can deactivate into a quiescent fibroblast (Kisseleva et al. 2012, Wang et al. 2012). The VECs differentiating to myofibroblast phenotype may be participating in the calcification of the aortic valve and go under differentiation to osteoblast-like phenotype, under the similar mentioned mechanisms as VICs behave in response to BMPs (Boström et al. 2011).

### 2.4.4 Inflammation

Since CAVD was categorized as a degenerative disease, inflammation, the primary response of innate immunity in the body, has been one of the main characterizations of this disease (Lee et al. 2018). The excised heart valves from patients undergoing aortic valve replacement showed evidence of chronic inflammatory infiltrates, providing further evidence of inflammatory response in the active remodeling process in this disease (Cote et al. 2013).

During inflammation, Toll-Like Receptors (TLRs) mediate inflammation that is caused by molecules released during tissue damage (García-Rodríguez et al. 2018), like lyse of apoptotic bodies, such as in lung inflammation, atherosclerosis, rheumatoid arthritis (Poon et al. 2014). The immune system's inability to clear apoptotic bodies results in the initiation of their secondary necrosis, which is a release of the intracellular components,

and causes an inflammatory response (Poon et al. 2014) that causes TLRs to moderate inflammation via NF- $\kappa$ B routes (García-Rodríguez et al. 2018).

### 2.4.5 Membrane-enclosed vesicles

Other than VICs, another cell type present in the aortic valve is smooth muscle cells that go under transition to become osteoblast-like cells (Leopold 2012) and, in the presence of calcium or phosphate, can release vesicles (Kapustin Alexander et al. 2011, Wuthier et al. 2011). These matrix vesicles play a role in bone formation and ectopic vascular calcification (Wuthier et al. 2011) and microcalcific nodules formation (Kapustin Alexander et al. 2011, Vengrenyuk et al. 2006, Wallin et al. 2010, Wuthier et al. 2011).

The mixture of proteins and enzymes present in the matrix vesicles makes them a probable candidate for initiating the calcification. The matrix vesicles include calcium-binding proteins, such as inorganic phosphate-generating enzyme alkaline phosphatase (ALP) and calcium ion pump Annexin V (Anderson et al. 2005, Hessel et al. 2002, Kirsch et al. 2003, Wuthier et al. 2011, Xiao et al. 2007), and phosphate to promote crystallization of calcium phosphate (Proudfoot et al. 2001).

## 2.5 Sex-related differences in CAVD

There is emerging evidence of sex-related differences in CAVD, stating that males are more prone to developing CAVD than females (Porrás et al. 2017) and more affected by external stimuli to show apoptosis and early osteogenic markers (Masjedi et al. 2017).

Not only is the progression of CAVD variable between individuals, but it is also different between different sexes (Summerhill et al. 2020), to the point that even the pathways involved in the development of the disease differs between males and females (Summerhill et al. 2020).

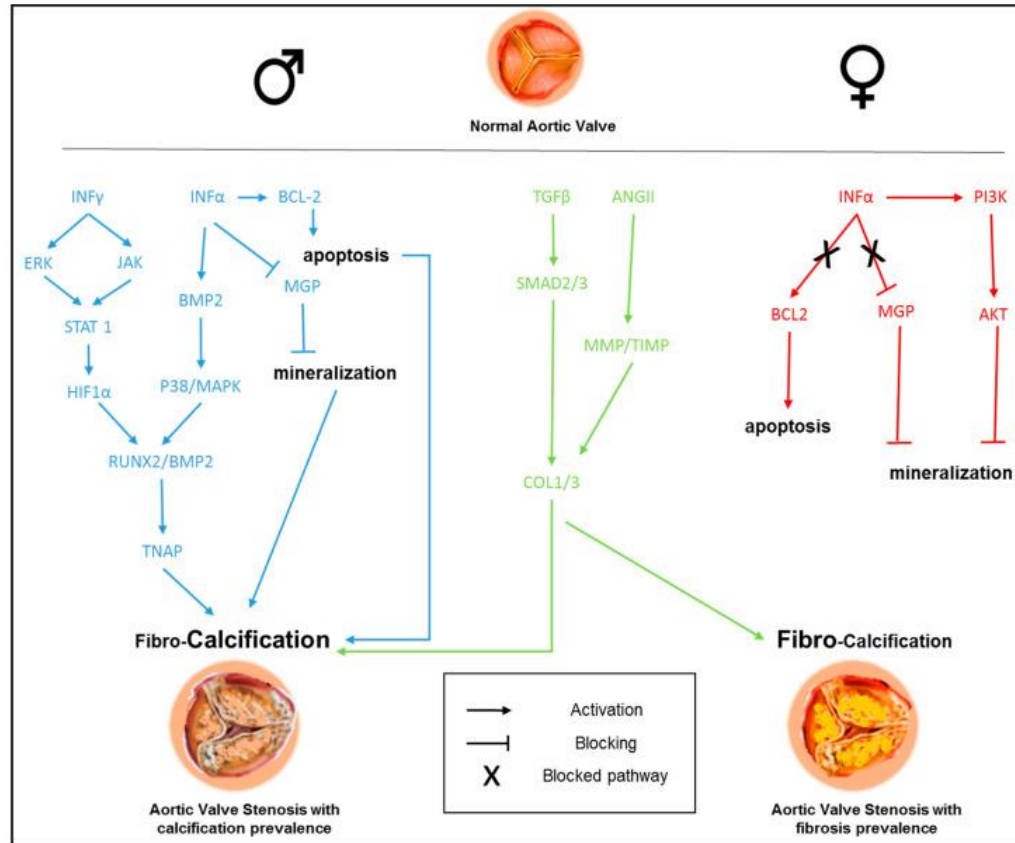


Figure 2-3. Sex-related signaling pathways in the development of CAVD. This schematic shows the known pathways involved in CAVD in different sexes, which results in males to more calcification and in females in more fibrosis. Blue represents the male, and red represents the female pathways. From (Summerhill et al. 2020) via [CC BY 4.0 license](#).

### 2.5.1 Apoptosis-mediated

In addition to prior causes, apoptosis can also trigger calcification (Cowell et al. 2005, Leopold 2012, Loscalzo 2006). Although there have been many researchers reporting a correlation between apoptosis and calcification (Cirka et al. 2017, Fujita et al. 2014, Gu et al. 2011, Kockx Mark et al. 1998, London et al. 2005, Nakahara et al. 2017, Otsuka et al. 2014, Proudfoot et al. 2000, Zazzeroni et al. 2018), the role of it in the progression of CAVD is not well understood (Leopold 2012).

Apoptosis, programmed cell death, is a necessary procedure to maintain the cells' homeostasis, repair, and growth. The changes that happen during apoptosis are a disruption in the asymmetry of the cell membrane - flipping of the phosphatidylserine to be exposed to the extracellular matrix - (Birge et al. 2016, Fadok et al. 1998, Mariño et al.

2013), shrinkage of the cell, formation of blebs on the membrane, secretion of apoptotic bodies (Kerr et al. 1972), fragmentation of DNA (Wyllie 1980), the release of the calcium in the intracellular environment by mitochondria (Kroemer et al. 2000), condensation of the chromatin (Wyllie et al. 1984), etc.

Many experimental studies have aimed to investigate the link between apoptosis and calcification. For example, there has been a significant increase in calcification for hMSC (human bone marrow mesenchymal stem cells) with the addition of necrotic dead cells or its membrane fraction (Fujita et al. 2014). In the same study, colocalization of the dead cells and calcification have been shown utilizing a localized cell death by photodynamic treatment (Fujita et al. 2014).

The dysregulation of calcium homeostasis and mitochondrial calcium overload has been shown to be pro-apoptotic (Giorgi et al. 2012, Mattson et al. 2003, Nicotera et al. 1998). Further, there is evidence that apoptotic cells that are not entirely removed by phagocytosis may serve as nucleation sites (Giachelli 2004, Leopold 2015, Proudfoot et al. 2000). For example, apoptotic cells are associated with atherosclerosis and blocking CD47 (“don’t eat me” signal) can reduce calcification in mouse models by increasing the clearance of apoptotic cells (Kojima et al. 2016).

TGF- $\beta$ 1 and its effect on the initiation of calcification of VSMCs and apoptosis of VICs (Jian et al. 2003) may be a potential mechanism for the correlation between apoptosis and calcification as TGF- $\beta$ 1 has osteogenic activity potential (Bonewald et al. 1994, Miyazono et al. 2001), as well as pro-apoptotic activity potential (Hishikawa et al. 1999, Matthey et al. 1997, Pollman Matthew et al. 1999). Another potential scenario is the role of VSMC “blebs” or ABs to initiate the crystallization of the calcium (Proudfoot et al. 2001) as apatite similar to calcium crystal present in bone (Proudfoot et al. 2001).

The VSMC “blebs,” ABs (Proudfoot et al. 2001), and porcine aortic valve fibroblasts vesicles (Kim et al. 1999) are calcium-rich. The present calcium is in the form of calcium carbonate (Proudfoot et al. 2001), a predecessor in apatite formation (Zapanta LeGeros 1981). It should be mentioned that this property is not shared amongst all types of matrix vesicles but only among those enriched in calcium and phosphatases (Kirsch et al. 1997).

Another hypothesized portion of the apoptotic cells responsible for calcium deposition and further nodule formation are the cytoskeletal remains of those cells (Leopold 2012). These apoptotic cells, although variable in size and content, have phospholipid-rich membranes and concentrated calcium that may initiate mineralization (Giachelli 2004, Leopold 2015, Loscalzo 2006, Proudfoot et al. 2000) and, if not properly cleared by immune cells, may serve as nucleation sites for calcification (Jian et al. 2003, Kim 1995).

The resultant dystrophic calcification of VICs going under apoptosis has been observed in vitro (Jian et al. 2003, Yip et al. 2009). During apoptosis, Vascular smooth muscle cells (VSMC) secrete apoptotic bodies, which share similarities with matrix vesicles (Proudfoot et al. 2000). These structures can initiate calcification by attracting and crystallizing calcium (Proudfoot et al. 2000). On the other hand, the inhibition of apoptosis (Cirka et al. 2017, Proudfoot et al. 2001) as well as overexpression of Bcl-2, an anti-apoptotic molecule (Nagase et al. 2009), results in the reduction of calcification.

## 2.6 The potential mechanism linking apoptosis and calcification

Investigation of collective cell behavior is vital as individual cells' behavior differs in communication with other cells, whereas in the body, the cells are in proximity of other cells and affected by neighboring cells. The collective behavior arises from individual cell behaviors (Wickert et al. 2016) and is not always uniform. In addition to the many benefits of collective behavior in many biological processes such as morphogenesis or tissue repair, it could lead to many diseases such as cancer or calcification.

Collective behavior is not always uniform and may include heterogeneity. Heterogeneities in local collective orientation for human fibroblasts monolayer (Turiv et al.) cancerous cells (Deisboeck et al. 2009), in migration within a confluent monolayer, for MDCK cells (Angelini Thomas et al. 2011), in experimental velocity field (Deforet et al. 2014), in simulations of the velocity field (Doxzen et al. 2013), in our observation in apoptosis signals in VICs 2D aggregates (Goldblatt et al. 2020).

Apoptosis is non-linearly correlated with the tensional state of the cell (Chan et al. 2011). The tensional state depends on multiple items that should be considered together and not as independent reasons. In detail, healthy cells under homeostatic conditions have low instances of apoptosis. Although when the cells experience extracellular high-stress conditions, such as when cells are excessively stretched in vitro, cells experience an increase in their intracellular stress levels. As all of them try to regain their homeostasis condition, they will go under apoptosis if they cannot revert their stress level to homeostatic conditions. This is where we believe calcification initiates in CAVD; as a result of the inability to retrieve their homeostatic state and going under excess apoptosis, the unremoved apoptotic cells go under secondary necrosis and result in calcium nucleation (Paone et al. 2019). Similar to cells in the high-stress region, cells with low intracellular stresses, such as when cells are seeded on soft substrates or restricted to small areas through micro-contact printing, will undergo apoptosis if they cannot achieve homeostatic levels. Hence, the correlation between apoptosis and the tensional state of cells is nonlinear.

PtdSer is a major phospholipid component of mammalian cell membranes that contributes to many regulatory processes of biological response, such as apoptosis (Uchida et al. 1998), memory function (Kim et al. 2014), and blood clotting (Kay et al. 2019). Prior to apoptosis, PtdSer resides in the inner leaflet of the plasma membrane (Uchida et al. 1998) but is translocated to the outer leaflet during the early stages of apoptosis (Birge et al. 2016, Fadok et al. 1998, Mariño et al. 2013) when there is a decreased activity of a calcium-dependent scramblase (Fadok et al. 1998). This process allows the phagocytes to recognize and remove the apoptotic cells (Uchida et al. 1998).

The exposure of PtdSer to the extracellular environment may play a role in calcification due to its extremely high binding affinity for  $\text{Ca}^{2+}$  (Boyan et al. 1989), which causes calcium ions to naturally bind to this negatively charged phospholipid in the membrane (Sinn et al. 2006). Specifically, in heart valves, the binding of phospholipids and calcium has been investigated (Demer 1997, Tintut et al. 2018, Zheng et al. 2019), although not linked with apoptotic cells specifically. For example, in patients with aortic stenosis, it has been observed that oxidized phospholipids promote valve calcification and disease progression (Zheng et al. 2019).

The presence of PtdSer in the membrane increases the calcium concentration and enhances the binding of calcium to PtdSer (Sinn et al. 2006). Calcium ions have many essential roles in cellular processes. Their interaction with biological membranes is essential for endocytosis and exocytosis and assists in the transport of small molecules across cell membranes.

## 2.7 Summary

In this thesis, we first investigate the collective behavior of VICs, the cells more involved in the pathology of CAVD. And how it affects the mechanical state of the cells in proximity of other VICs. We will measure different stress markers such as apoptosis, shown to be strongly correlated with calcification. Then we will evaluate the changes in the calcification as we exogenously add PtdSer into our model, as we believe this specific part of the apoptotic bodies is correlated with the calcification. Following is the model for the path from collective behavior to calcification studied in this thesis.

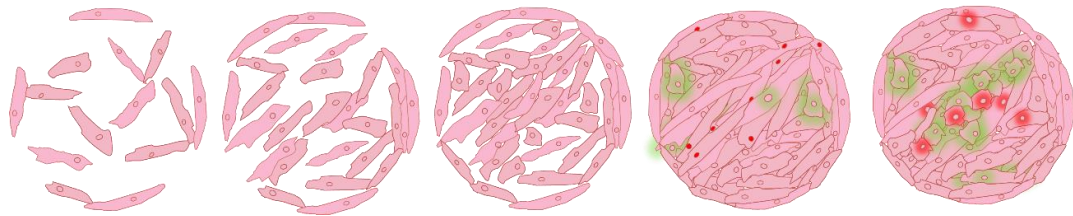


*Figure 2-4: Our proposed model of the Progression of confluency band formation), apoptosis, and YAP nucleation and how we believe each precedes from sub-confluent to hyper-confluent. Pink is a cell, green shows the hypothetical apoptosis signaling, red circles show YAP inside nuclei, and the red halo shows the YAP outside nuclei.*

We believe our study will help us to understand the importance and mechanisms of the link between apoptosis and calcification on VICs, more in-depth. This obtained knowledge will significantly impact future therapeutic targets for CAVD.

## 2.8 References

Alexopoulos, A., V. Bravou, S. Peroukides, L. Kaklamanis, J. Varakis, D. Alexopoulos and H. Papadaki (2010). "Bone Regulatory Factors Nfatc1 and Osterix in Human Calcific Aortic Valves." *International Journal of Cardiology* **139**(2): 142-149.

Allison Matthew, A., H. Criqui Michael and C. M. Wright (2004). "Patterns and Risk Factors for Systemic Calcified Atherosclerosis." *Arteriosclerosis, thrombosis, and vascular biology* **24**(2): 331-336.

Alushi, B., L. Curini, M. R. Christopher, H. Grubitzch, U. Landmesser, A. Amedei and A. Lauten (2020). "Calcific Aortic Valve Disease-Natural History and Future Therapeutic Strategies." Frontiers in Pharmacology **11**: 685.

Anderson, H. C., R. Garimella and S. E. Tague (2005). "The Role of Matrix Vesicles in Growth Plate Development and Biomineralization." Frontiers in Bioscience **10**: 822-837.

Angelini Thomas, E., E. Hannezo, X. Trepas, M. Marquez, J. Fredberg Jeffrey and A. Weitz David (2011). "Glass-Like Dynamics of Collective Cell Migration." Proceedings of the National Academy of Sciences **108**(12): 4714-4719.

Arad, Y., L. A. Spadaro, K. Goodman, D. Newstein and A. D. Guerci (2000). "Prediction of Coronary Events with Electron Beam Computed Tomography." Journal of the American College of Cardiology **36**(4): 1253-1260.

Balachandran, K., P. Sucusky, H. Jo and A. P. Yoganathan (2010). "Elevated Cyclic Stretch Induces Aortic Valve Calcification in a Bone Morphogenetic Protein-Dependent Manner." The American journal of pathology **177**(1): 49-57.

Birge, R. B., S. Boeltz, S. Kumar, J. Carlson, J. Wanderley, D. Calianese, M. Barcinski, R. A. Brekken, X. Huang, J. T. Hutchins, B. Freimark, C. Empig, J. Mercer, A. J. Schroit, G. Schett and M. Herrmann (2016). "Phosphatidylserine Is a Global Immunosuppressive Signal in Efferocytosis, Infectious Disease, and Cancer." Cell Death And Differentiation **23**: 962.

Bischoff, J. and E. Aikawa (2011). "Progenitor Cells Confer Plasticity to Cardiac Valve Endothelium." Journal of Cardiovascular Translational Research **4**(6): 710-719.

Bogdanova, M., A. Kostina, K. Zihlvanikova Enayati, A. Zibirnyk, A. Malashicheva, K.-O. Stensløkken, G. J. Sullivan, M.-L. Kaljusto, J.-P. E. Kvitting, A. Kostareva, J. Vaage and A. Rutkovskiy (2018). "Inflammation and Mechanical Stress Stimulate Osteogenic Differentiation of Human Aortic Valve Interstitial Cells." Frontiers in Physiology **9**.

Bonetti, A., M. Marchini and F. Ortolani (2019). "Ectopic Mineralization in Heart Valves: New Insights from in Vivo and in Vitro Procalcific Models and Promising Perspectives on Noncalcifiable Bioengineered Valves." Journal of thoracic disease **11**(5): 2126-2143.

Bonewald, L. F. and S. L. Dallas (1994). "Role of Active and Latent Transforming Growth Factor B in Bone Formation." Journal of Cellular Biochemistry **55**(3): 350-357.

Boström, K. I., N. M. Rajamannan and D. A. Towler (2011). "The Regulation of Valvular and Vascular Sclerosis by Osteogenic Morphogens." Circulation research **109**(5): 564-577.

Boyan, B. D., Z. Schwartz, L. D. Swain and A. Khare (1989). "Role of Lipids in Calcification of Cartilage." the Anatomical Record **224**(2): 211-219.

Caira, F. C., S. R. Stock, T. G. Gleason, E. C. McGee, J. Huang, R. O. Bonow, T. C. Spelsberg, P. M. McCarthy, S. H. Rahimtoola and N. M. Rajamannan (2006). "Human Degenerative Valve Disease Is Associated with up-Regulation of Low-Density Lipoprotein Receptor-Related Protein 5 Receptor-Mediated Bone Formation." Journal of the American College of Cardiology **47**(8): 1707-1712.

Chan, D. D., W. S. Van Dyke, M. Bahls, S. D. Connell, P. Critser, J. E. Kelleher, M. A. Kramer, S. M. Pearce, S. Sharma and C. P. Neu (2011). "Mechanostasis in Apoptosis and Medicine." Progress in Biophysics and Molecular Biology **106**(3): 517-524.

Chen, H. Y., J. C. Engert and G. Thanassoulis (2019). "Risk Factors for Valvular Calcification." Current Opinon in Endocrinology, Diabetes and Obesity **26**(2): 96-102.

Chen, J.-H., C. Y. Y. Yip, E. D. Sone and C. A. Simmons (2009). "Identification and Characterization of Aortic Valve Mesenchymal Progenitor Cells with Robust Osteogenic Calcification Potential." The American journal of pathology **174**(3): 1109-1119.

Chen, J., J. R. Peacock, J. Branch and W. D. Merryman (2015). "Biophysical Analysis of Dystrophic and Osteogenic Models of Valvular Calcification." Journal of biomechanical engineering(1528-8951 (Electronic)).

Cirka, H. A., J. Uribe, V. Liang, F. J. Schoen and K. L. Billiar (2017). "Reproducible in Vitro Model for Dystrophic Calcification of Cardiac Valvular Interstitial Cells: Insights into the Mechanisms of Calcific Aortic Valvular Disease." Lab Chip **17**(5): 814-829.

Cliff, W. J. (1970). "The Aortic Tunica Media in Aging Rats." Experimental and Molecular Pathology **13**(2): 172-189.

Cote, N., A. Mahmut, Y. Bosse, C. Couture, S. Page, S. Trahan, M. C. Boulanger, D. Fournier, P. Pibarot and P. Mathieu (2013). "Inflammation Is Associated with the Remodeling of Calcific Aortic Valve Disease." Inflammation **36**(3): 573-581.

Cowell, S. J., D. E. Newby, R. J. Prescott, P. Bloomfield, J. Reid, D. B. Northridge and N. A. Boon (2005). "A Randomized Trial of Intensive Lipid-Lowering Therapy in Calcific Aortic Stenosis." New England Journal of Medicine **352**(23): 2389-2397.

Deforet, M., V. Hakim, H. G. Yevick, G. Duclos and P. Silberzan (2014). "Emergence of Collective Modes and Tri-Dimensional Structures from Epithelial Confinement." Nature Communications **5**(1): 3747.

Deisboeck, T. S. and I. D. Couzin (2009). "Collective Behavior in Cancer Cell Populations." BioEssays **31**(2): 190-197.

Demer, L. L. (1997). "Lipid Hypothesis of Cardiovascular Calcification." Circulation **95**(2): 297-298.

Demer, L. L. and Y. Tintut (2014). "Inflammatory, Metabolic, and Genetic Mechanisms of Vascular Calcification." Arteriosclerosis, Thrombosis, and Vascular Biology **34**(4): 715-723.

Doxzen, K., S. R. K. Vedula, M. C. Leong, H. Hirata, N. S. Gov, A. J. Kabla, B. Ladoux and C. T. Lim (2013). "Guidance of Collective Cell Migration by Substrate Geometry." Integrative Biology **5**(8): 1026-1035.

Egan, K. P., J.-H. Kim, E. R. Mohler, 3rd and R. J. Pignolo (2011). "Role for Circulating Osteogenic Precursor Cells in Aortic Valvular Disease." Arteriosclerosis, thrombosis, and vascular biology **31**(12): 2965-2971.

- El-Hamamsy, I., A. H. Chester and M. H. Yacoub (2010). "Cellular Regulation of the Structure and Function of Aortic Valves." Journal of Advanced Research **1**(1): 5-12.
- Fadok, V. A., D. L. Bratton, S. C. Frasch, M. L. Warner and P. M. Henson (1998). "The Role of Phosphatidylserine in Recognition of Apoptotic Cells by Phagocytes." Cell Death & Differentiation **5**(7): 551-562.
- Fadok, V. A., D. L. Bratton, S. C. Frasch, M. L. Warner and P. M. Henson (1998). "The Role of Phosphatidylserine in Recognition of Apoptotic Cells by Phagocytes." Cell Death And Differentiation **5**(7): 551-562.
- Freeman Rosario, V. and M. Otto Catherine (2005). "Spectrum of Calcific Aortic Valve Disease." Circulation **111**(24): 3316-3326.
- Fujita, H., M. Yamamoto, T. Ogino, H. Kobuchi, N. Ohmoto, E. Aoyama, T. Oka, T. Nakanishi, K. Inoue and J. Sasaki (2014). "Necrotic and Apoptotic Cells Serve as Nuclei for Calcification on Osteoblastic Differentiation of Human Mesenchymal Stem Cells in Vitro." Cell Biochemistry and Function **32**(1): 77-86.
- García-Rodríguez, C., I. Parra-Izquierdo, I. Castaños-Mollor, J. López, J. A. San Román and M. Sánchez Crespo (2018). "Toll-Like Receptors, Inflammation, and Calcific Aortic Valve Disease." Frontiers in Physiology **9**.
- Giachelli, C. M. (1999). "Ectopic Calcification: Gathering Hard Facts About Soft Tissue Mineralization." The American journal of pathology **154**(3): 671-675.
- Giachelli, C. M. (2004). "Vascular Calcification Mechanisms." Journal of the American Society of Nephrology **15**(12): 2959-2964.
- Giachelli, C. M. (2004). "Vascular Calcification Mechanisms." J Am Soc Nephrol **15**(12): 2959-2964.
- Giorgi, C., F. Baldassari, A. Bononi, M. Bonora, E. De Marchi, S. Marchi, S. Missiroli, S. Patergnani, A. Rimessi, J. M. Suski, M. R. Wieckowski and P. Pinton (2012). "Mitochondrial Ca(2+) and Apoptosis." Cell Calcium **52**(1): 36-43.
- Goldblatt, Z. E., H. Ashouri Choshali, H. A. Cirka, V. Liang, Q. Wen, D. McCollum, N. Rahbar and K. L. Billiar (2020). "Heterogeneity Profoundly Alters Emergent Stress Fields in Constrained Multicellular Systems." Biophysical Journal **118**(1): 15-25.
- Gomel, M. A., R. Lee and K. J. Grande-Allen (2019). "Comparing the Role of Mechanical Forces in Vascular and Valvular Calcification Progression." Frontiers in Cardiovascular Medicine **5**.
- Gössl, M., S. Khosla, X. Zhang, N. Higano, K. L. Jordan, D. Loeffler, M. Enriquez-Sarano, R. J. Lennon, U. McGregor, L. O. Lerman and A. Lerman (2012). "Role of Circulating Osteogenic Progenitor Cells in Calcific Aortic Stenosis." Journal of the American College of Cardiology **60**(19): 1945-1953.
- Gould Sarah, T., S. Srigunapalan, A. Simmons Craig and S. Anseth Kristi (2013). "Hemodynamic and Cellular Response Feedback in Calcific Aortic Valve Disease." Circulation research **113**(2): 186-197.

Gu, X. and K. S. Masters (2011). "Role of the Rho Pathway in Regulating Valvular Interstitial Cell Phenotype and Nodule Formation." American Journal of Physiology-Heart and Circulatory Physiology **300**(2): H448-H458.

Hashimoto, S., R. L. Ochs, F. Rosen, J. Quach, G. McCabe, J. Solan, J. E. Seegmiller, R. Terkeltaub and M. Lotz (1998). "Chondrocyte-Derived Apoptotic Bodies and Calcification of Articular Cartilage." Proceedings of the National Academy of Sciences of the United States of America **95**(6): 3094-3099.

Hessle, L., K. A. Johnson, H. C. Anderson, S. Narisawa, A. Sali, J. W. Goding, R. Terkeltaub and J. L. Millan (2002). "Tissue-Nonspecific Alkaline Phosphatase and Plasma Cell Membrane Glycoprotein-1 Are Central Antagonistic Regulators of Bone Mineralization." Proceedings of the National Academy of Sciences of the United States of America **99**(14): 9445-9449.

Hinton, R. B. and K. E. Yutzey (2011). "Heart Valve Structure and Function in Development and Disease." Annual review of physiology **73**: 29-46.

Hinz, B., S. H. Phan, V. J. Thannickal, M. Prunotto, A. Desmoulière, J. Varga, O. De Wever, M. Mareel and G. Gabbiani (2012). "Recent Developments in Myofibroblast Biology: Paradigms for Connective Tissue Remodeling." The American journal of pathology **180**(4): 1340-1355.

Hishikawa, K., T. Nakaki and T. Fujii (1999). "Transforming Growth Factor-B1 Induces Apoptosis Via Connective Tissue Growth Factor in Human Aortic Smooth Muscle Cells." European Journal of Pharmacology **385**(2): 287-290.

Jenkins, G. (2008). "The Role of Proteases in Transforming Growth Factor-B Activation." The International Journal of Biochemistry and Cell Biology **40**(6): 1068-1078.

Jian, B., N. Narula, Q.-y. Li, E. R. Mohler and R. J. Levy (2003). "Progression of Aortic Valve Stenosis: Tgf-B1 Is Present in Calcified Aortic Valve Cusps and Promotes Aortic Valve Interstitial Cell Calcification Via Apoptosis." The Annals of thoracic surgery **75**(2): 457-465.

Johnson Rebecca, C., A. Leopold Jane and J. Loscalzo (2006). "Vascular Calcification." Circulation research **99**(10): 1044-1059.

Kapustin Alexander, N., D. Davies John, L. Reynolds Joanne, R. McNair, T. Jones Gregory, A. Sidibe, J. Schurgers Leon, N. Skepper Jeremy, D. Proudfoot, M. Mayr and M. Shanahan Catherine (2011). "Calcium Regulates Key Components of Vascular Smooth Muscle Cell-Derived Matrix Vesicles to Enhance Mineralization." Circulation research **109**(1): e1-e12.

Kay, J. G. and G. D. Fairn (2019). "Distribution, Dynamics and Functional Roles of Phosphatidylserine within the Cell." Cell Communication and Signaling **17**(1): 126.

Keelan Paul, C., F. Bielak Lawrence, K. Ashai, S. Jamjoum Lama, E. Denktas Ali, A. Rumberger John, I. I. P. F. Sheedy, A. Peyser Patricia and S. Schwartz Robert (2001). "Long-Term Prognostic Value of Coronary Calcification Detected by Electron-Beam Computed Tomography in Patients Undergoing Coronary Angiography." Circulation **104**(4): 412-417.

Kerr, J. F., A. H. Wyllie and A. R. Currie (1972). "Apoptosis: A Basic Biological Phenomenon with Wide-Ranging Implications in Tissue Kinetics." British journal of cancer **26**(4): 239-257.

Kim, H. Y., B. X. Huang and A. A. Spector (2014). "Phosphatidylserine in the Brain: Metabolism and Function." Progress in Lipid Research **56**: 1-18.

Kim, K. M. (1995). "Apoptosis and Calcification." Scanning Microscopy **9**(4): 1137-1175; discussion 1175-1138.

Kim, K. M., G. A. Herrera and H. D. Battarbee (1999). "Role of Glutaraldehyde in Calcification of Porcine Aortic Valve Fibroblasts." The American journal of pathology **154**(3): 843-852.

Kirsch, T., H. D. Nah, I. M. Shapiro and M. Pacifici (1997). "Regulated Production of Mineralization-Competent Matrix Vesicles in Hypertrophic Chondrocytes." The Journal of Cell Biology **137**(5): 1149-1160.

Kirsch, T., W. Wang and D. Pfander (2003). "Functional Differences between Growth Plate Apoptotic Bodies and Matrix Vesicles." J Bone Miner Res **18**(10): 1872-1881.

Kisseleva, T., M. Cong, Y. Paik, D. Scholten, C. Jiang, C. Benner, K. Iwaisako, T. Moore-Morris, B. Scott, H. Tsukamoto, S. M. Evans, W. Dillmann, C. K. Glass and D. A. Brenner (2012). "Myofibroblasts Revert to an Inactive Phenotype During Regression of Liver Fibrosis." Proceedings of the National Academy of Sciences of the United States of America **109**(24): 9448-9453.

Klotz, O. (1905). "Studies Upon Calcareous Degeneration : I. The Process of Pathological Calcification." The Journal of experimental medicine **7**(6): 633-674.

Kockx Mark, M., R. Y. De Meyer Guido, J. Muhring, W. Jacob, H. Bult and G. Herman Arnold (1998). "Apoptosis and Related Proteins in Different Stages of Human Atherosclerotic Plaques." Circulation **97**(23): 2307-2315.

Kojima, Y., J. P. Volkmer, K. McKenna, M. Civelek, A. J. Lusis, C. L. Miller, D. Direnzo, V. Nanda, J. Ye, A. J. Connolly, E. E. Schadt, T. Quertermous, P. Betancur, L. Maegdefessel, L. P. Matic, U. Hedin, I. L. Weissman and N. J. Leeper (2016). "Cd47-Blocking Antibodies Restore Phagocytosis and Prevent Atherosclerosis." Nature **536**(7614): 86-90.

Krishnamurthy, V. K., F. Guilak, D. A. Narmoneva and R. B. Hinton (2011). "Regional Structure-Function Relationships in Mouse Aortic Valve Tissue." Journal of biomechanics **44**(1): 77-83.

Kroemer, G. and J. C. Reed (2000). "Mitochondrial Control of Cell Death." Nature Medicine **6**(5): 513-519.

Le, C. and P. M. Bedocs. (2021 Jul 17, 2021 Jul 17). "Calcinosis Cutis." from <https://www.ncbi.nlm.nih.gov/books/NBK448127/>.

Lee, H. J. and W. S. Sung (2018). "Calcification of the Urinary Bladder and Ureter in Schistosomiasis." Kidney Research and Clinical Practice **37**(3): 304-305.

Lee, S.-E., J. M. Sung, D. Andreini, M. H. Al-Mallah, M. J. Budoff, F. Cademartiri, K. Chinnaiyan, J. H. Choi, E. J. Chun, E. Conte, I. Gottlieb, M. Hadamitzky, Y. J. Kim, B. K. Lee, J. A. Leipsic, E. Maffei, H. Marques, P. de Araújo Gonçalves, G. Pontone, S. Shin, P. H. Stone, H. Samady, R. Virmani, J. Narula, D. S. Berman, L. J. Shaw, J. J. Bax, F. Y. Lin, J. K. Min and H.-J.

- Chang (2021). "Association between Aortic Valve Calcification Progression and Coronary Atherosclerotic Plaque Volume Progression in the Paradigm Registry." Radiology **300**(1): 79-86.
- Lee, S. H. and J.-H. Choi (2018). "Involvement of Inflammatory Responses in the Early Development of Calcific Aortic Valve Disease: Lessons from Statin Therapy." Animal Cells and Systems **22**(6): 390-399.
- Leopold, J. A. (2012). "Cellular Mechanisms of Aortic Valve Calcification." Circulation. Cardiovascular interventions **5**(4): 605-614.
- Leopold, J. A. (2015). "Vascular Calcification: Mechanisms of Vascular Smooth Muscle Cell Calcification." Trends in Cardiovascular Medicine **25**(4): 267-274.
- Leopold, J. A. (2015). "Vascular Calcification: Mechanisms of Vascular Smooth Muscle Cell Calcification." Trends Cardiovasc Med **25**(4): 267-274.
- Lerman, D. A., S. Prasad and N. Alotti (2015). "Calcific Aortic Valve Disease: Molecular Mechanisms and Therapeutic Approaches." European Cardiology Review **10**(2): 108-112.
- Lindman, B. R., M.-A. Clavel, P. Mathieu, B. Iung, P. Lancellotti, C. M. Otto and P. Pibarot (2016). "Calcific Aortic Stenosis." Nature reviews. Disease primers **2**: 16006-16006.
- Lindroos, M., M. Kupari, J. Valvanne, T. Strandberg, J. Heikkilä and R. Tilvis (1994). "Factors Associated with Calcific Aortic Valve Degeneration in the Elderly." European Heart Journal **15**(7): 865-870.
- Liu, A. C., V. R. Joag and A. I. Gotlieb (2007). "The Emerging Role of Valve Interstitial Cell Phenotypes in Regulating Heart Valve Pathobiology." The American journal of pathology **171**(5): 1407-1418.
- Liu, F., J. D. Mih, B. S. Shea, A. T. Kho, A. S. Sharif, A. M. Tager and D. J. Tschumperlin (2010). "Feedback Amplification of Fibrosis through Matrix Stiffening and Cox-2 Suppression." The Journal of Cell Biology **190**(4): 693-706.
- London, G. M., S. J. Marchais, A. P. Guérin and F. Métivier (2005). "Arteriosclerosis, Vascular Calcifications and Cardiovascular Disease in Uremia." Current opinion in nephrology and hypertension **14**(6): 525-531.
- Loscalzo, J. (2006). "Vascular Calcification: Pathobiological Mechanisms and Clinical Implications." Circulation research : journal of the American Heart Association. **99**(10): 1044-1059.
- Mariño, G. and G. Kroemer (2013). "Mechanisms of Apoptotic Phosphatidylserine Exposure." Cell research **23**(11): 1247-1248.
- Masjedi, S., Y. Lei, J. Patel and Z. Ferdous (2017). "Sex-Related Differences in Matrix Remodeling and Early Osteogenic Markers in Aortic Valvular Interstitial Cells." Heart and Vessels **32**(2): 217-228.
- Mattey, D. L., P. T. Dawes, N. B. Nixon and H. Slater (1997). "Transforming Growth Factor Beta 1 and Interleukin 4 Induced Alpha Smooth Muscle Actin Expression and Myofibroblast-Like

Differentiation in Human Synovial Fibroblasts in Vitro: Modulation by Basic Fibroblast Growth Factor." Annals of the Rheumatic Diseases **56**(7): 426-431.

Mattson, M. P. and S. L. Chan (2003). "Calcium Orchestrates Apoptosis." Nature Cell Biology **5**(12): 1041-1043.

Merryman, W. D. and F. J. Schoen (2013). "Mechanisms of Calcification in Aortic Valve Disease: Role of Mechanokinetics and Mechanodynamics." Current Cardiology Reports **15**(5): 355.

Mezzabotta, F., R. Cristofaro, M. Ceol, D. Del Prete, G. Priante, A. Familiari, A. Fabris, A. D'Angelo, G. Gambaro and F. Anglani (2015). "Spontaneous Calcification Process in Primary Renal Cells from a Medullary Sponge Kidney Patient Harboring a Gdnf Mutation." Journal of cellular and molecular medicine **19**(4): 889-902.

Miller, J. D., R. M. Weiss and D. D. Heistad (2011). "Calcific Aortic Valve Stenosis: Methods, Models, and Mechanisms." Circulation research **108**(11): 1392-1412.

Miller, J. D., R. M. Weiss, K. M. Serrano, L. E. Castaneda, R. M. Brooks, K. Zimmerman and D. D. Heistad (2010). "Evidence for Active Regulation of Pro-Osteogenic Signaling in Advanced Aortic Valve Disease." Arteriosclerosis, thrombosis, and vascular biology **30**(12): 2482-2486.

Miyazono, K., K. Kusanagi and H. Inoue (2001). "Divergence and Convergence of Tgf-B/Bmp Signaling." Journal of Cellular Physiology **187**(3): 265-276.

Mizobuchi, M., D. Towler and E. Slatopolsky (2009). "Vascular Calcification: The Killer of Patients with Chronic Kidney Disease." Journal of the American Society of Nephrology **20**(7): 1453.

Mohler, E. R., R. Nichols, W. P. Harvey, M. J. Sheridan, B. F. Waller and B. F. Waller (1991). "Development and Progression of Aortic Valve Stenosis: Atherosclerosis Risk Factors—A Causal Relationship? A Clinical Morphologic Study." Clinical Cardiology **14**(12): 995-999.

Mundy, G. R. and T. J. Martin (1993). Physiology and Pharmacology of Bone, Springer.

Nagase, Y., M. Iwasawa, T. Akiyama, Y. Kadono, M. Nakamura, Y. Oshima, T. Yasui, T. Matsumoto, J. Hirose, H. Nakamura, T. Miyamoto, P. Bouillet, K. Nakamura and S. Tanaka (2009). "Anti-Apoptotic Molecule Bcl-2 Regulates the Differentiation, Activation, and Survival of Both Osteoblasts and Osteoclasts." J Biol Chem **284**(52): 36659-36669.

Nakahara, T., M. R. Dweck, N. Narula, D. Pisapia, J. Narula and H. W. Strauss (2017). "Coronary Artery Calcification: From Mechanism to Molecular Imaging." JACC Cardiovascular Imaging **10**(5): 582-593.

Nasir, K., R. Katz, M. Al-Mallah, J. Takasu, D. M. Shavelle, J. J. Carr, R. Kronmal, R. S. Blumenthal, K. O'Brien and M. J. Budoff (2010). "Relationship of Aortic Valve Calcification with Coronary Artery Calcium Severity: The Multi-Ethnic Study of Atherosclerosis (Mesa)." Journal of Cardiovascular Computed Tomography **4**(1): 41-46.

Nicotera, P. and S. Orrenius (1998). "The Role of Calcium in Apoptosis." Cell Calcium **23**(2-3): 173-180.

- Oliveira, J. R. M. and M. F. Oliveira (2016). "Primary Brain Calcification in Patients Undergoing Treatment with the Biphosphonate Alendronate." Scientific Reports **6**(1): 22961.
- Otsuka, F., K. Sakakura, K. Yahagi, M. Joner and R. Virmani (2014). "Has Our Understanding of Calcification in Human Coronary Atherosclerosis Progressed?" Arteriosclerosis, thrombosis, and vascular biology **34**(4): 724-736.
- Paone, S., A. A. Baxter, M. D. Hulett and I. K. H. Poon (2019). "Endothelial Cell Apoptosis and the Role of Endothelial Cell-Derived Extracellular Vesicles in the Progression of Atherosclerosis." Cellular and Molecular Life Sciences **76**(6): 1093-1106.
- Paranya, G., S. Vineberg, E. Dvorin, S. Kaushal, S. J. Roth, E. Rabkin, F. J. Schoen and J. Bischoff (2001). "Aortic Valve Endothelial Cells Undergo Transforming Growth Factor-Beta-Mediated and Non-Transforming Growth Factor-Beta-Mediated Transdifferentiation in Vitro." The American journal of pathology **159**(4): 1335-1343.
- Pho, M., W. Lee, D. R. Watt, C. Laschinger, C. A. Simmons and C. A. McCulloch (2008). "Cofilin Is a Marker of Myofibroblast Differentiation in Cells from Porcine Aortic Cardiac Valves." American Journal of Physiology-Heart and Circulatory Physiology **294**(4): H1767-H1778.
- Pollman Matthew, J., L. Naumovski and H. Gibbons Gary (1999). "Vascular Cell Apoptosis." Circulation **99**(15): 2019-2026.
- Poon, I. K., C. D. Lucas, A. G. Rossi and K. S. Ravichandran (2014). "Apoptotic Cell Clearance: Basic Biology and Therapeutic Potential." Nat Rev Immunol **14**(3): 166-180.
- Porras, A. M., C. M. McCoy and K. S. Masters (2017). "Calcific Aortic Valve Disease: A Battle of the Sexes." Circ Res **120**(4): 604-606.
- Priante, G., M. Ceol, L. Giancesello, C. Furlan, D. Del Prete and F. Anglani (2019). "Human Proximal Tubular Cells Can Form Calcium Phosphate Deposits in Osteogenic Culture: Role of Cell Death and Osteoblast-Like Transdifferentiation." Cell Death Discovery **5**(1): 57.
- Proudfoot, D., J. N. Skepper, L. Hegyi, M. R. Bennett, C. M. Shanahan and P. L. Weissberg (2000). "Apoptosis Regulates Human Vascular Calcification in Vitro." Circulation research **87**(11): 1055-1062.
- Proudfoot, D., J. N. Skepper, L. Hegyi, A. Farzaneh-Far, C. M. Shanahan and P. L. Weissberg (2001). "The Role of Apoptosis in the Initiation of Vascular Calcification." Zeitschrift für Kardiologie **90**(3): 43-46.
- Quinlan, A. M. T. and K. L. Billiar (2012). "Investigating the Role of Substrate Stiffness in the Persistence of Valvular Interstitial Cell Activation." Journal of biomedical materials research. Part A **100**(9): 2474-2482.
- Rajamannan, N. M., F. J. Evans, E. Aikawa, K. J. Grande-Allen, L. L. Demer, D. D. Heistad, C. A. Simmons, K. S. Masters, P. Mathieu, K. D. O'Brien, F. J. Schoen, D. A. Towler, A. P. Yoganathan and C. M. Otto (2011). "Calcific Aortic Valve Disease: Not Simply a Degenerative Process: A Review and Agenda for Research from the National Heart and Lung and Blood

- Institute Aortic Stenosis Working Group. Executive Summary: Calcific Aortic Valve Disease-2011 Update." Circulation **124**(16): 1783-1791.
- Rockley, G. J. (1965). "Acase of Renal Cortical Necrosis with Dystrophic Calcification Demonstrated at the Postgraduate Medical School of London." British medical journal **2**(5462): 633-636.
- Schrijvers Dorien, M., R. Y. De Meyer Guido, M. Kockx Mark, G. Herman Arnold and W. Martinet (2005). "Phagocytosis of Apoptotic Cells by Macrophages Is Impaired in Atherosclerosis." Arteriosclerosis, thrombosis, and vascular biology **25**(6): 1256-1261.
- Sewell-Loftin, M.-K., C. B. Brown, H. S. Baldwin and W. D. Merryman (2012). "A Novel Technique for Quantifying Mouse Heart Valve Leaflet Stiffness with Atomic Force Microscopy." The Journal of heart valve disease **21**(4): 513-520.
- Shekar, C. and M. Budoff (2018). "Calcification of the Heart: Mechanisms and Therapeutic Avenues." Expert Review of Cardiovascular Therapy **16**(7): 527-536.
- Sinn, C. G., M. Antonietti and R. Dimova (2006). "Binding of Calcium to Phosphatidylcholine-Phosphatidylserine Membranes." Colloids and Surfaces A: Physicochemical and Engineering Aspects **282-283**: 410-419.
- Stella, J. A. and M. S. Sacks (2007). "On the Biaxial Mechanical Properties of the Layers of the Aortic Valve Leaflet." Journal of biomechanical engineering **129**(5): 757-766.
- Summerhill, V. I., D. Moschetta, A. N. Orekhov, P. Poggio and V. A. Myasoedova (2020). "Sex-Specific Features of Calcific Aortic Valve Disease." International journal of molecular sciences **21**(16).
- Thompson, B. and D. A. Towler (2012). "Arterial Calcification and Bone Physiology: Role of the Bone-Vascular Axis." Nature reviews. Endocrinology **8**(9): 529-543.
- Thubrikar M Fau - Piegrass, W. C., T. W. Piegrass Wc Fau - Shaner, S. P. Shaner Tw Fau - Nolan and S. P. Nolan (1979). "Design and Dynamic Variations of Aortic Valve Leaflets in Vivo." Surgical forum **30**: 241-243.
- Tintut, Y., J. J. Hsu and L. L. Demer (2018). "Lipoproteins in Cardiovascular Calcification: Potential Targets and Challenges." Frontiers in Cardiovascular Medicine **5**: 172.
- Turiv, T., J. Krieger, G. Babakhanova, H. Yu, V. Shiyanovskii Sergij, Q.-H. Wei, M.-H. Kim and D. Lavrentovich Oleg "Topology Control of Human Fibroblast Cells Monolayer by Liquid Crystal Elastomer." Science Advances **6**(20): eaaz6485.
- Uchida, K., K. Emoto, D. L. Daleke, K. Inoue and M. Umeda (1998). "Induction of Apoptosis by Phosphatidylserine." The Journal of Biochemistry **123**(6): 1073-1078.
- Vengrenyuk, Y., S. Carlier, S. Xanthos, L. Cardoso, P. Ganatos, R. Virmani, S. Einav, L. Gilchrist and S. Weinbaum (2006). "A Hypothesis for Vulnerable Plaque Rupture Due to Stress-Induced Debonding around Cellular Microcalcifications in Thin Fibrous Caps." Proceedings of the National Academy of Sciences of the United States of America **103**(40): 14678-14683.

- Walker Gennyne, A., S. Masters Kristyn, N. Shah Darshita, S. Anseth Kristi and A. Leinwand Leslie (2004). "Valvular Myofibroblast Activation by Transforming Growth Factor-B." Circulation research **95**(3): 253-260.
- Wallin, R., L. J. Schurgers and R. F. Loeser (2010). "Biosynthesis of the Vitamin K-Dependent Matrix Gla Protein (Mgp) in Chondrocytes: A Fetuin&#X2013;Mgp Protein Complex Is Assembled in Vesicles Shed from Normal but Not from Osteoarthritic Chondrocytes." Osteoarthritis and Cartilage **18**(8): 1096-1103.
- Wang, H.-B., M. Dembo and Y.-L. Wang (2000). "Substrate Flexibility Regulates Growth and Apoptosis of Normal but Not Transformed Cells." American Journal of Physiology-Cell Physiology **279**(5): C1345-C1350.
- Wang, H., S. M. Haeger, A. M. Kloxin, L. A. Leinwand and K. S. Anseth (2012). "Redirecting Valvular Myofibroblasts into Dormant Fibroblasts through Light-Mediated Reduction in Substrate Modulus." PLoS One **7**(7): e39969-e39969.
- Wang, H., L. A. Leinwand and K. S. Anseth (2014). "Cardiac Valve Cells and Their Microenvironment--Insights from in Vitro Studies." Nature reviews. Cardiology **11**(12): 715-727.
- Wang, H., B. Sridhar, L. A. Leinwand and K. S. Anseth (2013). "Characterization of Cell Subpopulations Expressing Progenitor Cell Markers in Porcine Cardiac Valves." PLoS One **8**(7): e69667-e69667.
- Wayhs, R., A. Zelinger and P. Raggi (2002). "High Coronary Artery Calcium Scores Pose an Extremely Elevated Risk for Hard Events." Journal of the American College of Cardiology **39**(2): 225-230.
- Weiler, M., C. H. Yap, K. Balachandran, M. Padala and A. P. Yoganathan (2011). "Regional Analysis of Dynamic Deformation Characteristics of Native Aortic Valve Leaflets." Journal of biomechanics **44**(8): 1459-1465.
- Wickert, L. E., S. Pomeranke, I. Mitchell, K. S. Masters and P. K. Kreeger (2016). "Hierarchy of Cellular Decisions in Collective Behavior: Implications for Wound Healing." Scientific Reports **6**(1): 20139.
- Wuthier, R. E. and G. F. Lipscomb (2011). "Matrix Vesicles: Structure, Composition, Formation and Function in Calcification." Frontiers in Biosciences-Landmark(1093-4715): 812-902.
- Wyllie, A. H. (1980). "Glucocorticoid-Induced Thymocyte Apoptosis Is Associated with Endogenous Endonuclease Activation." Nature **284**(5756): 555-556.
- Wyllie, A. H., R. G. Morris, A. L. Smith and D. Dunlop (1984). "Chromatin Cleavage in Apoptosis: Association with Condensed Chromatin Morphology and Dependence on Macromolecular Synthesis." The Journal of Pathology **142**(1): 67-77.
- Xiao, Z., C. E. Camalier, K. Nagashima, K. C. Chan, D. A. Lucas, M. J. d. I. Cruz, M. Gignac, S. Lockett, H. J. Issaq, T. D. Veenstra, T. P. Conrads and G. R. Beck Jr (2007). "Analysis of the Extracellular Matrix Vesicle Proteome in Mineralizing Osteoblasts." Journal of Cellular Physiology **210**(2): 325-335.

Yip, C. Y. Y., J.-H. Chen, R. Zhao and C. A. Simmons (2009). "Calcification by Valve Interstitial Cells Is Regulated by the Stiffness of the Extracellular Matrix." Arteriosclerosis, thrombosis, and vascular biology **29**(6): 936-942.

Yurdagul, A., A. C. Doran, B. Cai, G. Fredman and I. A. Tabas (2018). "Mechanisms and Consequences of Defective Efferocytosis in Atherosclerosis." Frontiers in Cardiovascular Medicine **4**(86).

Zapanta LeGeros, R. (1981). "Apatites in Biological Systems." Progress in Crystal Growth and Characterization **4**(1): 1-45.

Zazzeroni, L., G. Faggioli and G. Pasquinelli (2018). "Mechanisms of Arterial Calcification: The Role of Matrix Vesicles." European Journal of Vascular and Endovascular Surgery **55**(3): 425-432.

Zhang, Y.-H., C.-Q. Zhao, L.-S. Jiang and L.-Y. Dai (2011). "Substrate Stiffness Regulates Apoptosis and the Mrna Expression of Extracellular Matrix Regulatory Genes in the Rat Annular Cells." Matrix Biology **30**(2): 135-144.

Zhao, R., K. L. Sider and C. A. Simmons (2011). "Measurement of Layer-Specific Mechanical Properties in Multilayered Biomaterials by Micropipette Aspiration." Acta Biomaterialia **7**(3): 1220-1227.

Zheng, K. H., S. Tsimikas, T. Pawade, J. Kroon, W. S. A. Jenkins, M. K. Doris, A. C. White, N. Timmers, J. Hjortnaes, M. A. Rogers, E. Aikawa, B. J. Arsenaault, J. L. Witztum, D. E. Newby, M. L. Koschinsky, Z. A. Fayad, E. S. G. Stroes, S. M. Boekholdt and M. R. Dweck (2019). "Lipoprotein(a) and Oxidized Phospholipids Promote Valve Calcification in Patients with Aortic Stenosis." Journal of the American College of Cardiology **73**(17): 2150-2162.

## Chapter III: Multicellular Aligned Bands Disrupt Global Collective Cell Behavior<sup>1</sup>

Mahvash Jebeli<sup>1</sup>, Samantha K. Lopez<sup>1</sup>, Zachary E. Goldblatt<sup>1</sup>, Dannel McCollum<sup>2</sup>, Sebastian Mana-Capelli<sup>2</sup>, Qi Wen<sup>3</sup>, Kristen Billiar<sup>1</sup>

<sup>1</sup> Biomedical Engineering Department, Worcester Polytechnic Institute, Worcester MA, USA

<sup>2</sup> University of Massachusetts Medical School, Worcester MA, USA

<sup>3</sup> Physics Department, Worcester Polytechnic Institute, Worcester MA, USA

*Supported by grants:*

American Heart Association (20AIREA35120448); National Science Foundation (CMMI 1761432)

### **Keywords**

Valvular interstitial cell, collective cell behavior, microcontact printing, traction force microscopy, mechanical stretch

---

<sup>1</sup> A version of this work is published in the special issue “The Mechanics of Cells and Fibers” of Acta Biomaterialia (Jebeli et al. 2022).

### 3.1 Abstract

Mechanical stress patterns emerging from collective cell behavior have been shown to play critical roles in morphogenesis, tissue repair, and cancer metastasis. In our previous work, we constrained valvular interstitial cell (VIC) monolayers on circular protein islands to study emergent behavior in a controlled manner and demonstrated that the general patterns of cell alignment, size, and apoptosis correlate with predicted mechanical stress fields if radially increasing stiffness or contractility are used in the computational models. However, these radially symmetric models did not predict the existence of local regions of dense aligned cells observed in seemingly random locations of individual aggregates. The goal of this study is to determine how the heterogeneities in cell behavior emerge over time and diverge from the predicted collective cell behavior. Cell-cell interactions in circular multicellular aggregates of VICs were studied with time-lapse imaging ranging from hours to days, and migration, proliferation, and traction stresses were measured. Our results indicate that elongated cells create strong local alignment within preconfluent cell populations on the microcontact printed protein islands. These cells influence the alignment of additional cells to create dense, locally aligned bands of cells which disrupt the predicted global behavior. Cells are highly elongated at the endpoints of the bands yet have decreased spread area in the middle and reduced mobility. Although traction stresses at the endpoints of bands are enhanced, even to the point of detaching aggregates from the culture surface, the cells in dense bands exhibit reduced proliferation, less nuclear YAP, and increased apoptotic rates indicating a low stress environment. These findings suggest that strong local cell-cell interactions between primary fibroblastic cells can disrupt the global collective cellular behavior leading to substantial heterogeneity of cell behaviors in constrained monolayers. This local emergent behavior within aggregated fibroblasts may play an important role in development and disease of connective tissues.

## 3.2 Introduction

Morphogenesis, tissue repair, and cancer metastasis are driven by collective cell behaviors which differ substantially from independent cell behavior. Studies that use voids, scratch assays (Camley et al. 2017, Ladoux et al. 2017, Nanavati et al. 2020, Trepate et al. 2011, Vishwakarma et al. 2020), and micropatterned protein “islands” (He et al. 2015, Streichan et al. 2014) in specific geometries (Li et al. 2009, Moussus et al. 2014, Nelson et al. 2005, Ng et al. 2014, Trepate et al. 2009) demonstrate that emergent mechanical stress patterns contribute in large part to the collective cell behavior. In particular, maximum traction stresses at the surface correlate positively with proliferation at pattern edges (Uroz et al. 2018), while the anisotropy of computed cell layer stresses correlate with cell alignment and elongation (Wyatt et al. 2015). The majority of studies on collective cell behavior utilize epithelial cells and cell lines which exhibit relatively uniform cell area when in a monolayer as well as strong contact inhibition. Emergent patterns in the behavior of these cell types are explained relatively well with computational mechanical models that assume uniform cell mechanical properties such as modulus and contractility (Li et al. 2009, Moussus et al. 2014, Nelson et al. 2005, Paek et al. 2021). However, primary mesenchymal and spindle like cells, which are more contractile and have strong cell-cell interactions, exhibit less uniform behavior when cultured as monolayers (Duclos et al. 2017, Ladoux et al. 2017, Xie et al. 2021).

The complex collective cell behavior of primary valvular interstitial cells (VICs) is implicated in calcific aortic valve disease (Bogdanova et al. 2019, Yip Cindy Ying et al. 2009). VICs cultured as monolayers, sheets of cells without any confinement, detach under high tension and form multicellular aggregates which become hyperconfluent. The cells in these high-density regions undergo apoptosis and calcification (Bogdanova et al. 2019, Jian et al. 2003, Yip Cindy Ying et al. 2009). Previously, we used uniform circular protein islands to form consistent multicellular aggregates, with confined sizes, to study the effects of collective cell behavior on calcification of these cells (Cirka et al. 2017). We found that the general patterns of cell alignment, size, and apoptosis correlate with predicted mechanical stress fields if nonuniform cell properties are used in computational

models (Goldblatt et al. 2020). However, these radially symmetric models did not predict the substantial heterogeneity in cell behavior observed in individual circular aggregates. In particular, we observed asymmetric apoptotic patterns associated with local hyperconfluent regions. We also observed groups of aligned elongated cells spanning the 200  $\mu\text{m}$ -diameter collagen islands. Similar collective alignment of spindle-shaped cells forming well-aligned nematic domains have been reported in boundary-free monolayers and on circular patterned protein islands by Silberzan and colleagues (Duclos et al. 2017). In particular, they show the alignment pattern of NIH 3T3 cells and C2C12 myoblasts (both spindle-shaped cells similar to VICs) stabilizes when the cells reach confluence, and on circular protein islands the aligned regions span between two facing “ $+1/2$  defects” located at  $2/3$  of the radius from the center (Duclos et al. 2017). In contrast, the groups of aligned VICs in our system terminate closer to the edge and can be observed in many different locations. Further, the VICs do not stabilize in density or size over time in culture, rather they proceed to local hyperconfluency and subsequently detach from the substrate at later timepoints (multiple days) indicating that high traction forces emerge from the collective cell behavior. The observed hyperconfluency of VICs in our model may have importance in the pathology of diseases involving calcification where densification and elevated cell-cell forces are postulated to play critical roles.

The goal of this work is to uncover the mechanisms underlying the observed heterogeneous collective cell behaviors within micropatterned VIC aggregates. Circular stamps are employed to provide a uniform radially symmetric global constraint, and relatively large 400  $\mu\text{m}$ -diameter collagen islands were chosen to minimize the spanning of single cells across the patterns. We use long-term time-lapse imaging to follow the evolution of individual aggregates over four days as substantial heterogeneity between aggregates has been observed even in a single dish of uniformly printed cell islands. Short-term time-lapse is used to observe cell-cell interactions in real time and to quantify cell velocity and traction stresses in distinct sub-regions over the span of hours. To determine if cells act independently or collectively in response to an imposed global stimulus, we cyclically stretch aggregates and quantify changes in orientation and elongation. As Yes-associated protein (YAP) is implicated in mechanosensing in many

cell types (Aragona et al. 2013, Calvo et al. 2013, Codelia et al. 2014, Das et al. 2016), we investigate the relationship between YAP activation and apoptosis stemming from the collective cell behavior. The knowledge obtained from this study provides further insight into how collective cell behaviors drive biological phenomena that are implicated in many developmental and pathological conditions.

### 3.3 Methods

#### 3.3.1 Substrate preparation

Microcontact printed 400  $\mu\text{m}$  diameter circular protein islands were formed by coating plasma-treated and 70% EtOH pre-rinsed polydimethylsiloxane (PDMS) stamps with collagen and placing them onto untreated 22x22 mm square coverslips for 1 hr; a 50 g weight was lightly applied to create uniform pressure on the stamp (Fig. S.3-1). The collagen solution consisted of 25  $\mu\text{L}$  of 4 mg/mL collagen, 75  $\mu\text{L}$  of 0.1 M acetic acid, 900  $\mu\text{L}$  sodium acetate buffer, and sodium periodate. Prior to transfer, excess collagen was removed from the stamp using a combination of air drying and nitrogen stream. In a subset of experiments, the uniformity of the circular collagen prints was verified with the addition of 1  $\mu\text{L}$  Alexa Fluor-488 carboxylic acid, succinimidyl ester (A20000, Invitrogen) to the collagen solution for 1 hr at room temperature. To determine the effects of island size, we used 200  $\mu\text{m}$  and 600  $\mu\text{m}$  circular patterns in a subset of experiments.

Circular collagen patterns were printed onto polyacrylamide (PA) gels by indirect microcontact printing (Cirka et al. 2017). Briefly, for each substrate, 50  $\mu\text{L}$  of PA solution (acrylamide:bisacrylamide (Biorad) of percentages of 7.5/0.24 for  $\sim 20$  kPa ) were pipetted onto an activated coverslip. The coverslips were activated by soaking in 1.5% (aminopropyl) trimethoxysilane solution for 30 min then in 0.5% glutaraldehyde solution overnight at 4  $^{\circ}\text{C}$  and dried completely before use. After placement of PA solution on activated coverslips an inactivated collagen microcontact printed coverslip was gently placed on top. Following 12 min of polymerization of the PA-gel, the coverslips were separated by a razor blade. A modulus of  $\sim 20$  kPa was chosen because it

is in the range of reported stiffness values for healthy and diseased valves (Kloxin et al. 2010, Wang et al. 2012).

### 3.3.2 Traction force microscopy

To quantify the shear stresses that the cells apply to the surface of the substrate via traction force microscopy (TFM), 0.2  $\mu\text{m}$  red fluorescent micro-beads were coated on plasma treated glass coverslips, allowed to dry, and then applied to the top surface of the PA gel solution during polymerization. Collagen patterns were then stamped onto the PA gel using direct microcontact printing methods as previously described (Cirka et al. 2016). At various timepoints, phase and fluorescent images were acquired to determine the aggregate borders and bead locations, respectively. Cells were then trypsinized, and a reference image of the bead locations was acquired. Displacements of the beads were calculated with a custom MATLAB code and input into a finite element model (modulus: 19 kPa; Poisson ratio: 0.4; material property: linear elastic) to calculate the stresses on the surface of the gel (ANSYS Inc.) (Cirka et al. 2016). To calculate the total traction force of an aligned band, the stresses exceeding a certain threshold in the “hotspots” at the ends of the band were extracted using a custom written MATLAB code. Then the sum of the stresses multiplied times the areas over which they act were calculated and the total force magnitudes for the two opposing hotspots in each aggregate were averaged, please see Appendix 1.

### 3.3.3 Dynamic stretching

To determine the effect of cyclic stretching on collective behavior in aggregates, PA gels were affixed in each well of a 16-well compliant Elastasil culture plate (CellScale), patterned using indirect microcontact printing, and seeded with cells. After 24 hr post-seeding, the substrates were stretched 10% uniaxially at 1 Hz for 8 hr using a MechanoCulture FX (CellScale). PA gels were attached to the compliant substrate by treating wells with 1.5% (aminopropyl) trimethoxysilane solution for 5 min, drying, and then treating with 0.5% glutaraldehyde solution for 5 min. After removing the liquid, the wells were dried with nitrogen stream, 4  $\mu\text{L}$  of PA were placed at the bottom of the well

and covered with a collagen patterned circular 5 mm coverslip. The wells were then transferred to a vacuum chamber filled with nitrogen for 45 min to facilitate polymerization, then diH<sub>2</sub>O was added to the wells for 30 min to promote detachment of the coverslips from the PA gel surface.

### 3.3.4 Cell culture and media

Aortic VICs were isolated from porcine hearts obtained from a local abattoir (Blood Farm, Groton, MA) using previous protocols (Gould et al. 2010). Porcine VICs are primary fibroblastic cells and were chosen as VIC aggregation is implicated in the pathology of CAVD, in addition to their similarity to human VICs. VICs at passages 3-6 were seeded at 12,500 cells/cm<sup>2</sup> (Cirka et al. 2017). In one set of experiments, neonatal human dermal fibroblasts (courtesy G. Pins, Worcester Polytechnic Institute) were used with the same passage range, cell density, and culture conditions as VICs. The cells were cultured in DMEM supplemented with 10% FBS and 1% Antibiotic/Antifungal at 37 °C with 10% CO<sub>2</sub>. Media were exchanged every 48 hr. In cell-cell interaction inhibition experiments, calcium was depleted from DMEM with 1 mM ethylenediaminetetraacetic acid (EDTA), a concentration reported to not affect cell viability (Voccoli et al. 2014).

### 3.3.5 Stable YAP-VIC cell line

To determine if apoptosis is YAP-dependent, YAP-6A, a constitutively active version of YAP that cannot be inhibited by LATS, was obtained from Addgene (#42562), packaged into lentivirus particles, and transduced into VIC cells. Lentiviral particles were generated by transfecting 293T cells with pLX304-YAP-S6A-V5, pSPAX.2, and PMD2.G. After 48 hr, the supernatant was collected and filtered through a 45 µm sterile filter. Viral supernatant was then mixed 1:1 with culture media, added with 1 µg/mL of polybrene (Millipore), and incubated with VICs overnight. The next day, cells were fed with culture media, and after 24 hr, cells were selected with 1 µg/mL of Puromycin until all control (uninfected) cells died after approximately 48 hr. Expression of the YAP S6A-V5 construct was visualized in pooled puromycin-resistant cells through immunofluorescence using anti-V5 (Invitrogen).

### 3.3.6 Imaging and immunohistochemistry

Individual aggregates were tracked for four days utilizing a motorized stage and automated position tracking software (Zeiss Axiovision 4.8.2 SP1) on an inverted microscope (Axiovert 200M, Zeiss) and imaged with phase contrast every 24 hr at 10x (AxioCam MRm camera; 1.4 MP, 1388 X 1040 pixels). To track individual aggregates at specific locations, coordinates of each aggregate were saved with respect to a reference point at the top left corner of the coverslip on each day. Samples were incubated for 30 min in standard media with CellEvent Caspase 3/7 (1:400, C10423, Invitrogen) prior to imaging to observe apoptosis. To quantify cell death in longer time lapses of 24 hrs, propidium iodide (1:100, P1304MP, Invitrogen) was added to the samples 30 min before imaging.

YAP staining was completed following published methods (Dutta et al. 2018, Ma et al. 2017). VIC aggregates were fixed in 4% paraformaldehyde for 45 min at room temperature, rinsed twice in PBS, and permeabilized using 0.1% TritonX-100 in PBS for 1 hr. Samples were then blocked with 5% bovine serum albumin (BSA) overnight at 4°C to minimize nonspecific protein binding. Samples were stained with Anti-YAP in 5% BSA (1:250, mouse, sc-398182, Santa Cruz) primary antibody and incubated for 1 hr at room temperature. Samples were rinsed in PBST (0.5 wt% Tween-20 in PBS) two times for 10 min following incubation with primary antibody. Samples were then incubated in secondary antibody with goat anti-mouse AlexaFluor 647 (1:200, A21241, Invitrogen) while counterstained with Alexa Fluor 488 Phalloidin (1:100, A12379, Life Technologies) to visualize F-actin and Hoechst 33342 (1:200, H3570, Life Technologies) to visualize nuclei in 1% BSA for 1 hr at room temperature. Samples were rinsed three times for 10 min with PBST, mounted, and imaged using a BioTek Cytation Gen5 inverted microscope. To quantify the YAP deactivation, the colocalization of YAP and Hoechst signals was quantified as nuclear, nuclear/cytoplasmic, or cytoplasmic in the hyperconfluent bands identified in phase images. Two different fluorescent channels were compared by merging the channels in ImageJ. If the YAP signal was present around the cell nuclei, it was categorized as nuclear/cytosolic; and if there were no signal of YAP around the nuclei, it was categorized as nuclear. An example of nuclear/cytosolic YAP is

in Fig. 1-D of (Aragona et al. 2013). In acquired images, no cells with completely cytosolic YAP were observed. More details on the YAP colocalization with nuclei are provided in Appendix 2.

To visualize migration of individual cells within the aggregates, 20% of cells were treated with CellTracker™ Green CMFDA Dye (5:1000, C2925, Invitrogen) and imaged via fluorescence microscopy (Axiovert 200M, Zeiss). Only staining a portion of the cells is required so that individual cells can be tracked when cells become dense. To trace the cells in time lapses of velocity, the center of a rectangle containing the cell's area in each frame was marked. In the final frame, these centers are connected; the red dot corresponds to the location of that center of the area in the last frame. To calculate the mean squared distances (MSD), we manually tracked the coordinates each cell's centroid on each frame using ImageJ and calculated the square of the distance moved. To visualize the coordinated movement of cells in hyperconfluent aggregates, we performed particle image velocimetry (PIV) analysis using the PIV tool in ImageJ.

To quantify proliferation, Click-iT™ Plus EdU Cell Proliferation Kit for Imaging, Alexa Fluor™ 488 dye was used per manufacturer's instructions (C10637, Invitrogen). We performed both a 24 hr-long exposure to visualize proliferation over an entire population doubling and a 1-hr pulse experiment for short-term visualization with minimal migration away from the site of proliferation.

To visualize if the collagen island remained after aggregates detached, a subset of samples was stained with Ponceau S and imaged with transmitted light and color camera (Cytation 5, BioTek), as well as another subset that were fixed and stained with picosirius red/fast green (120M1516V, Sigma-Aldrich) and imaged with transmitted light and color camera (Cytation 5, BioTek).

### 3.3.7 Quantification of confluency level, cell density, and cell alignment

To quantify the observed confluency levels in each aggregate, the area of the cells in phase images was measured using ImageJ and divided by the total area of the collagen

island in the same image. To quantify the average density of cells in different confluency levels, the number of the cells in each aggregate was divided by its area.

To qualify the orientation of aligned cell regions from phase images, the aggregates were analyzed with the OrientationJ plugin in ImageJ to produce color orientation maps. To calculate the percentage of aligned area, we divided the size of the local aligned area (i.e., area with the same color) by the total area of the aggregate.

To quantify the alignment of cells in live cultures before and after stretch, F-actin was stained using CellMask™ Actin Tracking at 1:1000 dilution (A57249, Invitrogen). As this staining of live cells is not as efficient as phalloidin staining of fixed and permeabilized cells, only a portion of the cells are stained brightly. Further, imaging through the 400  $\mu\text{m}$ -thick silicone well and the  $\sim 200$   $\mu\text{m}$ -thick PA gel degrades the quality of the images. Together, these limitations make quantification of the stress fiber angular distribution problematic; however, as individual cells could be identified clearly, we were able to track these individual cells before and after stretch and quantify their direction and elongation by tracing each stained cell and calculating the angle and elongation of the stained fibers with the Directionality tool in ImageJ.

### 3.3.8 Statistical Analysis

Data are presented as mean and standard deviation. One-way ANOVA was performed to evaluate the significance of cell density values between the five different confluency levels. Two-way ANOVAs were used to assess the significance of cell location (inside/outside of bands), and inter-aggregate variability on YAP nuclear localization and separately on proliferation. Holm-Sidak (HSD) post-hoc test was used with all pairwise comparison. Student's t-test was used to evaluate the significance in differences of cell speed between confluent and hyperconfluent regions. Paired t-tests were used to evaluate of the significance of changes in the cell orientation and aspect ratio before and after stretch and to compare apoptosis levels of YAP activated and control cells. Analyses were completed in SPSS, and a p-value of less than 0.05 was considered statistically significant.

## 3.4 Results

### 3.4.1 Aggregates have variable rates of progression towards confluency

Across the span of 4 days, 53 aggregates were tracked following initial seeding. On the 400  $\mu\text{m}$ -diameter collagen islands containing 50-300 cells, cells migrate, proliferate, and fill the islands at varying rates. As the density of cells was variable within each aggregate, we manually categorized aggregates in terms of confluency level and measured the percentage of the island area that is covered with cells (Fig. 3-1A). In the “sparse” stage, relatively large regions of islands are visible between cells and coverage is  $80.0\pm 9.0\%$ . Due to these visible relatively large areas of underneath substrate, the cells are not in contact. In the “pre-confluent” stage, cells fill most of the circular area ( $89.6\pm 5.1\%$  coverage) and only small areas of the surface are visible. At the “confluent” stage, cells cover almost the entire area ( $95.6\pm 1.7\%$  coverage), slight areas of the underneath substrate is visible, and cell density is approximately uniform. The “hyperconfluent” stage is characterized by regions in which cells are highly dense and rounded, although there are still small gaps in some aggregates ( $97.3\pm 0.8\%$  coverage). There were aggregates with a hyperconfluent region while another region in the same aggregate might be at pre-confluency; in the cases of any hyperconfluency existence in the aggregate, it was categorized as hyperconfluent. In the “self-detached” stage, highly dense areas are formed when portions of the aggregate pull away from the culture surface. In case of any self-detachment, regardless of the confluency level of other regions inside of the aggregate, it was categorized as self-detached. The average cell density correlates with the confluency level (Supplemental Fig. S.3-2A), although there is not a one-to-one correspondence due to the heterogeneity within each aggregate e.g., some aggregates with highly dense regions are categorized as hyperconfluent yet have an average cell density in the confluent range.

To account for potential inconsistencies in initial seeding, we set the pre-confluent level to be “time zero.” Despite this data shift, we still observe substantial variability in

how long it takes aggregates to progress through confluency levels (Fig 3-1C). The majority of aggregates progress from pre-confluent to confluent within 12 hr (as indicated by the thickness of the line). Note that the aggregate shown in Fig. 3-1A corresponds to a line in Fig. 3-1C where every 24 hours the level of confluency moves one higher. Rather than seeding density, it appears that banding plays a predominate role in variability in timing. Aggregates with a high area of alignment (>30% on average) of the cells in sparse level on Day 1 detach by Day 4, whereas those with a lower percentage area aligned (>20% on average) do not. The percentage of area aligned is significantly higher in the prior group on each day of culture (ANOVA,  $p < 0.05$ ; Supplemental Fig. S.3-2). These multicellular bands can be observed more clearly in phase imaging following fixation when individual cells separate due to the dehydration process, and fluorescent staining shows continuous F-actin structures spanning regions with high numbers of nuclei (Fig. 3-1D).

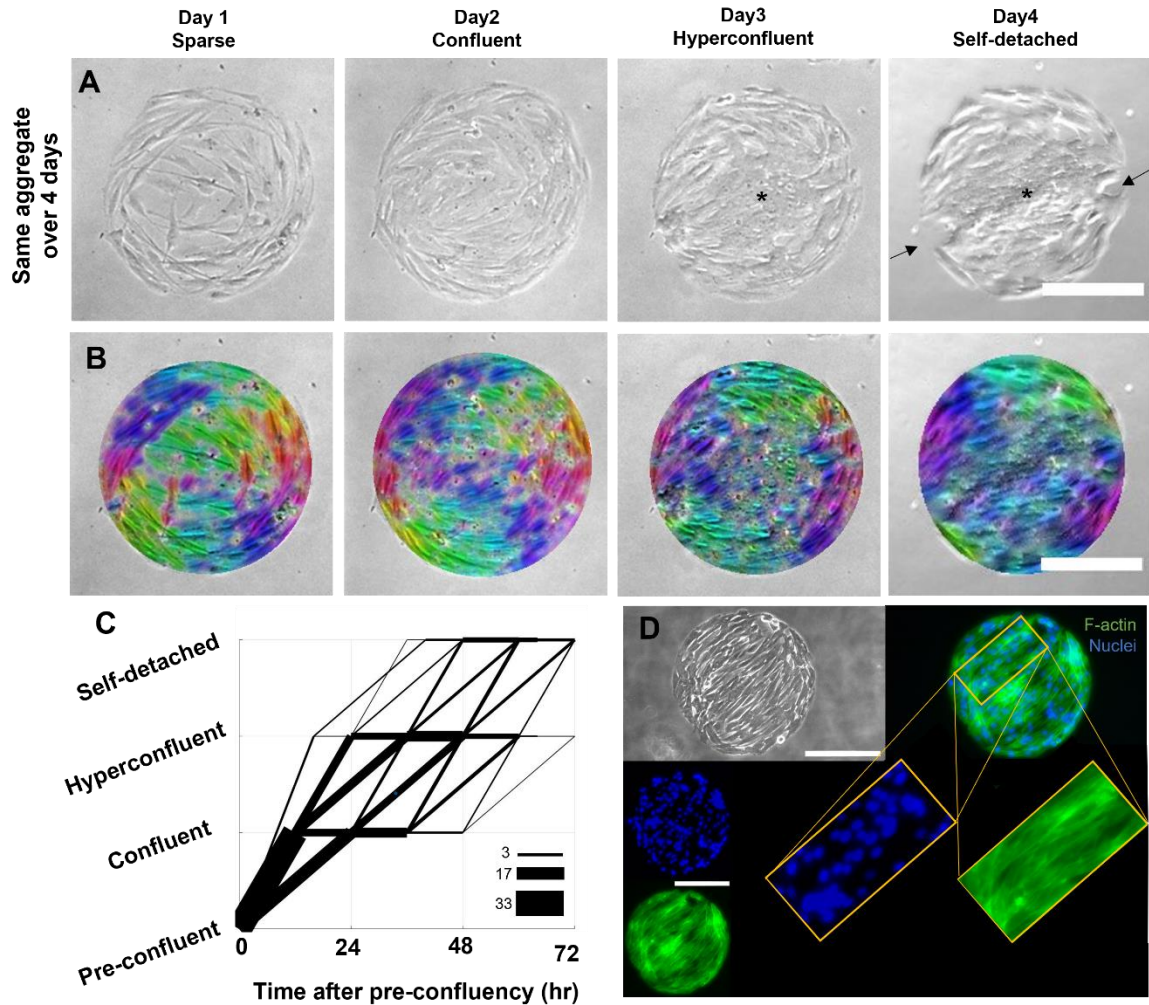


Figure. 3-1. The progression between levels of confluency varies in time from aggregate to aggregate. A) Time-lapse of the same aggregate over 4 days showing the evolution of its confluency starting sparse 24 hr after seeding, proceeding to confluent at day 2, hyperconfluent on day 3 (\* indicates high density region), and finally self-detachment on day 4 (arrow indicate regions detached from substrate). B) Orientation analyses by OrientationJ in ImageJ show the development of aligned cells across aggregate. C) Plot of levels of confluency versus time adjusted to time when each particular aggregate reached the pre-confluent level to remove variability in initial seeding in a single dish ( $n = 53$  aggregates; thickness of lines indicates number of aggregates following a given path). The majority of aggregates take 12 hr to reach confluency, yet there remains high variability in confluency rates from pre-confluent to higher levels of confluency after removal of heterogeneity in initial seeding (see other

*examples in Fig. 3-2 and Supplemental Fig. S. 3-2). C) Local clustering of aligned cells forms banding and hyperconfluent regions. F-actin staining (green) shows the direction of the band, and high density of nuclei (blue) demonstrates hyperconfluency. The shown banding was observed in 86.7% of 53 tracked aggregates, which is the major observed banding behavior. The phase image in panel C (gray) was captured after fixation and permeabilization which creates spaces between cells not seen in live imaging in panel A.*

*Scale bar = 200  $\mu$ m.*

### 3.4.2 Local hyperconfluency occurs following band formation

Despite the simple circular shape of the collagen islands, few aggregates had the expected radially symmetric patterns with circumferential alignment at edges and isotropic cells in the center (see Fig 2A right column for example). Even these relatively symmetric aggregates (e.g., Fig. 2A, 4<sup>th</sup> column) exhibit short regions of aligned cells at intermediate timepoints (Fig. 2A, 2<sup>nd</sup> and 3<sup>rd</sup> columns) which become hyperconfluent in the central region but do not span the entire aggregate and thus do not self-detach. In most aggregates, multicellular banding was observed disrupting the radial symmetry, even at early timepoints (Fig. 3-2B left panels). After 4 days, pronounced hyperconfluent bands were observed in all aggregates (Fig. 3-2B right panels). If banding is pronounced at the pre-confluent stage (Fig. 3-2C left panels), the band becomes highly dense within 24 hr and leads to self-detachment of cells from the substrate at the two endpoints of the banded region (Fig. 3-2C right panels, Fig. S.3-2F).

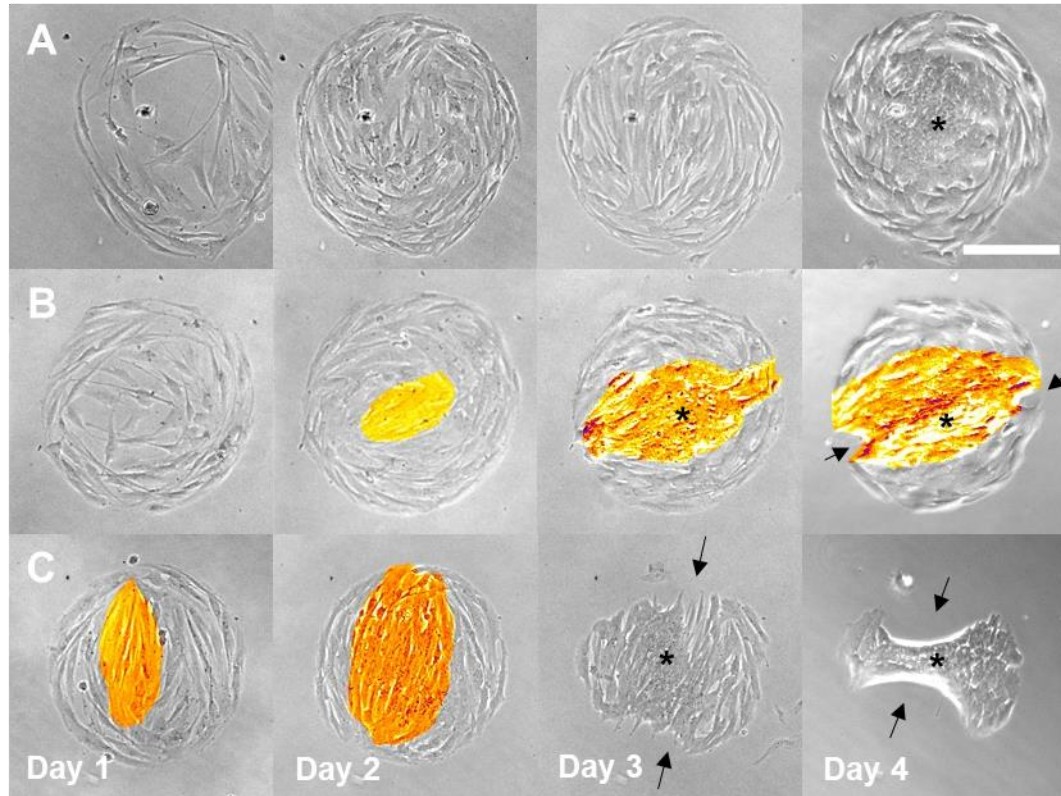


*Figure. 3-2. Three examples of different time courses of confluency progression in aggregates. A) Aggregate with relatively uniform cell distribution exhibiting circumferentially aligned cells around the edge and high density in the center by day 4 but no banding or self-detachment. This cell distribution was observed in 1 out of 53 tracked aggregates. B) Aggregate with formation of band starting day 2 and leading hyperconfluency by day 4 and slight self-detachment by day 4. C) Aggregate with banding occurring early which proceeds quickly to hyperconfluency and self-detachment by day 3. This kind of banding as a straight line was observed in 86.7% of 53 tracked aggregates. Meanwhile, in 2 out of 53, the alignment was a curvature, and in 5 out of 53, it was a triangle. (see examples of these alignments in Supplemental Fig. S. 3-3) Banding of aligned cells is highlighted in orange color, \* indicates high density region, and arrows indicate regions detached from substrate. Scale bar = 200  $\mu\text{m}$ .*

In the majority of aggregates, bands form a straight line from one edge of the aggregate to the other. Less often the bands are curved, only span a small internal region,

or connect into triangular patterns (Supplemental Fig. S.3-3). Most bands eventually lead to some degree of self-detachment within the 4-day culture period.

### 3.4.3 Banding occurs regardless of aggregate size

In previous studies, we microcontact-printed 200  $\mu\text{m}$ -diameter protein islands and observed VICs forming confluent aggregates with cells generally oriented circumferential at the edges but highly heterogeneous orientation and cell area in the central region (Goldblatt et al. 2020). In this study, we used 400  $\mu\text{m}$ -diameter to minimize the “edge effect,” yet we still observed highly heterogeneous structures within most aggregates. To further lessen the proximity to the edges, 600  $\mu\text{m}$ -diameter islands were created, and similar hyperconfluent bands formed in these large aggregates as well (Fig. 3-3). This finding, in conjunction with our time-lapse studies where cells aligned with individual elongated cells in aggregate centers, indicates that bands are not forming by cells interacting with the edges. To determine if this behavior is unique for VICs, we cultured primary human dermal fibroblasts on 400  $\mu\text{m}$  islands, and we observed similar banding and hyperconfluency (Supplemental Fig. S.3-4).

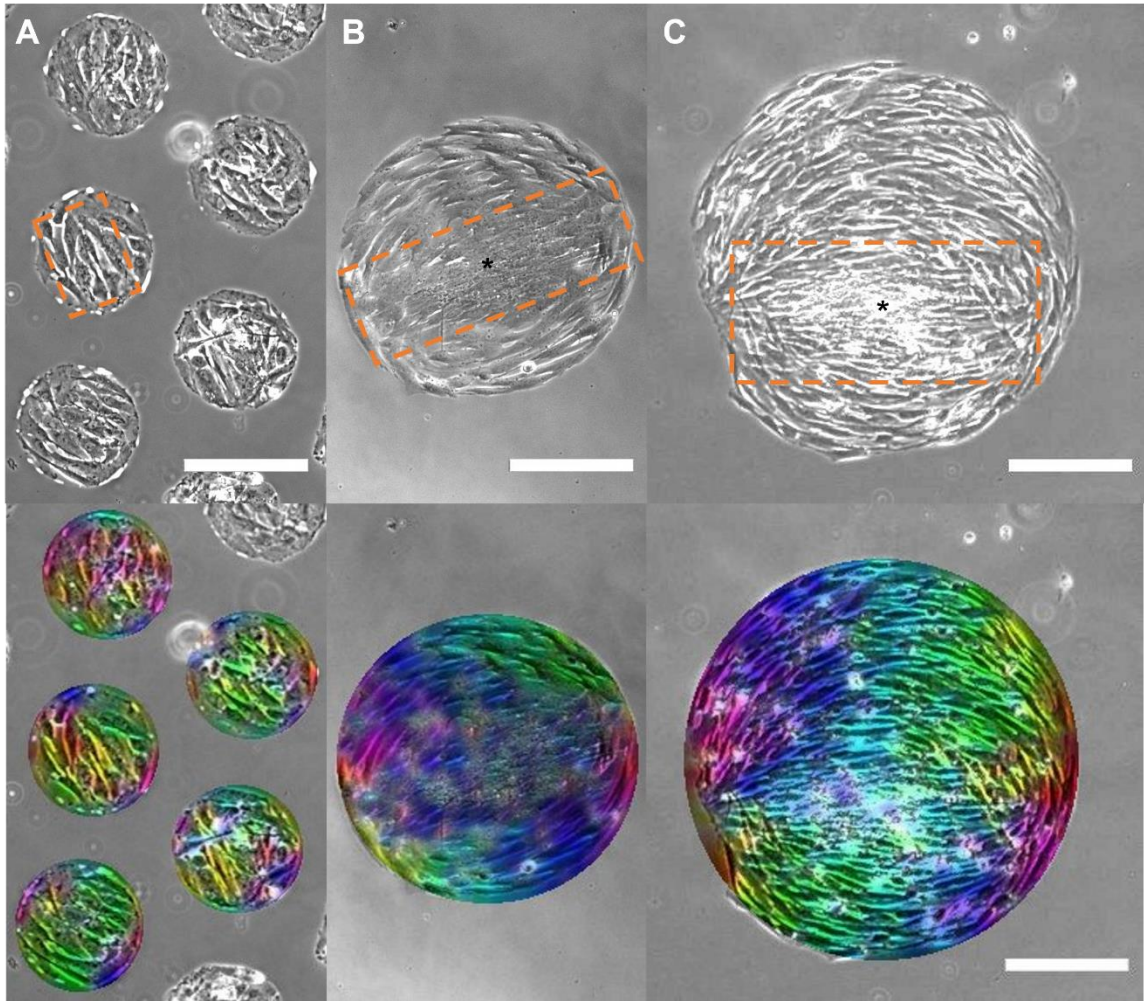


*Figure 3-3. Banding and hyperconfluency occur independent of aggregate size as observed in A) 200  $\mu\text{m}$ , B) 400  $\mu\text{m}$ , and C) 600  $\mu\text{m}$  day 4 aggregates. A dashed orange rectangle highlights banding, and \* indicates a high density region. The lower panel shows the orientation analysis by OrientationJ in ImageJ. Scale bar = 200  $\mu\text{m}$ .*

### 3.4.4 Cells migrate to connect with bands and then move in coordination

To better understand how cell migration plays a role in band formation, we performed 4.5 hr time-lapse imaging of aggregates with approximately 20% of cells fluorescently labeled so that individual cells could be tracked. Following 162 cells, we observed that cells in relatively sparse regions moved independently, whereas cells within

bands moved coherently (Fig. S.3-5). The vast majority of cells (~96%) remain within their respective regions (sparse, band, or edge) over the 4.5 hours (Supplemental Movie M.1). Five cells in sparse regions merged with bands and one cell joined a band from the edge. Four cells from relatively sparse regions joined the ring of aligned cells along the edge in the absence of any band. Although the behavior of cells in different regions were qualitatively different with cells in sparse regions migrating relatively independently and the cells in hyperconfluent regions oscillating in sync. Quantitatively, the mean squared displacement is lower in the hyperconfluent regions than the less confluent regions (Supplemental Fig. S.3-6), yet the average speed in less dense regions ( $8.2 \pm 0.8 \mu\text{m/hr}$ ) is not significantly different than in hyperconfluent regions ( $7.1 \pm 1.5 \mu\text{m/hr}$ , t-test,  $p = 0.07$ ).

To understand the events leading to band formation, we imaged aggregates every 30 minutes over 24 hours. Cells under lower confluency levels display a fluid-like behavior with edge cells rotating around the circumference and internal cells beginning to align to one another and forming bands, shown by orientation analysis by OrientationJ (Supplemental Movie M.2A). As confluency progresses, motility within aggregates decreases and cell migration is relatively uncoordinated (Supplemental Movie M.2B). Finally, during hyperconfluent stages, cells move back and forth together with limited migration similar to an oscillation (shown by PIV analysis in Supplemental Movie M.2C, and Fig. S.3-7). Cell proliferation is observed in the phase images at all confluency levels with less proliferation in hyperconfluent regions. Propidium iodide staining at the beginning of time-lapse experiments suggests that a small amount of apoptosis occurs throughout sub-confluent and confluent aggregates, whereas the rate of cell death is much higher in the middle of hyperconfluent bands. The propidium iodide signal dissipates with time due to photobleaching so is only seen at the early timepoints.

#### 3.4.5 Local hyperconfluency is inhibited by depleting calcium

To test whether band formation is driven by intercellular force transmission, we decreased cell-cell adhesion by precipitating calcium from the cell culture medium. After four days in culture, the last two of which were in calcium-free media, hyperconfluent

regions did not form, and we did not observe any self-detachment (Fig. 3-4). The concentration of cells is approximately  $1080 \text{ cells/mm}^2$ , which falls in the category of preconfluent to confluent as shown in Fig. S.3-2A. However, local regions of cell alignment were still observed. This local alignment may have been established in the first two days of culture in standard medium which is necessary for forming aggregates as proliferation is calcium dependent (Kahl et al. 2003). When the EDTA was added 24 hr post seeding, some of the cells in the middle remain aligned; however, the confluency did not progress within the 4 days of the experiment (Fig. 3-4C), thus this earlier depletion of calcium was not used for the final experiments.

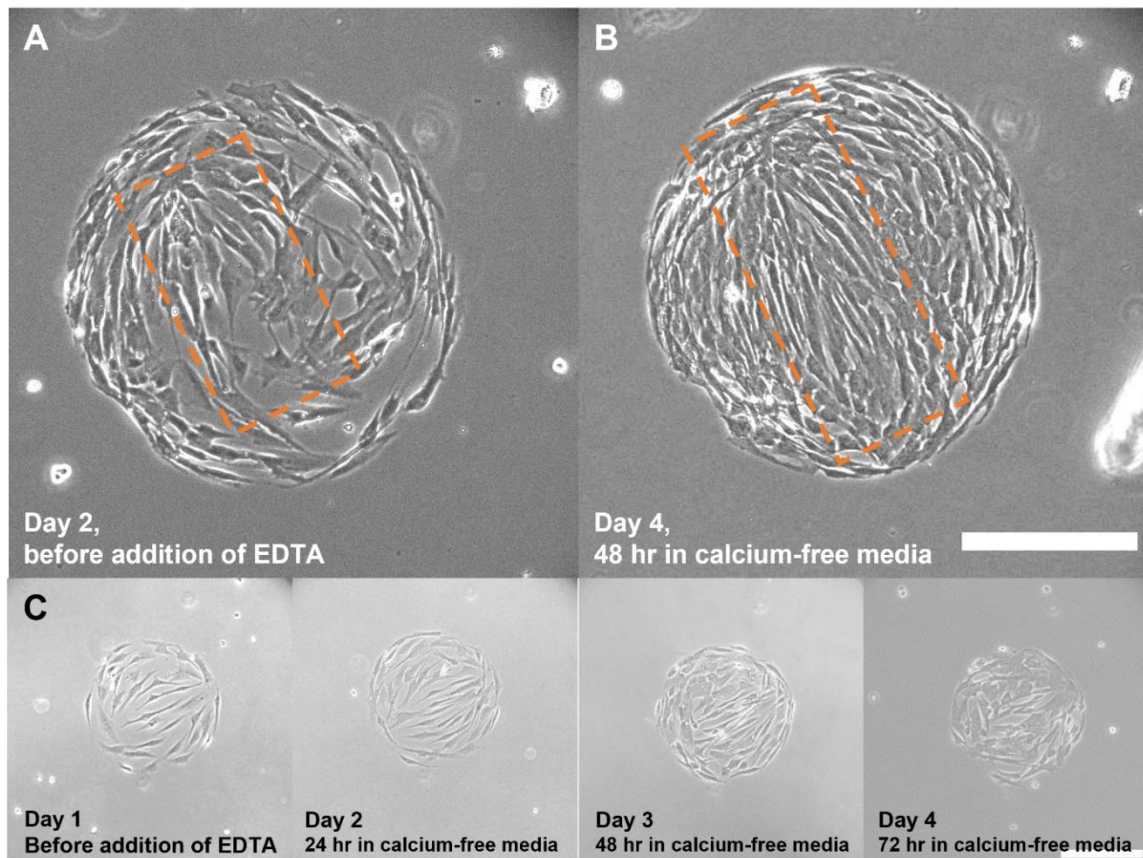


*Figure 3-4. Inhibiting cell-cell adhesion via calcium depletion prevents hyperconfluency, although banding is still observed. A) A day 2 aggregate before the addition of EDTA (1 mM) shows pre-alignment of the cells. B) The same aggregate on day 4 after 2 days in a calcium-free medium shows aligned cells in a band; however, the cells are not tightly contacting, and hyperconfluent regions are absent. Banding is*

*highlighted by a dashed orange rectangle. The concentration of cells is equal to 1080, which falls in the category of pre-confluent to confluent, following quantifications on Fig. S2A. C) Representative image of an aggregate with the addition of EDTA 24 hrs post-seeding, no confluent aggregates were observed after 4 days of culture; however, alignment of the cells in the middle remains. Scale bar = 200  $\mu\text{m}$ .*

### 3.4.6 Hyperconfluent bands increase local traction stresses

Unlike traction stress maps for homogeneous aggregates in which the traction is high and relatively uniform at the edges (Li et al. 2009), we observe that the bands accentuate the traction stresses at their endpoints (Fig. 3-5). When aggregates are confluent, traction “hot spots” are relatively low, then become much higher when large hyperconfluent bands form. For example, for the representative pre-confluent aggregate shown in Fig. 6A & B, the total traction force at the end of the band is 21.3  $\mu\text{N}$  (averaged between the two hotspots) compared to 118.0  $\mu\text{N}$  for the band in the representative hyperconfluent aggregate shown in Fig. 6C & D. Analysis of the principal stress vector directions indicates that stresses are highly anisotropic and predominantly in the direction of bands (Fig. 3-5 insets 1-4). Full vector fields are provided in the Supplemental Information (Supplemental Fig. S.3-8). Time-lapse traction stress maps show that stresses dynamically change in magnitude ( $F=299\pm 138$   $\mu\text{N}$ , a significantly large standard deviation compared to mean, showing the large fluctuation in magnitude of the forces applied by cells to the substrate) and location over 4.5 hr with cell movement, but peak traction stresses remain at the band ends (Supplemental Movie 3). Eventually, high traction stresses at band ends lead to self-detachment by exceeding the strength of the collagen-PA substrate bond/entanglement (Supplemental Fig. S.3-9).

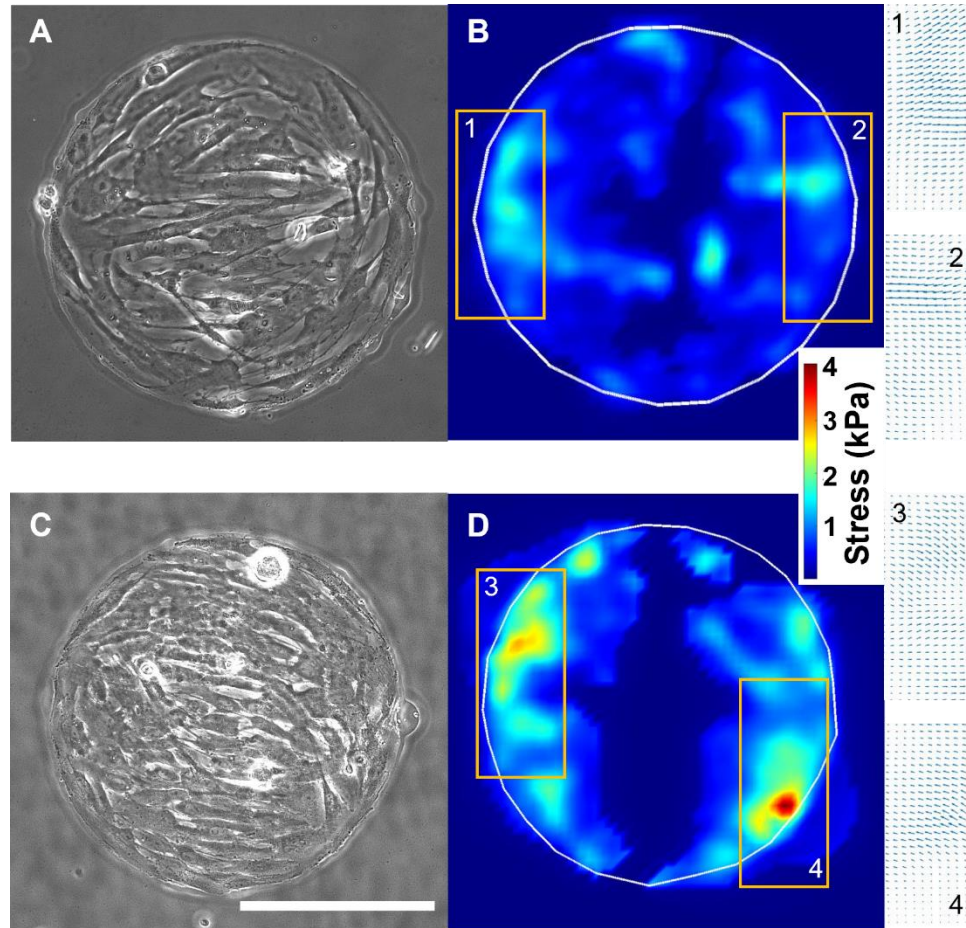


*Figure 3-5. Heterogeneous traction stress fields are produced by alignment and banding of cells and peak stresses increase with cell density. A) Phase image of a pre-confluent aggregate shows initial alignment of cells. B) TFM analysis of the pre-confluent aggregate shows low magnitude stress hotspots at ends of aligned cells with inward direction of applied stress (insets 1 & 2). C) Phase image of a hyperconfluent aggregate shows strong banding. D) TFM analysis of hyperconfluent aggregate shows high magnitude stress hotspots with inward direction of applied stress (insets 3 & 4). 5 aggregates with different confluency levels were tracked, which all showed hot spot in their traction stress field. Scale bar = 200  $\mu\text{m}$ .*

### 3.4.7 Cytosolic YAP indicates low tension in hyperconfluent bands

Despite measurement of high traction stress at the ends of the bands, biological markers consistent with a low stress environment such as high cell density, low spread

area, and apoptosis indicate low tension within the hyperconfluent bands. As an indirect measure of cell stress, we stained for YAP, a mechanosensitive protein which is shuttled preferentially to the nucleus under high tension and remains cytosolic in low tension environments (Aragona et al. 2013). In our aggregates, cells inside of bands have more cytosolic YAP (Fig. 3-6B, inset 1) compared to cells outside of bands, which have more nuclear YAP (Fig. 3-6B, inset 2). At band endpoints, where cells are more elongated, YAP is predominantly nuclear (Fig. 3-6B, inset 3). We did not observe any purely cytosolic YAP.

Quantification of nuclear (N) and nuclear/cytosolic (N/C) YAP in the center, end of bands, and non-banded regions was performed for four confluent aggregates (Fig 7.C). There was no purely cytosolic YAP observed. The remaining 37 stained aggregates had pronounced hyperconfluent bands in which this analysis was not possible due to difficulty in distinguishing individual nuclei. A two-way ANOVA was performed to analyze the effect of the region with respect to bands and heterogeneity between aggregates (treating aggregates as separate realizations) on YAP deactivation. The YAP nuclear localization is significantly lower in the central region ( $p = 0.001$ ,  $df = 2$ ,  $F$  value = 24.4). There are no significant differences between different aggregates ( $p = 0.24$ ). A post-hoc Tukey HSD test showed that YAP deactivation significantly differs between cells in the band and endpoints ( $p = 0.001$ ), also between cells in the band and outside of bands ( $p = 0.004$ ).

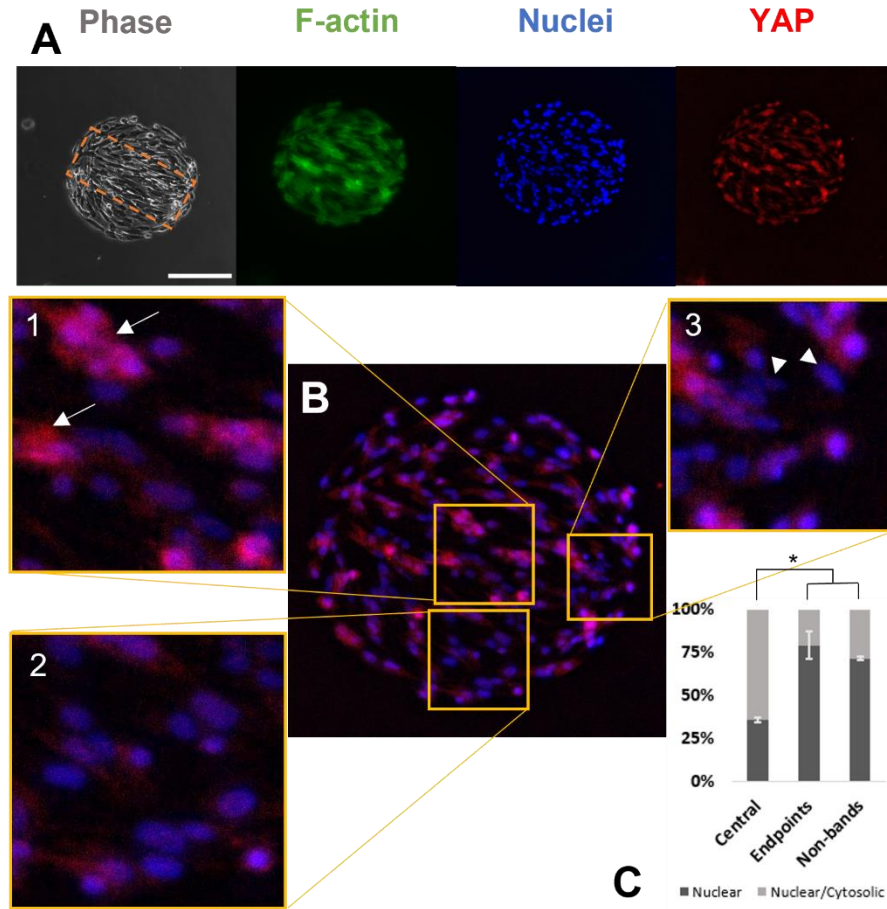


*Figure. 3-6. A greater proportion of cytosolic YAP is observed in the center of hyperconfluent bands than at the ends. A) Phase image of fixed and permeabilized and fluorescent images of F-actin, nuclei, and YAP in a hyperconfluent aggregate exhibiting banding (dashed orange box). B) YAP/Hoechst merged image shows mixed cytosolic/nuclear YAP in the hyperconfluent center (inset 1), outside of the band (inset 2), and nuclear YAP at the endpoint of the band (inset 3). Arrows point to examples of cytosolic/nuclear YAP, and arrowheads point to examples of nuclear YAP. Scale bar = 200  $\mu\text{m}$ . C) Quantification of nuclear (N) and nuclear/cytosolic (N/C) YAP in the center, end of bands, and non-banded regions ( $n = 615$  cells, 4 aggregates); there was no purely cytosolic YAP observed.*

### 3.4.8 Cells in bands reorient towards stretch but not completely

To examine the response of cells to external loading, we applied 10% cyclic uniaxial stretch for eight hours at 1 Hz frequency. Due to the heterogeneity of band locations, we tracked 38 individual aggregates before and after stretch rather than averaging overall cell behavior between aggregates. Actin fibers were observable with a live stain taken up by cells and imaged in compliant stretch wells without fixation; thus, since not all cells were stained, we manually tracked and quantified the morphology of 56 individual cells within those aggregates before and after stretch.

In general, the cells reorient towards the direction of stretch but are not able to completely reorient to the stretch axis, and the extent of cell reorientation depends upon initial angle of the bands. For cells inside bands originally aligned within  $\pm 15^\circ$  of the direction of stretch (Fig. 3-7A, circled cells), the alignment of the cytoskeleton becomes more pronounced, and the cells do not reorient in a detectable manner (from  $5.2^\circ \pm 7.9^\circ$  to  $2.7^\circ \pm 3.2^\circ$ ,  $p=0.45$ ,  $n=9$ ). The aspect ratio of these cells in the direction of stretch increases significantly from  $3.7 \pm 1.4$  to  $6.3 \pm 3.2$  ( $p=0.04$ ). When bands are at a moderate angle ( $15^\circ$  to  $45^\circ$ ) relative to the stretch direction, cells reorient significantly towards the direction of stretch but not fully, from  $28.0^\circ \pm 13.2^\circ$  to  $18.4^\circ \pm 13.8^\circ$  ( $p=0.001$ ,  $n=23$ ), and aspect ratio trends higher from  $2.5 \pm 0.7$  to  $3.0 \pm 1.3$ , but the change is not significant ( $p = 0.53$ ) (Fig. 3-7B, Supplemental Fig. S.3-10A). When bands are at a large angle relative to the stretch direction, initially at  $45^\circ$  to  $90^\circ$ , a subset of cells reorient towards the stretch direction significantly from  $59.1^\circ \pm 8.8^\circ$  to  $30.0^\circ \pm 18.3^\circ$  ( $p=0.003$ ,  $n=9$ ), whereas in others the cytoskeleton is 63ehave63ted, and the cells appear more rounded and the orientation was not quantified (Fig. 3-7C, Supplemental Fig. S.3-10B).

Cells on island edges that align with the global circular constraint and are in the direction of stretch (top and bottom of the images) are relatively stable and do not reorient in a detectable manner (from  $-2.5^\circ \pm 16.0^\circ$  to  $1.8^\circ \pm 12.0^\circ$ ,  $p=0.30$ ,  $n=16$ ). Conversely, for cells that align to the edges that are perpendicular to the stretch (left and right sides of the images), the cytoskeletons are disrupted, observed by presence of bright F-actin signal before the stretch and no F-actin signal after the stretch, thus the

reorientation of the perpendicular cells could not be quantified (Fig. 3-7B, 3-7C); this cytoskeletal disruption was observed in 20 of the 24 tracked aggregates where perpendicular cells were observed at the edges at pre-stretch.

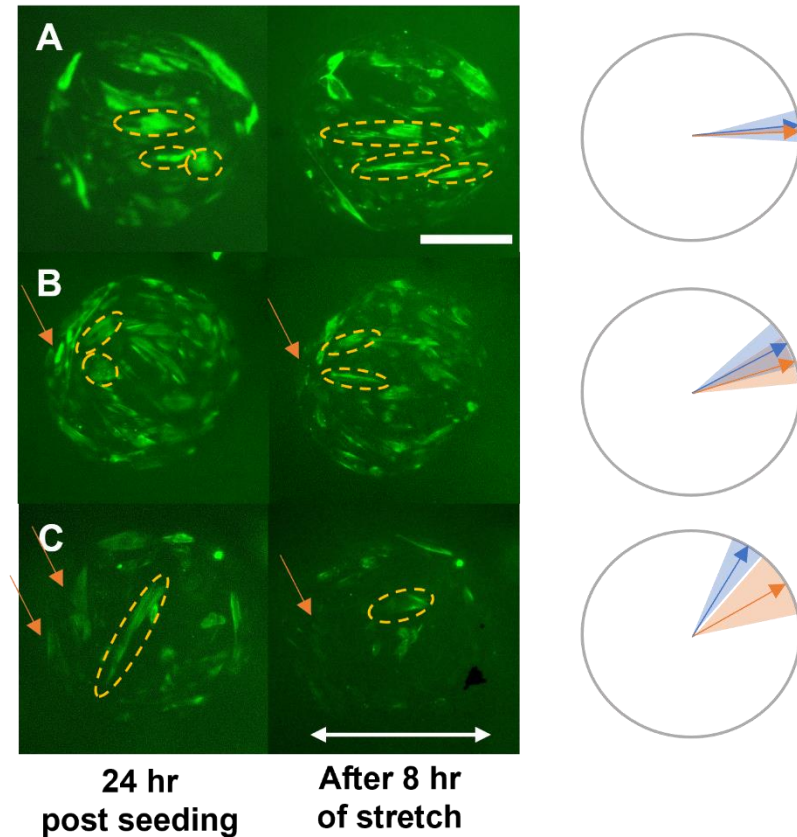


*Figure 3-7. Dynamic stretch reinforces F-actin alignment for cells in the direction of stretch and disrupts the cytoskeleton of cells aligned away from the stretch axis. A) Representative example of cells within a band roughly in the direction of stretch where the F-actin is intensified, and the cells are elongated after stretch. On the right is the schematic of reorientation, blue corresponds to pre-stretch, and orange is post-stretch. It appears there is no change of alignment after 8 hrs of stretch. B) Representative example of cells within bands that are oriented within  $45^\circ$  of the stretch axis showing reorientation towards the direction of stretch. The schematic shows the reorientation of cells towards the direction of stretch. C) Representative example of a highly elongated cell within a band oriented greater than  $45^\circ$  from the stretch axis becoming more rounded and reorienting towards the stretch direction. The schematic shows the reorientation of cells towards the direction of stretch. Panels B and C also show that*

*cells aligned along the edge perpendicular to the stretch direction retract (orange arrows). For all panels, F-actin of live VICs was stained with CellMask™ Actin before and after application of 10% uniaxial stretch for 8 hr at 1 Hz; brightly stained cells inside of bands are outlined by ellipses to show change in orientation and elongation.*

*Scale bar = 200  $\mu$ m.*

### 3.4.9 Proliferation occurs throughout aggregates but decreases in hyperconfluent regions

In contrast to studies showing proliferation of cells predominantly at the edges of constrained epithelial cell monolayers (Aragona et al. 2013, Li et al. 2006, Li et al. 2009, Silver et al. 2020), we observe proliferation throughout our confluent aggregates, observed with EdU signal in its fluorescent channel and compared to the number of cells observed in Hoechst fluorescent channel, representative of proliferation and nuclei, respectively. Images from 1 hr EdU pulse experiments show no distinct pattern of proliferation (Fig. 3-8A) even when images of positive cells from multiple aggregates are binarized and stacked (Fig. 3-8B). The 24 hr EdU exposure experiments indicate less proliferation in hyperconfluent bands (Fig. 3-8C, 3-8D).

A two-way ANOVA was performed to analyze the effect of the region (hyperconfluent or other regions) and heterogeneity between aggregates (treating aggregates as separate realizations) on proliferation. The proliferation rate is significantly lower in the hyperconfluent region than other regions ( $p = 0.02$ ,  $df = 1$ ,  $F$  value = 50.6). There were no significant differences between aggregates ( $p = 0.91$ ).

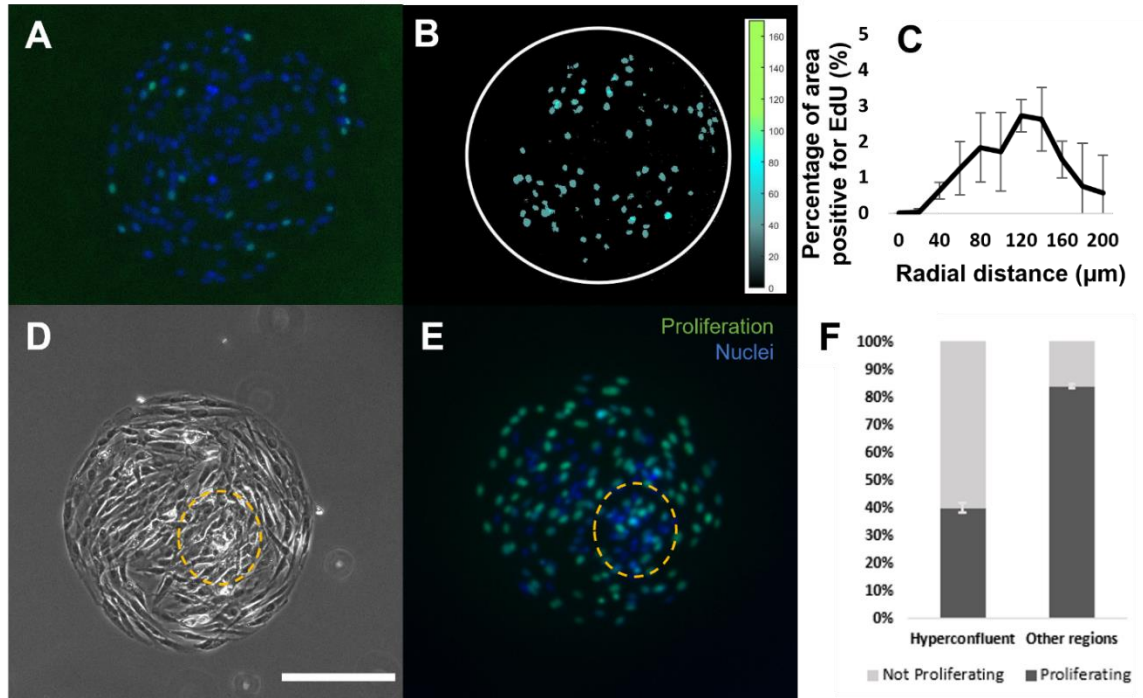


*Figure 3-8. Proliferation occurs throughout confluent aggregates except in high density regions. A) Representative aggregate after 1 hr pulse staining for proliferation with EdU. B) Overlay of binarized images of proliferation for 4 different aggregates after 1 hr EdU pulse shows proliferation throughout confluent aggregates. C) Frequency of proliferation presence at specific radii shows proliferation is not limited to the edge. D) Representative phase image of a fixed and permeabilized aggregate with a hyperconfluent region (orange outline). E) After 24 hr EdU exposure, proliferation occurs throughout the aggregate and significantly less in the hyperconfluent region, two-way ANOVA  $p = 0.06$  for  $p$ -value  $< 0.1$  to be significant.  $N = 3$  aggregates for 599 cells. Fluorescent images are merged Hoechst (blue) and EdU (green) images. Scale bar = 200  $\mu\text{m}$ .*

### 3.4.10 Apoptosis increases in high density regions in a YAP-dependent manner

As reported above, in time-lapse videos with PI staining (Supplemental Movies M.2A, B, C), we observe a low incidence of cell death throughout aggregates except within hyperconfluent regions. We confirmed that this cell death is likely due to

apoptosis by staining for cleaved caspase 3/7. Within the first 24 hr after pre-confluency, approximately 20% of aggregates show a caspase positive signal indicating apoptosis. Most caspase-positive aggregates are confluent aggregates as few hyperconfluent aggregates are present at this time (Fig. 3-9). At 24-48 hr after pre-confluency, almost half of the aggregates show caspase activity, and most of these aggregates are hyperconfluent. At 48-72 hr after pre-confluency, nearly all aggregates show a positive caspase signal with the majority having detached from the surface.

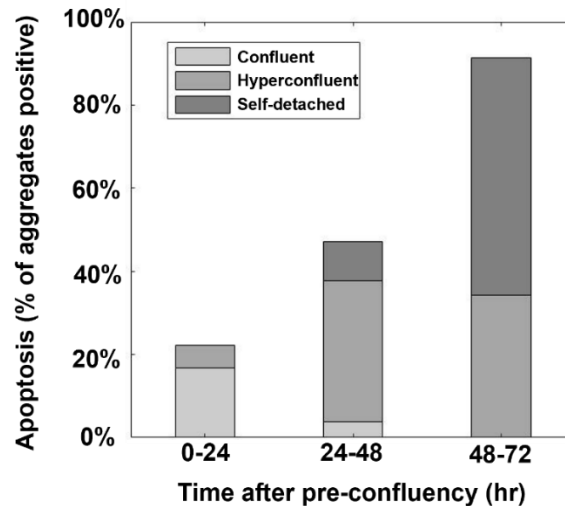


*Figure 3-9. Apoptosis increases with culture time. A small proportion of confluent aggregates have apoptotic cells at the early timepoint, whereas as the majority of aggregates become hyperconfluent and self-detached an increasing proportion exhibit apoptosis (n = 53 aggregates).*

As cytosolic YAP is not observed in sparse regions with low prevalence of apoptosis, we sought to determine if YAP activation (i.e., translocation to the nucleus) is sufficient to inhibit apoptosis. We stably expressed activated YAP in VICs and cultured them on circular collagen islands until hyperconfluent (but prior to self-detachment). Compared to control VICs (Fig. 3-10A), we observe a dramatic decrease in apoptotic activity in VICs with constitutively active YAP (Fig. 3-10B). The observed decrease is statistically significant (paired t-test,  $p < 0.001$ ).

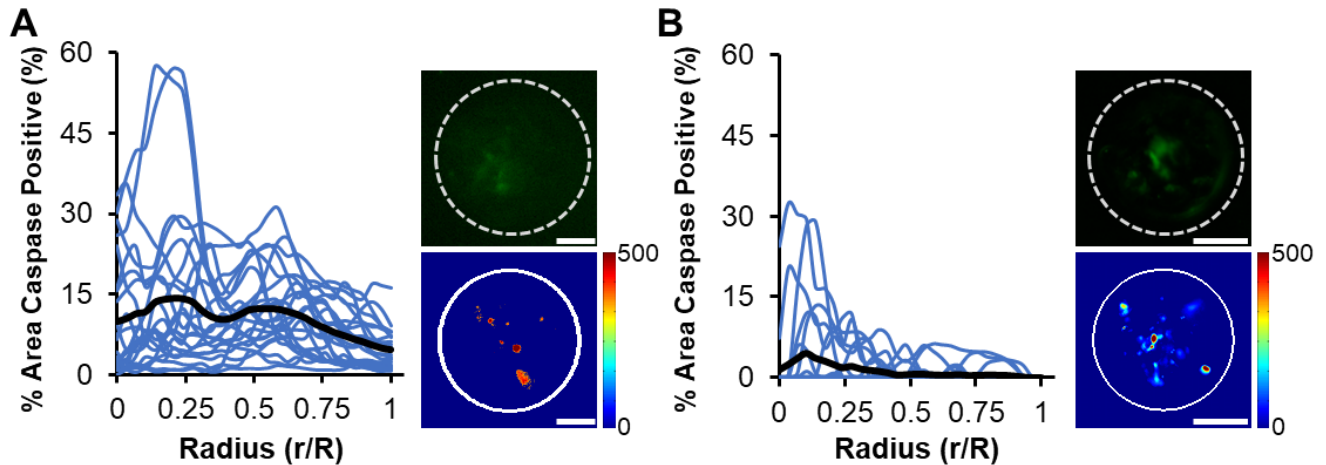


Figure. 3-10. Apoptosis is decreased substantially by YAP activation. A) The portion of aggregates positive for caspase in control VICs decreases from the center to edge. Image of a single aggregate stained for cleaved caspase-3/7 (top inset; green, dotted line indicates aggregate edge) and heat map for average caspase-3/7 intensity (bottom inset,  $n = 24$  aggregates from 3 replicates). B) The portion of aggregates positive for caspase in VICs with constitutively active YAP decreases from center to edge. Image of a single aggregate stained for cleaved caspase-3/7 (top inset; green, dotted line indicates aggregate edge) and heat map for average caspase-3/7 intensity (bottom inset,  $n = 23$  aggregates from 3 replicates). Scale bar =  $50 \mu\text{m}$ .

### 3.5 Discussion

Collective cell interactions drive distinct spatial patterning of cell behavior in monolayers of cells within confined geometries. These emergent patterns correlate strongly with predicted mechanical stress fields indicating a regulatory role of mechanics. Here, we extended studies conducted primarily on epithelial monolayers to more contractile and less contact inhibited primary fibroblastic cells. We analyzed the evolution of VIC confluency on circular micropatterned protein islands over a period of days, a long duration which is relevant for disease modeling. We aimed to determine how observed heterogeneities in spatial patterning are influenced by interactions between neighboring cells and under the influence of the circular global constraint to determine the relative effects of local and global collective behaviors. In contrast to previous reports

### Chapter III: Multicellular Aligned Bands Disrupt Global Collective Cell Behavior

of radially symmetric cell alignment, proliferation, and differentiation of epithelial cells and cell lines in circular and annular patterns (He et al. 2015, Nelson et al. 2005, Silver et al. 2020, Streichan et al. 2014), we observe that primary porcine VICs and human dermal fibroblasts align locally and form hyperconfluent bands spanning the circular patterns due to local cell-cell interactions, and this local alignment occurs regardless of pattern diameter (200-600  $\mu\text{m}$ ).

The banding behavior bears similarity to local collective behaviors reported in unconstrained fibroblast monolayers from a variety of sources (Carlson et al. 2009, Chansard et al. 2021, Lynch et al. 2018). VICs, like other spindle-shaped cells, evolve from a roughly isotropic state to an aligned nematic state as they proceed from sparse to confluent in 2D culture. Well-ordered nematic domains are disrupted by topological defects at high cell density and, when cultured on circular islands, create bands that span the majority of the diameter (Duclos et al. 2017); however, in contrast to cell lines such as NIH 3T3 and C2C12 cells (Duclos et al. 2017), VICs form bands that can terminate closer to the edges of the patterns than predicted for these characteristic defects, possibly due to the large size of the VICs relative to the pattern size and myofibroblast-like contractile behavior. More importantly, VIC and HDFs proceed to local hyperconfluency that is not predicted by the physics and nematic domains or observed for the cell lines, likely due to lower sensitivity to contact inhibition for these primary cells. The formation of hyperconfluent regions has biological ramifications in diseases involving increased rates of proliferation and apoptosis.

The asymmetric locations of bands largely explain the variability in patterns of proliferation, migration, and density observed in these aggregates. The formation of these highly aligned multicellular bands soon after seeding is correlated with self-detachment within 4 days of culture resulting in aggregate-to-aggregate heterogeneity within a single dish of identical collagen islands. Self-detachment and further nodule formation have been induced and studied in the context of dewetting behavior of the epithelial cells (Pérez-González et al. 2019). Dewetting is affected by E-cadherin adhesion, which influences the tissue mechanical properties and forces that later could alter the shape of the confined size aggregates, e.g., self-detachment (Pérez-González et al. 2019). In the

current study, self-detachment was the endpoint of our analysis, and we did not investigate further into nodule formation. These observations, along with traction force and time-lapse migration measurements, indicate that VICs exhibit strong local collective behavior that disrupts the emergent behavior emanating from the circular constraint of the islands. Such regional changes in cell shape, number, and confluency should be considered in the mechanical analysis of multicellular systems, especially for primary fibroblastic cells.

Non-uniform stress fields that emerge from transmission of forces between cells have been postulated as the driver of cell alignment and collective behavior in constrained cell islands (Li et al. 2009, Nelson et al. 2005, Silver et al. 2020). In contrast, our short-term (4.5 hr) time-lapse imaging shows that the cell alignment that drives the formation of bands is initiated by a few local cells migrating to and aligning with highly elongated spindle-shaped cells. Rather than acting individually until confluent as seen in epithelial cells (Doxzen et al. 2013), VICs often align with each other within the patterns at the pre-confluent stage. This local collective behavior may occur due to cells sensing the anisotropic displacement of the underlying PA gel generated by the cell (Reinhart-King et al. 2005) and/or by contact guidance provided by the elongated cell. This behavior occurs regardless of aggregate size up to 600  $\mu\text{m}$  diameter indicating that the banding is not formed due edge effects, i.e., cells do not attach to two points on the circular edge and elongate to span the island. We show that the banding also occurs with primary dermal fibroblasts. Sun and colleagues report that primary rat embryonic fibroblasts align radially at the edge of similar protein islands, and the central cells are smaller and more dense than edge cells, although without banding (Xie et al. 2021). This heterogeneous morphology is stark contrast to the patterns observed for NIH3T3 and osteoblast-like MC3T3-E1 cell lines which exhibit uniform spread area throughout the constrained monolayers and circumferentially aligned cells at the edges and less elongated cells in the center (He et al. 2015, Xie et al. 2021). Together, these results indicate that for the relatively large and contractile primary fibroblastic cells studied herein, the strong local collective behavior disrupts the global circular constraint that drives the radially symmetric emergent collective behavior of other cell types cultured on circular patterns.

### Chapter III: Multicellular Aligned Bands Disrupt Global Collective Cell Behavior

The long-term (24 hr) time-lapse videos clearly show that even when hyperconfluent, confined VIC cell layers are not static or “jammed” as observed for high-density epithelial monolayers (Atia et al. 2018, Garcia et al. 2015, Vig et al. 2017). We observe synchronized circumferential collective migration at the edges of pre-confluent and confluent VIC aggregates as well as substantial collective movement in the center along the multicellular bands. Similar collective cell migration is observed in epithelial monolayers on small (100-200  $\mu\text{m}$ ) circular islands, and vortices of local collective migration are observed in the central regions of larger islands (500-1000  $\mu\text{m}$ ) (Doxzen et al. 2013). The average cell speed was not significantly lower in hyperconfluent regions than in less confluent regions. Although this result is not consistent with the common finding that collective cell migration speed has an inverse correlation with cell density (Doxzen et al. 2013, Li et al. 2014, Lin et al. 2021), the motion of the cells in the bands appears qualitatively different in that it is less persistent in direction and more fluctuating; indeed, the MSD is significantly lower in hyperconfluent regions than less confluent regions.

The progression of bands to hyperconfluency appears to be driven by cells migration to and joining aggregates rather than proliferation within the bands. EdU staining and cell morphological features in time-lapse videos show that proliferation occurs throughout the aggregates and less within the hyperconfluent regions. Previous experiments with long EdU pulses (8 hr) show EdU staining throughout similar constrained monolayers (mouse MSC cell line) with a decrease in proliferation with cell density (Berent et al. 2022). In contrast, many studies of constrained epithelial monolayers report proliferation occurring predominantly at the edges corresponding to strong cell alignment and high traction forces (Li et al. 2006, Silver et al. 2020, Streichan et al. 2014). Utilization of low  $\text{Ca}^{2+}$  media, shown to disrupt cell-cell interactions and subsequently the traction and cell alignment at the edges of cell aggregates (Maruthamuthu et al. 2011, Xie et al. 2021), did not inhibit the alignment of cells into bands across our aggregates but did stop the bands from progressing to hyperconfluency and self-detachment. These results indicate that development of the hyperconfluent bands is dependent upon cell-cell force transmission; however, the results should be interpreted carefully as the initial cell alignment occurred in the 48 hours prior to depleting calcium

from media (Fig. 3-4A), and decreased proliferation rates in low-calcium media may contribute to the lower cell density (Kahl et al. 2003). Regardless, the results demonstrate that removing calcium from the media does not reverse the local collective behavior or fully block VIC proliferation.

The hyperconfluent bands produce high, localized traction stresses at their endpoints. In contrast, in previous studies with confluent islands of epithelial cells and cell lines that are not highly motile (Schaumann et al. 2018), traction stresses are highest and roughly uniform at the edges, and the predicted cell-layer stresses increase from the edge to the center (Aragona et al. 2013, Deglincerti et al. 2016, Li et al. 2009, Nelson et al. 2005, Tran et al. 2020). Time-lapse TFM heatmaps demonstrate that the magnitudes of traction stress vary with time but are consistently located at band endpoints and are directed inward indicating high uniaxial tension in bands. Traction stresses increase as bands progress from confluent to hyperconfluent and eventually lead to the detachment of portions of the aggregates from the substrate when the collagen/substrate bond strength is exceeded.

Despite the high total force at the ends of the bands, the biological markers examined suggest a low stress environment inside of the bands (as discussed below). Unfortunately, it is not feasible to calculate the stress or force per cell in the bands as they are not uniaxial cables attached only at the ends. The interactions with the adjacent cells are not known and there are additional (albeit low magnitude) traction stresses below the bands. In theory, monolayer stress microscopy (MSM) could be used to calculate the in-plane stresses of the cells throughout the aggregate from the traction stress maps; however, MSM assumes homogenous contractile and mechanical properties throughout the cell layer. We have previously shown that these calculations are not accurate for heterogeneous cell aggregates without incorporating the local cell properties which are not known for the banded aggregates (Goldblatt et al. 2020).

Cells in hyperconfluent regions have smaller areas and cytosolic YAP; markers that are characteristic of cells in low-stress environments such as when cultured on soft substrates or on small protein islands that constrain spreading (Aragona et al. 2013, Calvo et al. 2013, Mascharak et al. 2017, Wada et al. 2011). In contrast, cells at band endpoints

have more nucleated YAP similar to that observed for single cells on unpatterned stiff substrates (Dupont et al. 2011) and for confluent primary fibroblasts on protein islands (Xie et al. 2021). Apoptosis, which is also associated with low cell stress (Egerbacher et al. 2008, Humphrey et al. 2014), increases as aggregates progress to hyperconfluency. Consistent with this result, almost every aggregate that can no longer generate substantial traction due to being partially detached from the substrate is caspase positive. As YAP enhances the transcription of pro-survival genes (Codelia et al. 2014, Lin et al. 2015, Zhang et al. 2011), we wondered if YAP plays a defining role in apoptosis in VICs. We found that constitutively activating YAP substantially decreases apoptosis consistent with findings from studies of epithelial cell lines (Liu et al. 2017). While high traction stresses measured at the ends of the bands seem contradictory with low stress within the bands, it is possible that the high force in the band is generated/transmitted by many cells in parallel, i.e., high total force but low force per cell. This interpretation is consistent with our computational model of circular cell aggregates with radially increasing contractility from the center to the edge which predicts low stress in the central region despite high traction stresses transmitted to the substrate at the edges (Goldblatt et al. 2020).

To further investigate the state of stress in the bands, we applied cyclic uniaxial stretch to confluent aggregates. Under the assumption that cells attempt to reach a homeostatic stress level (Brown et al. 1998), we postulated that if cells within the bands were under high tension, they would reorient away from stretch to regain their preferred stress level, whereas if cells were confined due to high cell density and not able to generate their preferred level of homeostatic tension, they would spread out and reorient towards stretch. Isolated VICs (Cirka et al. 2016) and other fibroblasts cultured on stiff substrates exhibit strain avoidance (Greiner et al. 2013, Ristori et al. 2018, Shao et al. 2013, Wang et al. 2001) as do epithelial/endothelial sheets (G er emie et al. 2022, Kaunas et al. 2005). In contrast, when cells are cultured on collagen gels (Tondon et al. 2014), within low density soft collagen gels (Foolen et al. 2014, Sears et al. 2016) or when contractility is inhibited (Kaunas et al. 2005), cells reorient towards stretch. Consistent with the low stress interpretation, we observed that VICs within bands that are already oriented towards the direction of stretch elongate and have more pronounced and aligned cytoskeletal arrangement, whereas cells within bands roughly perpendicular to stretch

retracted or reoriented towards the direction of stretch. We did not observe increased aggregate detachment with stretch which also suggests low stress in the aggregates. Cyclic (equibiaxial) stretch of VIC monolayers, in combination with TGF-beta treatment, has been shown to potentiate cell detachment and formation of aggregates (Fisher et al. 2012). As we presumed that edge cells were under relatively high circumferential stress due to their elongated morphology and based on computational model predictions of high circumferential stresses at the edges of constrained monolayers (He et al. 2015), we expected these cells to reorient away from the stretch direction. Instead, we observed that the cells which were parallel to the direction of stretch maintained their elongation, and cells that were perpendicular to the direction of stretch retracted and/or reoriented away from the stretch direction. Cyclically stretched epithelial (MDCK) cells have been shown to increase their polarization (aspect ratio) when aligned around a “wound” edge in a monolayer model with a hole (essentially the inverse of our “island” system) consistent with the behavior we observe for cells aligned with the stretch axis, but the retraction of edge cells perpendicular to stretch has not been reported (Xu et al. 2022). It is possible that the aligned bands in our system disrupt the emergent radial-symmetric stress field resulting in relatively low stress in edge cells, thus these cells reorient in the stretch direction to increase their stress towards a homeostatic level or to minimize shear stress (Liu et al. 2016).

### 3.6 Conclusion

Our results indicate that cell alignment and subsequent local collective behavior leads to substantial heterogeneity between and within constrained monolayers of primary fibroblastic cells. Multicellular bands are formed by cell-cell interactions locally. As cells become more dense within the bands, the stress exerted by interior cells decrease, YAP becomes excluded from the nucleus and, consequently, apoptotic rates increase. These findings suggest that strong local cell-cell interactions between primary fibroblastic cells can disrupt the global collective cellular behavior; this local collective cell behavior may play an important role in development and disease of connective tissues.

The findings of this research are specifically crucial in the biology of VICs, as there is less information on their behavior compared to other cell types such as epithelial cells and fibroblast/myoblast cell lines. The mechanical environment of VICs is hypothesized to contribute to diseases such as calcification. In this research, we showed that emergent behavior arising from cell-cell interactions may be as important as the external mechanical environment of VICs on their behavior.

### 3.7 Acknowledgment

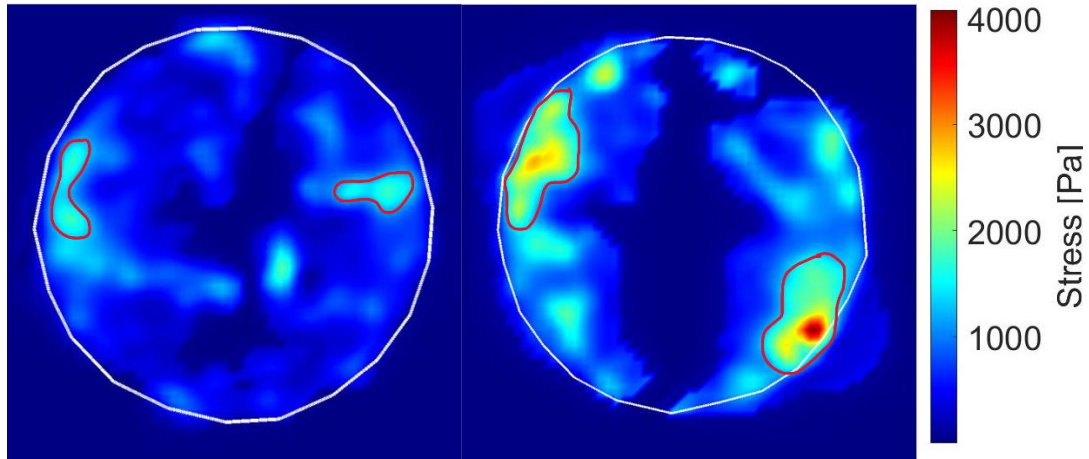
We would like to thank Sabine Hahn for her help editing the manuscript, Seyed Mohammad Jafar Sobhani for his help with graphical plotting with MATLAB, Milad Saadat for his help in visualization of data, as well as Marsha Rolle and CERES labs located in Worcester Polytechnic Institute for use of the Cytation microscope and George Pins for donation of neonatal human dermal fibroblastic cells. This work was funded in part by the American Heart Association (20AIREA35120448) and the National Science Foundation (CMMI 1761432).

### 3.8 Appendix 1

We picked the hotspots, red in the Figures below, at the end of the bands and extracted the stresses from those locations as we would also have the direction information. We perform these actions using a custom-written MATLAB code.

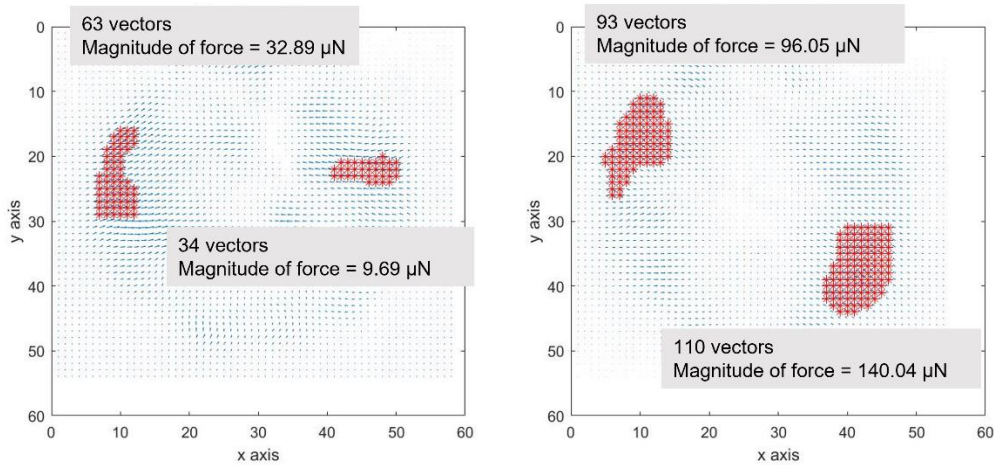
In this code, first, we extracted the data (Udata and Vdata of the plot related to the stress vectors). Each pixel has information on the coordination and the magnitudes of  $u$  and  $v$  components of the stress vector. Then, we entered the coordinate for a rectangle containing the hotspot, then visited each pixel in that area, and if it were higher than a minimum, which was determined by the graph's values, outlined by a red line.

These images are for presentation of the hot spots only. We used the stress information of these locations to execute our calculations.



We used the following plots, as they also have the information on the direction of the stress. Here we extracted u and v components of stresses.

Then, by multiplication of the stress vector to the area related to each vector and scaling from pixel to  $\mu\text{m}$ , we calculated the forces corresponding to each stress vector. Then we summed the forces in each hotspot to have a total traction force for each hotspot, as follows:

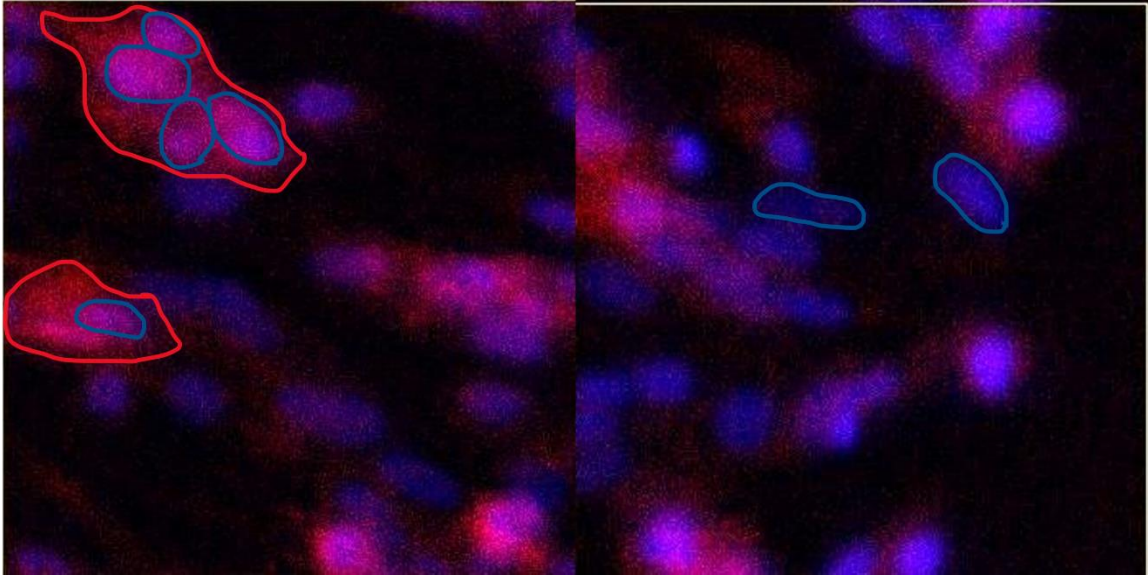


The same costume code was used for analyzing the frames of the TFM time lapse. The table below shows the average of the forces applied by cells in two hotspots at the end of the bands on each frame, as well as the average area of hotspots (the area that cells are applying traction forces higher than a threshold). The large standard deviations in both measurements, show the dynamic environment of the band.

Frame number	Average Force ( $\mu\text{N}$ )	Average area ( $\mu\text{m}^2$ )
1	356.22	6.29E+05
2	328.51	6.02E+05
3	181.72	4.80E+05
4	349.85	6.02E+05
5	560.09	7.45E+05
6	368.45	6.13E+05
7	374.33	5.79E+05
8	288.77	5.46E+05
9	141.17	3.20E+05
10	40.60	2.26E+05
Mean	298.97	5.34E+05
Standard Deviation	138.18	1.46E+05

### 3.9 Appendix 2

We merged the separate fluorescent channels corresponding to stained YAP and nuclei to quantify YAP colocalization with nuclei. To provide a better explanation of how the nucleated and nuclear/cytosolic YAP is recognized, please refer to the figure below:



The images above, from left to right, correspond to insets 1 and 3 of Fig. 3-6, respectively. In inset 1 of Fig. 3-6, the nuclear/cytosolic YAP is shown by arrows drawn here. The blue line outlines the nuclei, and the red outlines the area where the YAP signal is present. Please notice the red signal on the blue nuclei as well. On the right, which corresponds to inset 3 of Fig 3-6, the nucleated YAP is shown by an arrow. Here, the nuclei are outlined by a blue line. Please notice that there is no red signal present around the nuclei.

### 3.10 Supplemental Figures

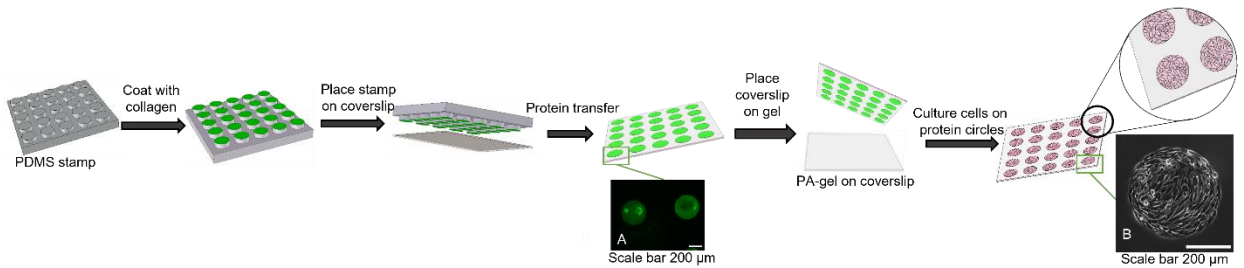


*Figure S.3-1. Indirect microcontact printing method schematic, modified from [26]. Inset (A) Collagen prints verified by Alexa Fluor-488 carboxylic acid succinimidyl ester. The uniform distribution of the collagen is shown in the indirect microcontact printing method used in this research. Inset (B) Pre-confluent 2D aggregate on 400  $\mu\text{m}$  in diameter collagen island showing cell coverage and circular shape of the print. The scale bar is 200  $\mu\text{m}$ .*

## Chapter III: Multicellular Aligned Bands Disrupt Global Collective Cell Behavior

Chapter III: Multicellular Aligned Bands Disrupt Global Collective Cell Behavior

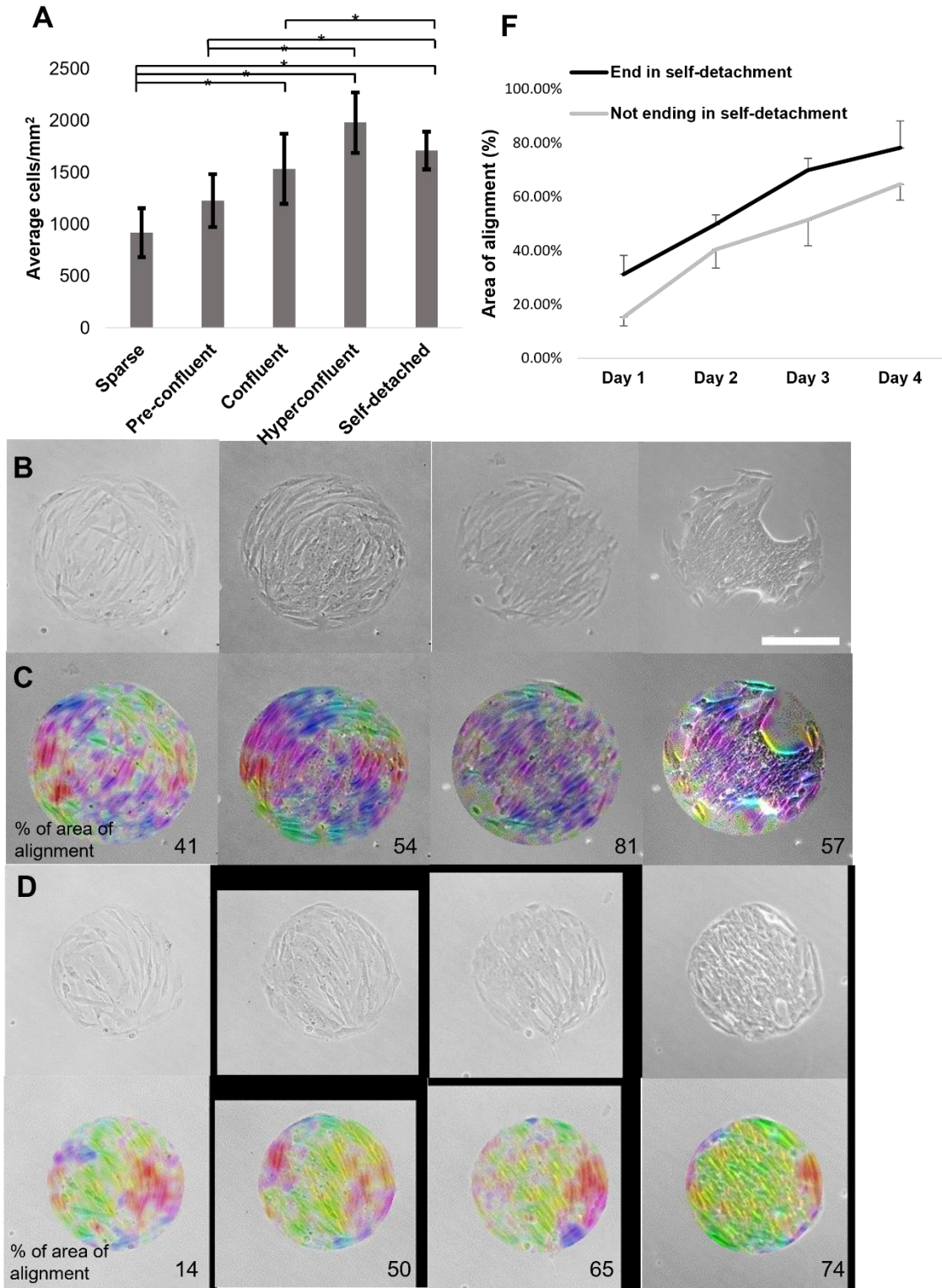
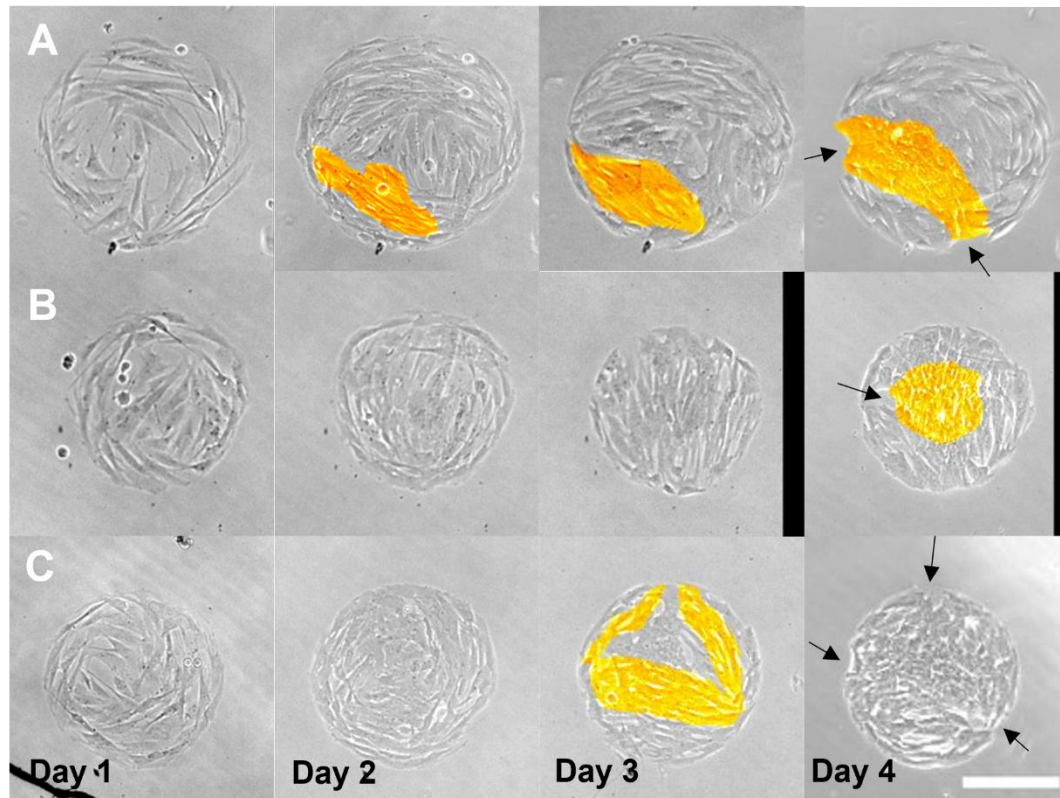


Figure S.3-2. The cell density increases with confluency level (A); non-adjacent confluency levels are statistically different (ANOVA, \* indicates  $p < 0.05$ ). If substantial regions are aligned by Day 1 in the preconfluent stage, the aggregate detaches from the

### Chapter III: Multicellular Aligned Bands Disrupt Global Collective Cell Behavior

substrate by Day 4 as shown for the representative aggregate in B (phase contrast) and C (orientation analyzed by OrientationJ in ImageJ). If only small regions are aligned at Day 1, the aggregate remains intact at Day 4 as shown for the representative aggregate in D (phase contrast) and E (orientation analyzed by OrientationJ in ImageJ). Scale bar = 200  $\mu\text{m}$ . F) Percentage of area of alignment in aggregates that end in self-detachment is significantly higher on each day of the experiment (two-way ANOVA,  $p < 0.001$  for different days,  $df = 3$ ,  $F = 68$ ;  $p < 0.001$  for different groups,  $df = 1$ ,  $F = 31.9$ ).



*Figure S.3-3. Local collective behavior results in hyperconfluent bands of many shapes. Banding is shown in orange, only for presentation purposes. A) Aggregate with banding initiating non-centrally. B) Aggregate with central banding that never spans the entire island to meet the edge, and hole appears in low density region. C) Aggregate with banding in three directions forming a triangular pattern and detachment in three locations. Yellow/orange highlight indicates aligned region; blue highlight indicates detachment of the cells from the substrate. Scale bar = 200  $\mu\text{m}$ .*

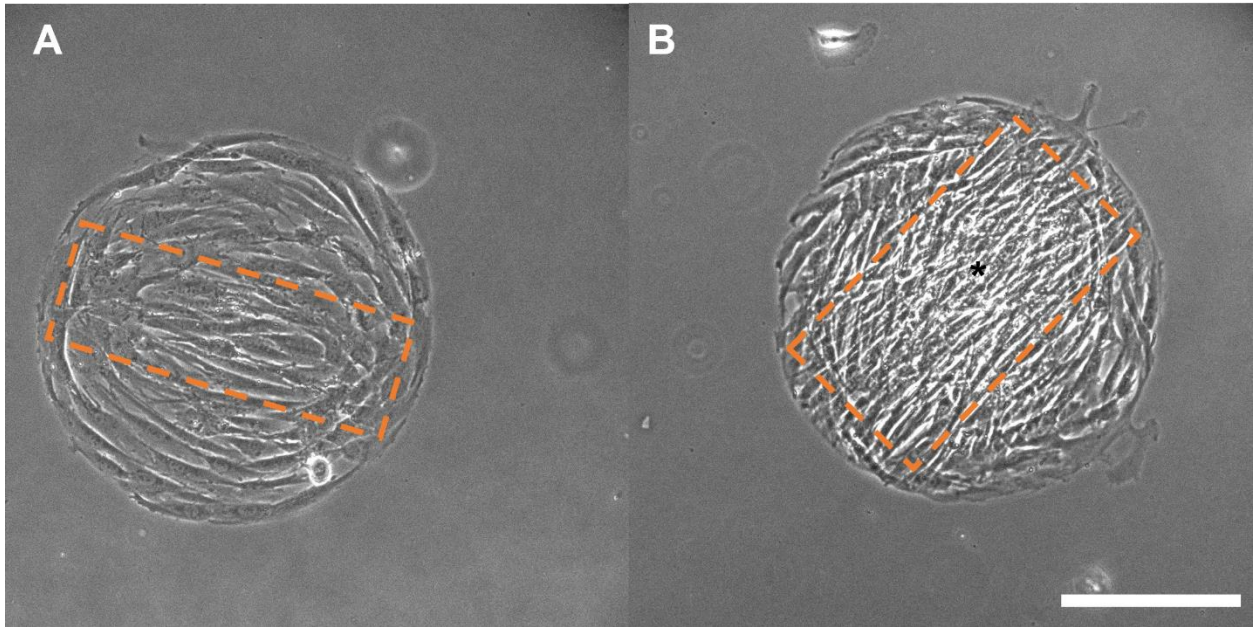
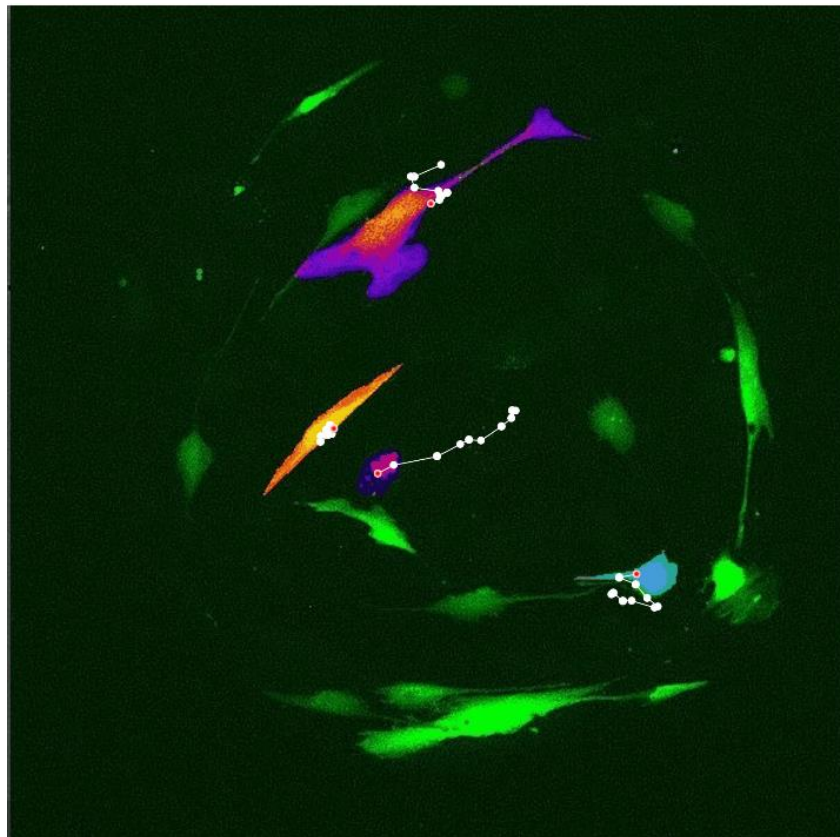


*Figure S.3-4. Banding (A, B) and hyperconfluency (B) are observed in human dermal fibroblast (HDF) aggregates (\* indicates hyperconfluent region). Scale bar = 200  $\mu\text{m}$ .*



### Chapter III: Multicellular Aligned Bands Disrupt Global Collective Cell Behavior

Figure S.3-5. Trace of the cells in Movie S1 is shown. Each dot is the center of the rectangle containing the cell's area. The red dot on each trace corresponds to the last frame

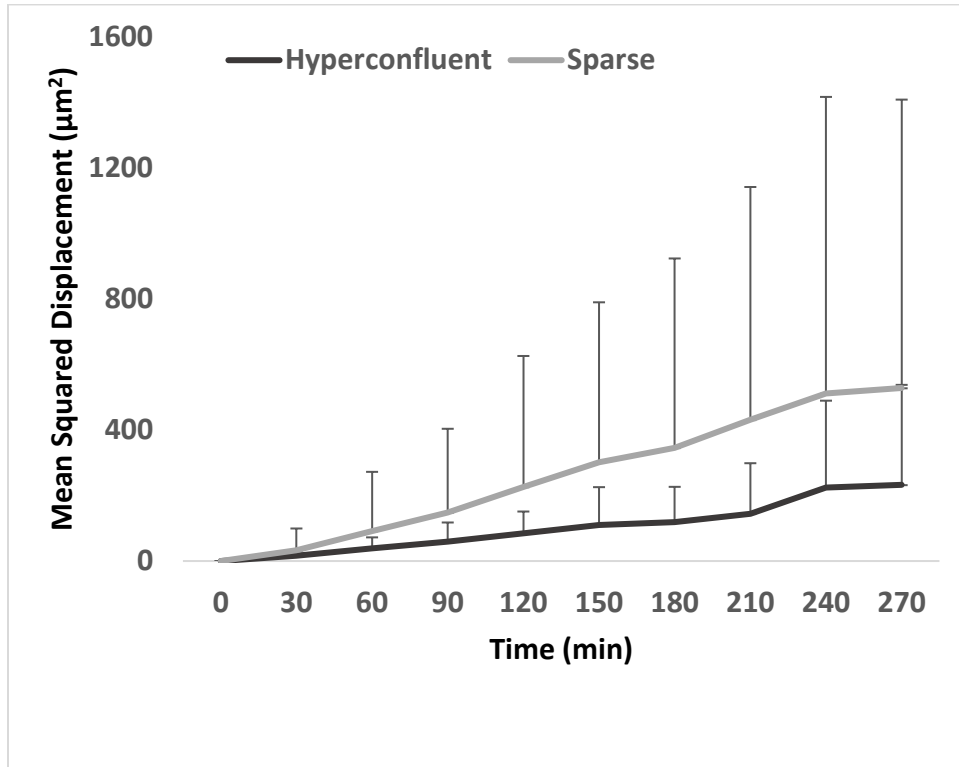
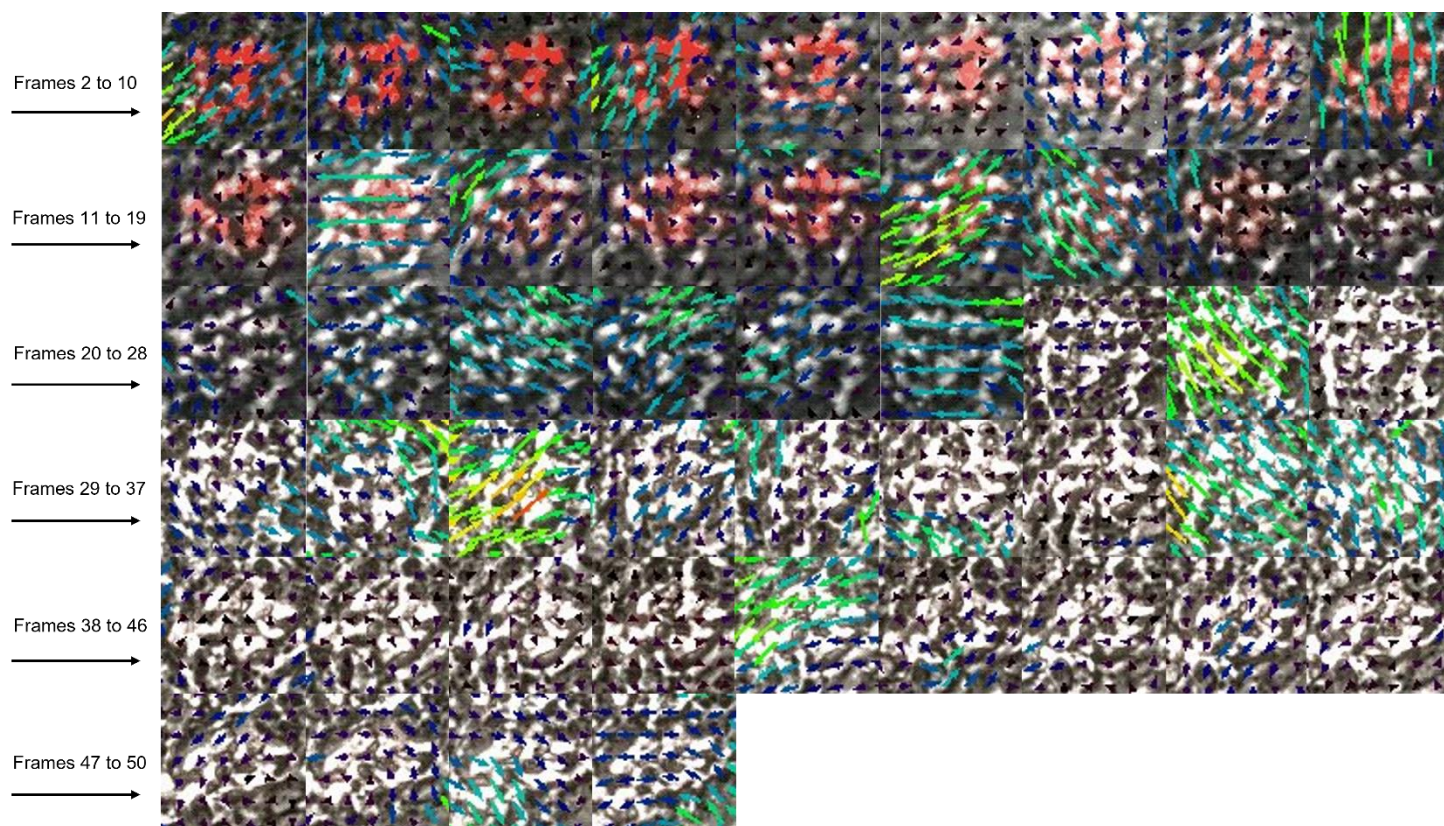
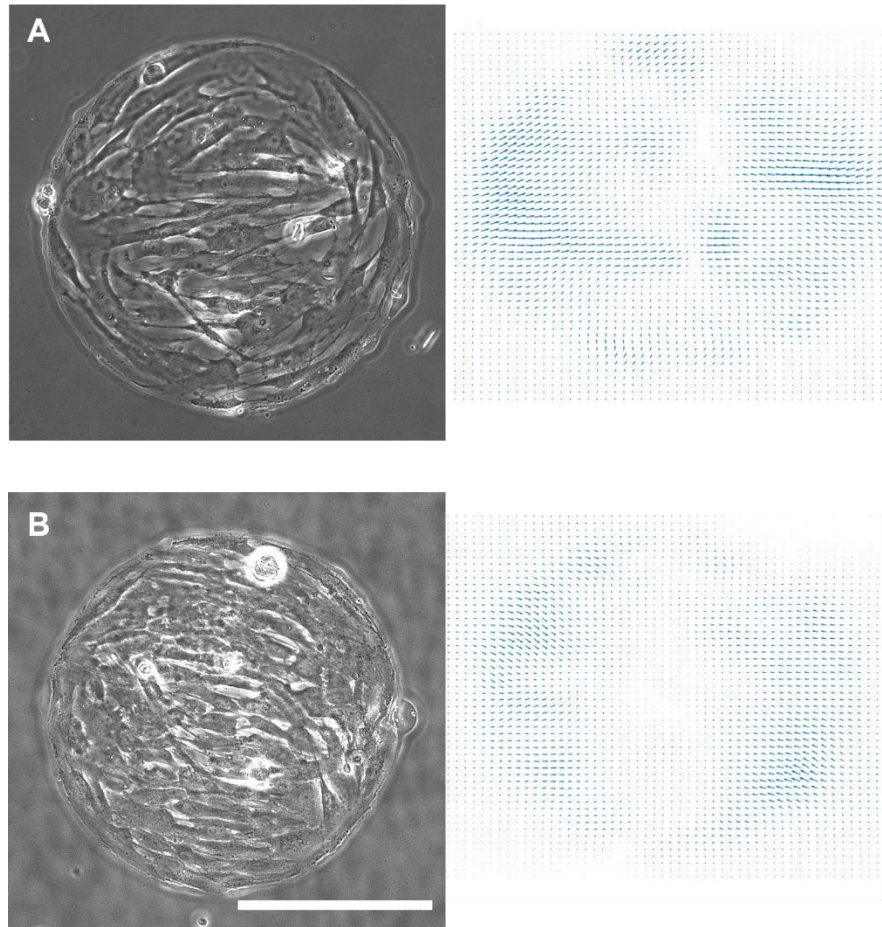


Figure S.3-6. Cells in hyperconfluency move coherently, significantly less farther from their starting point ( $p < 0.01$ ). Mean Squared Displacement for cells in hyperconfluent regions vs other regions shows the cells in hyperconfluency compared to the cells in other regions do not move far from their initial location ( $n = 56$  cells including 10 cells in hyperconfluent regions in 6 different aggregates and 46 cells in 9 different aggregates in sparse regions).

### Chapter III: Multicellular Aligned Bands Disrupt Global Collective Cell Behavior



*Figure S.3-7. Cells move together in hyperconfluency. Corresponding to frames, 30 mins apart, of the hyperconfluent region in the Supplemental Movie 2C. In 60% of the frames there is little to now movement, black arrows, where in others there is no random and independent movement of the cells, and the arrows are mostly in cool colors showing low magnitude of the movement.*



*Figure S.3-8. TFM vector plots show direction of traction force is along the long axis of the band. A) Phase image of a sparse aggregate and corresponding traction force vectors. B) Phase image of a confluent aggregate and corresponding traction force vectors. Scale bar = 200  $\mu\text{m}$ .*

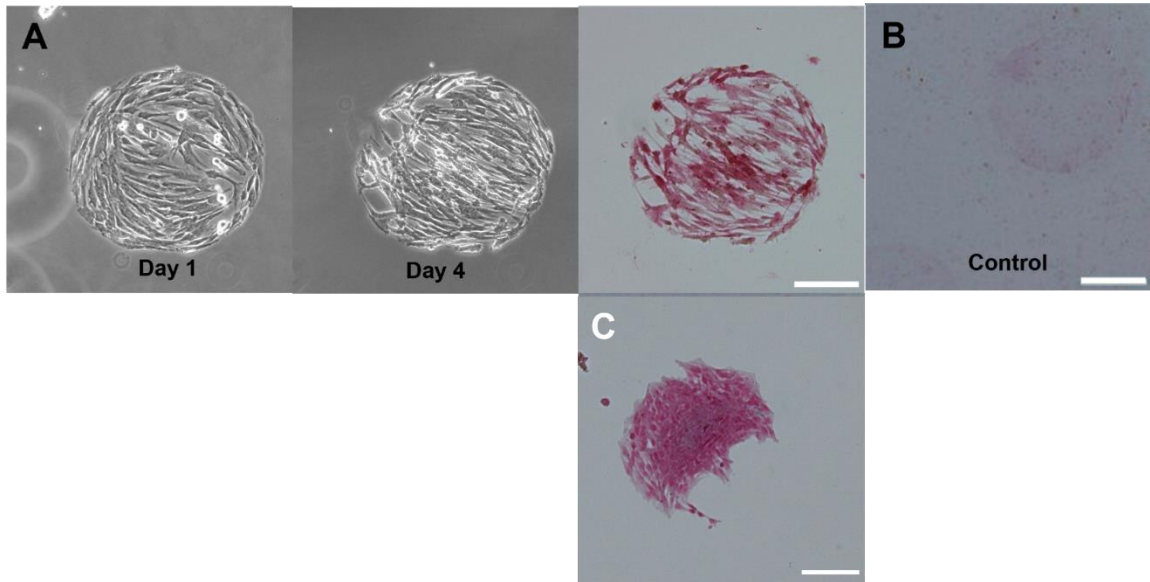


*Figure S.3-9. Collagen stained with Ponceau S after self-detached stage shows the removal of the collagen from the PA gel surface. A) shows the same aggregate with cells on areas where later the cells are detached. B) Control substrate with printed collagen stained with Ponceau S, showing pink halos on the surface. C) An aggregate stained with Picrosirius red. Scale bar = 200  $\mu\text{m}$ . The brightness of images has been manipulated for the purpose of presentation.*

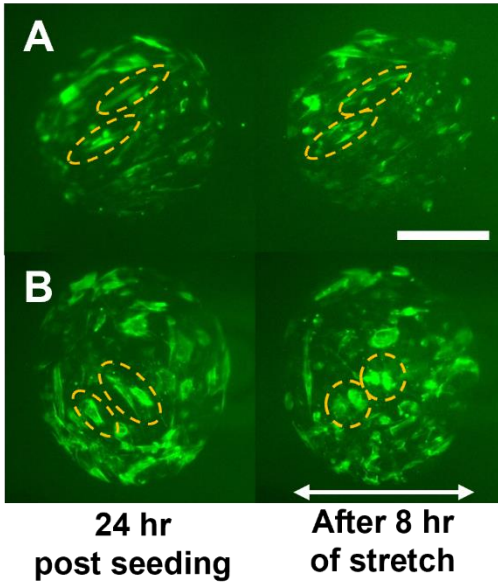
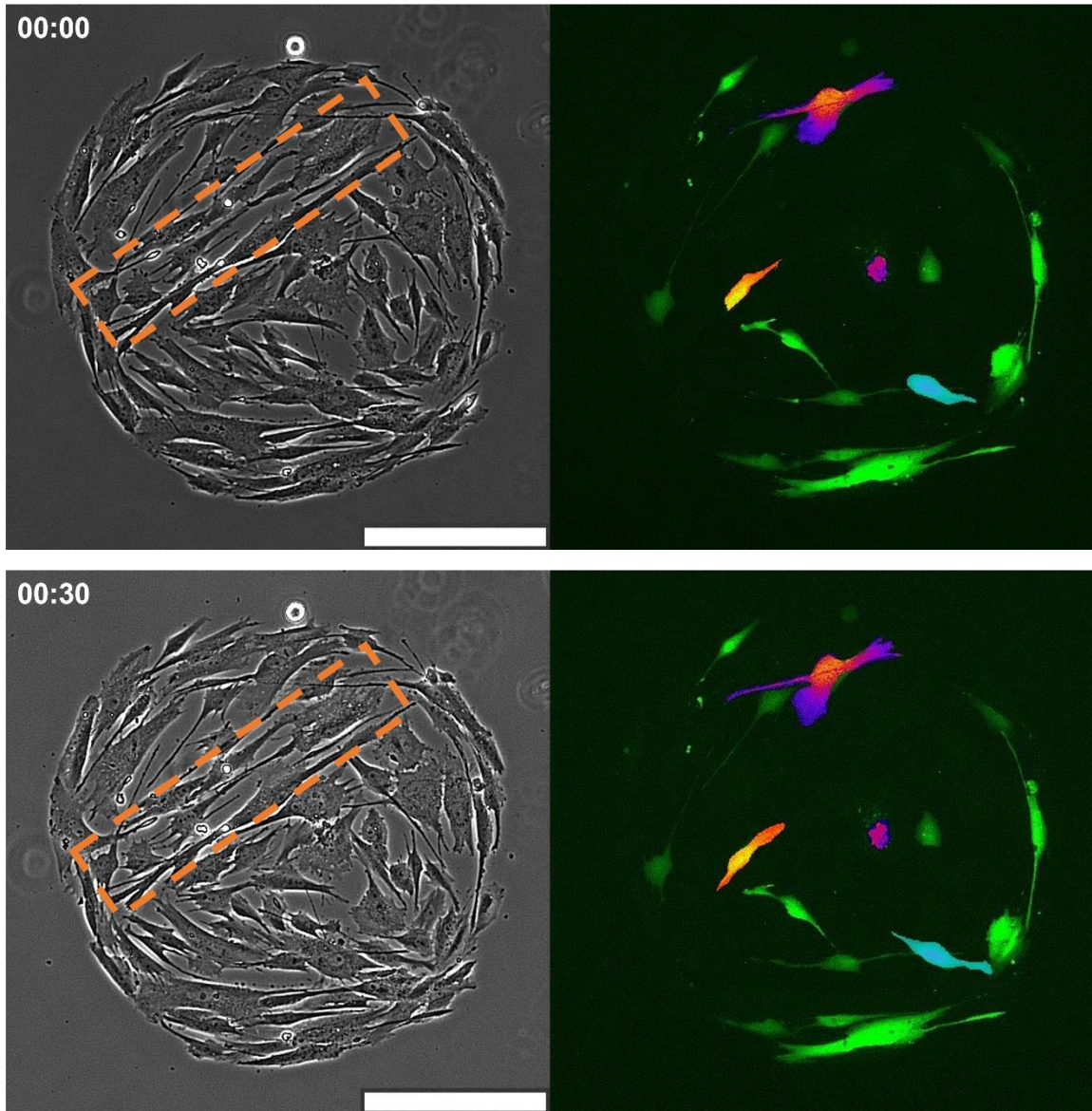


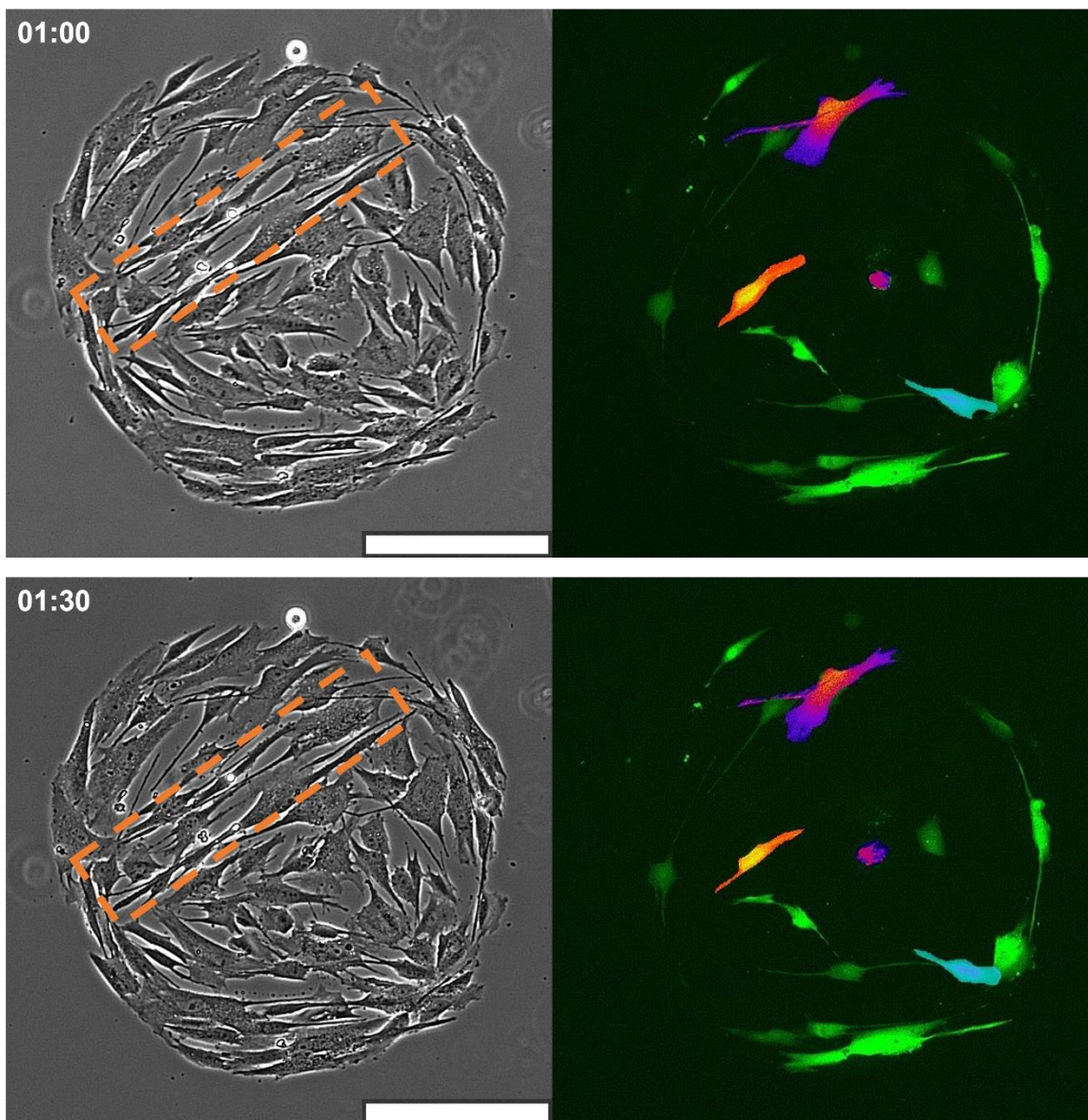
*Figure S.3-10. Dynamic stretch reinforces F-actin alignment for cells in the direction of stretch and disrupts the cytoskeleton of cells aligned away from the stretch axis. A) Representative example of cells within a band aligned at an intermediate angle ( $\sim 30^\circ$ ) in which the F-actin is intensified but the cell reorientation is minimal. B) Representative example of elongated cells within a band oriented greater than  $45^\circ$  from the stretch axis in which the F-actin cytoskeleton is disrupted and the cells become rounded. For all panels, F-actin of live VICs was stained with CellMask™ Actin before and after application of 10% uniaxial stretch for 8 hr at 1 Hz; brightly stained cells inside of bands are outlined by ellipses to show change in orientation and elongation. Scale bar = 200  $\mu\text{m}$ .*

### 3.11 Appendix 3

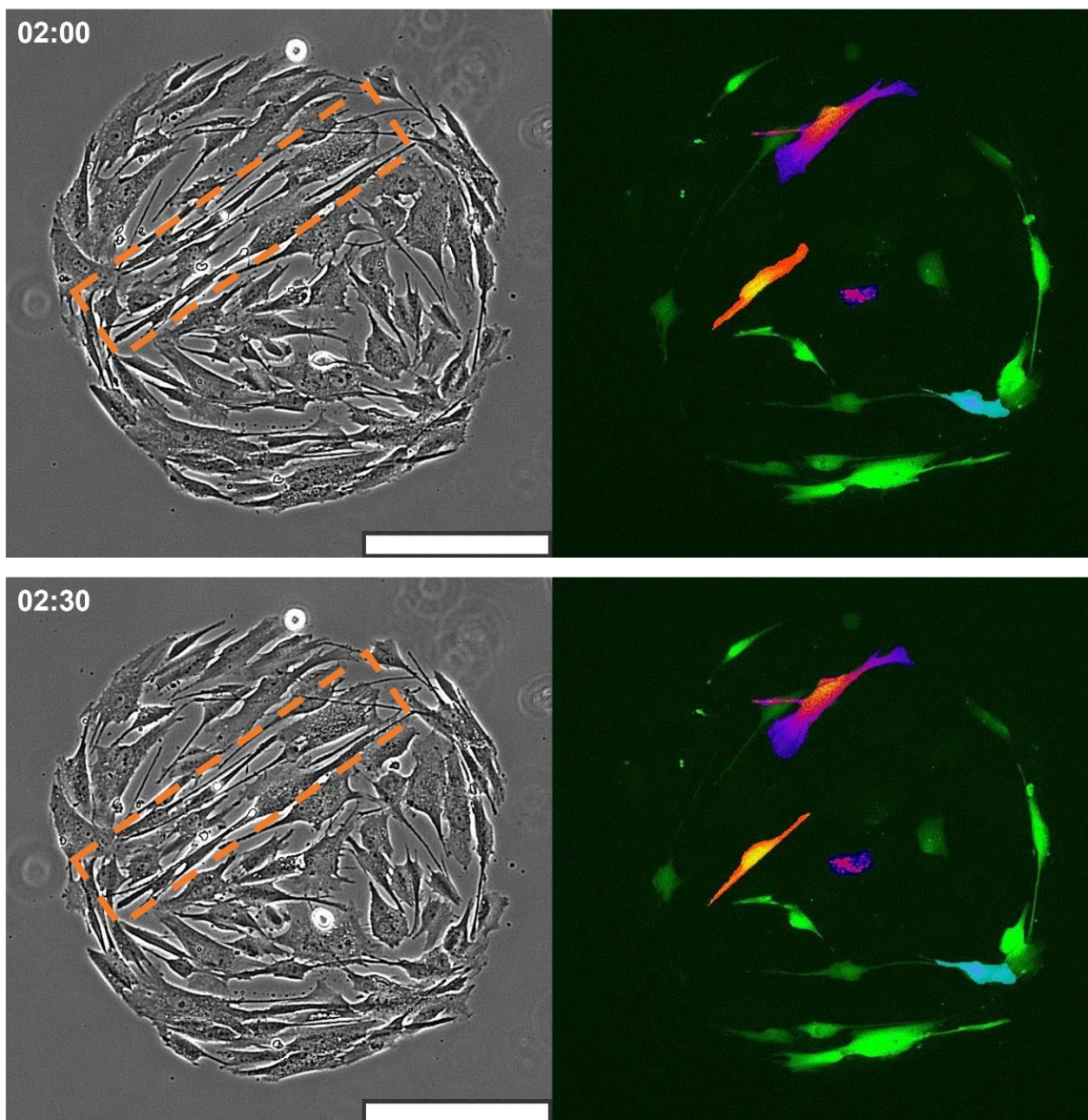
#### 3.11.1 Movie 1:



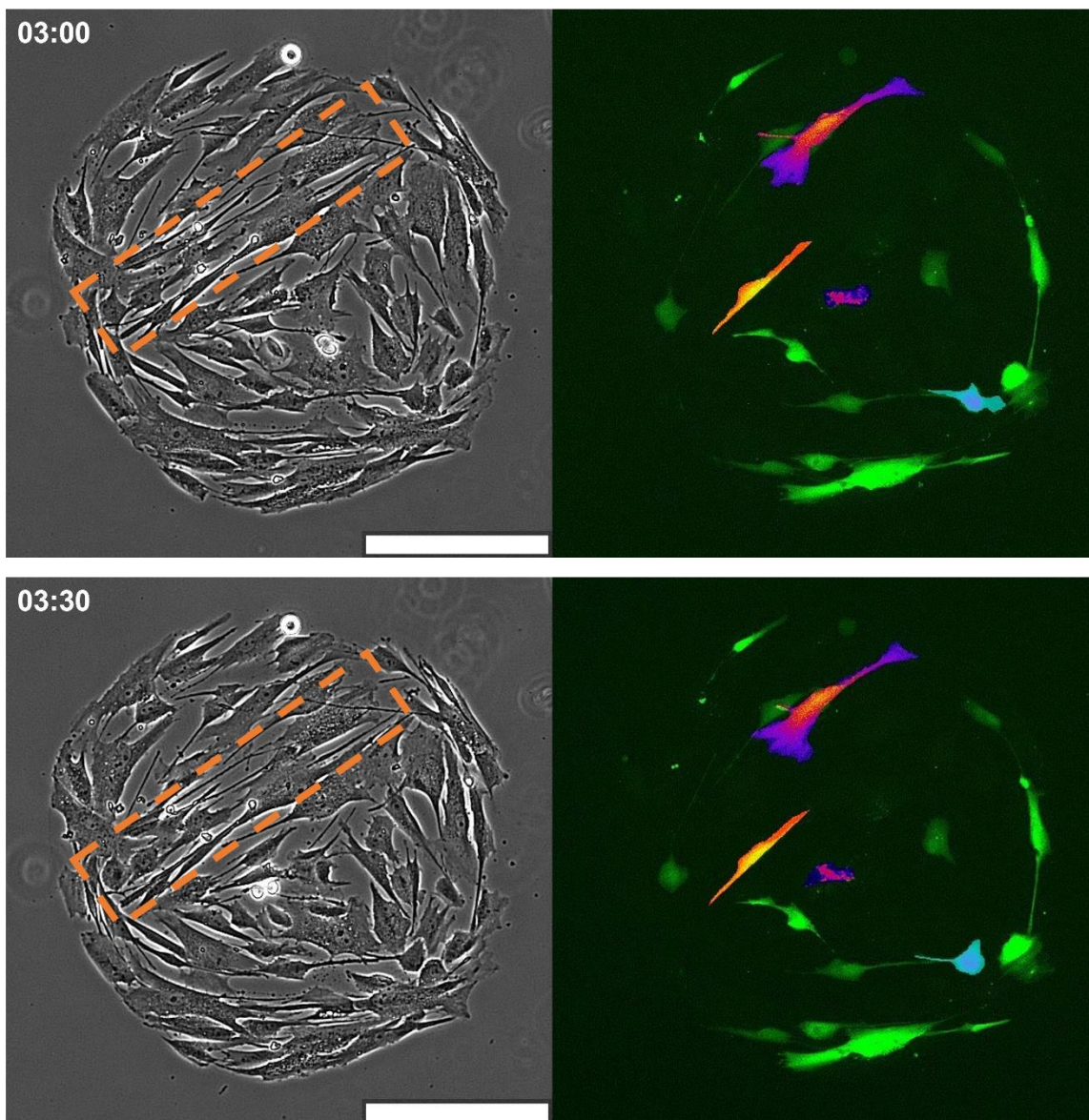
Chapter III: Multicellular Aligned Bands Disrupt Global Collective Cell Behavior



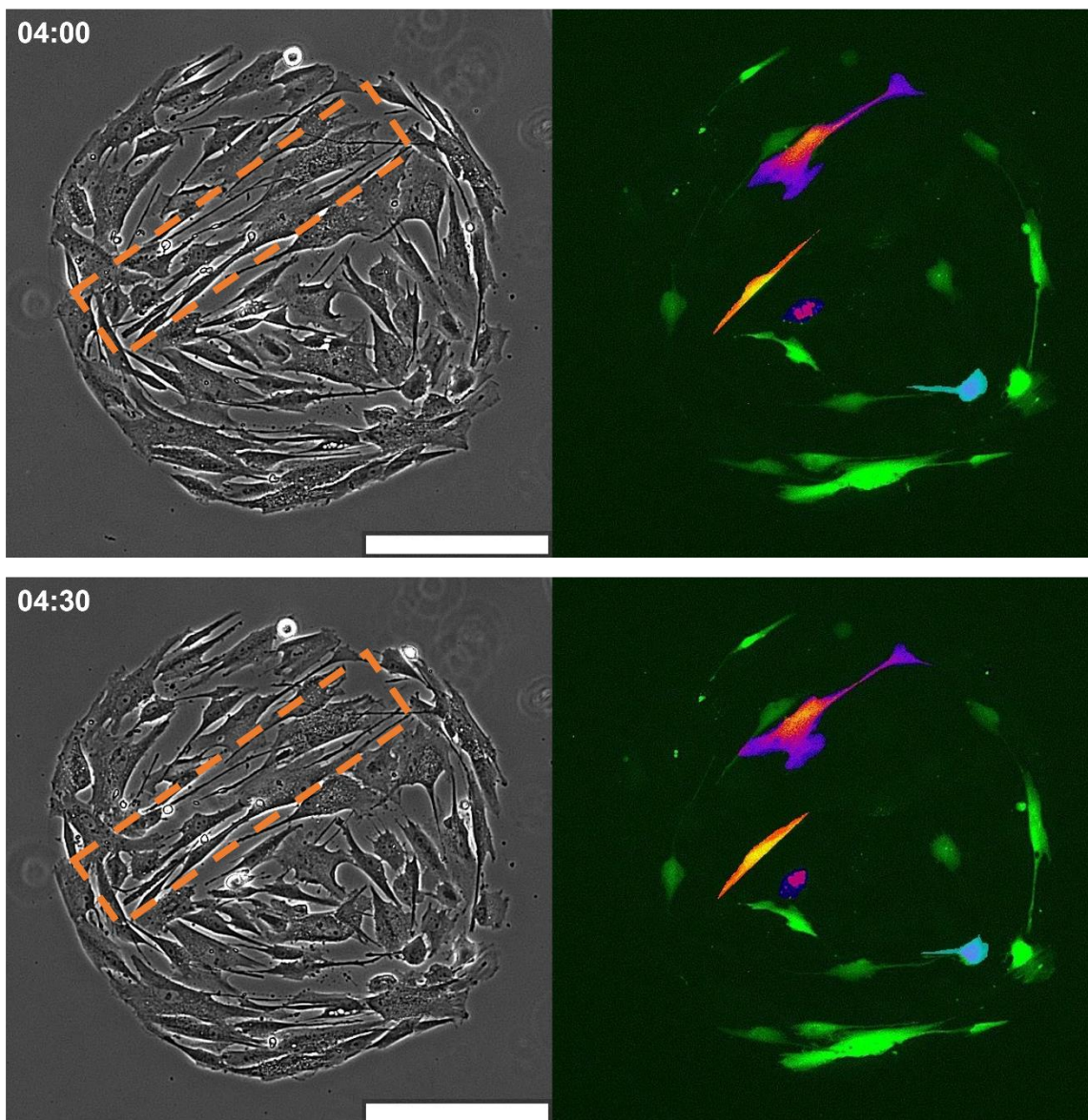
Chapter III: Multicellular Aligned Bands Disrupt Global Collective Cell Behavior

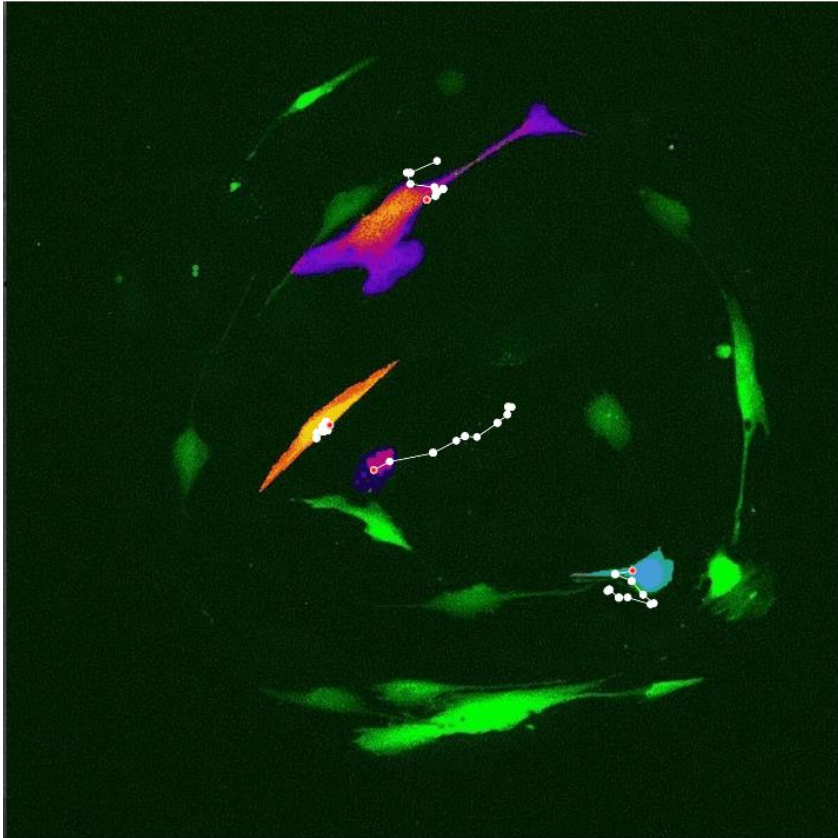


Chapter III: Multicellular Aligned Bands Disrupt Global Collective Cell Behavior



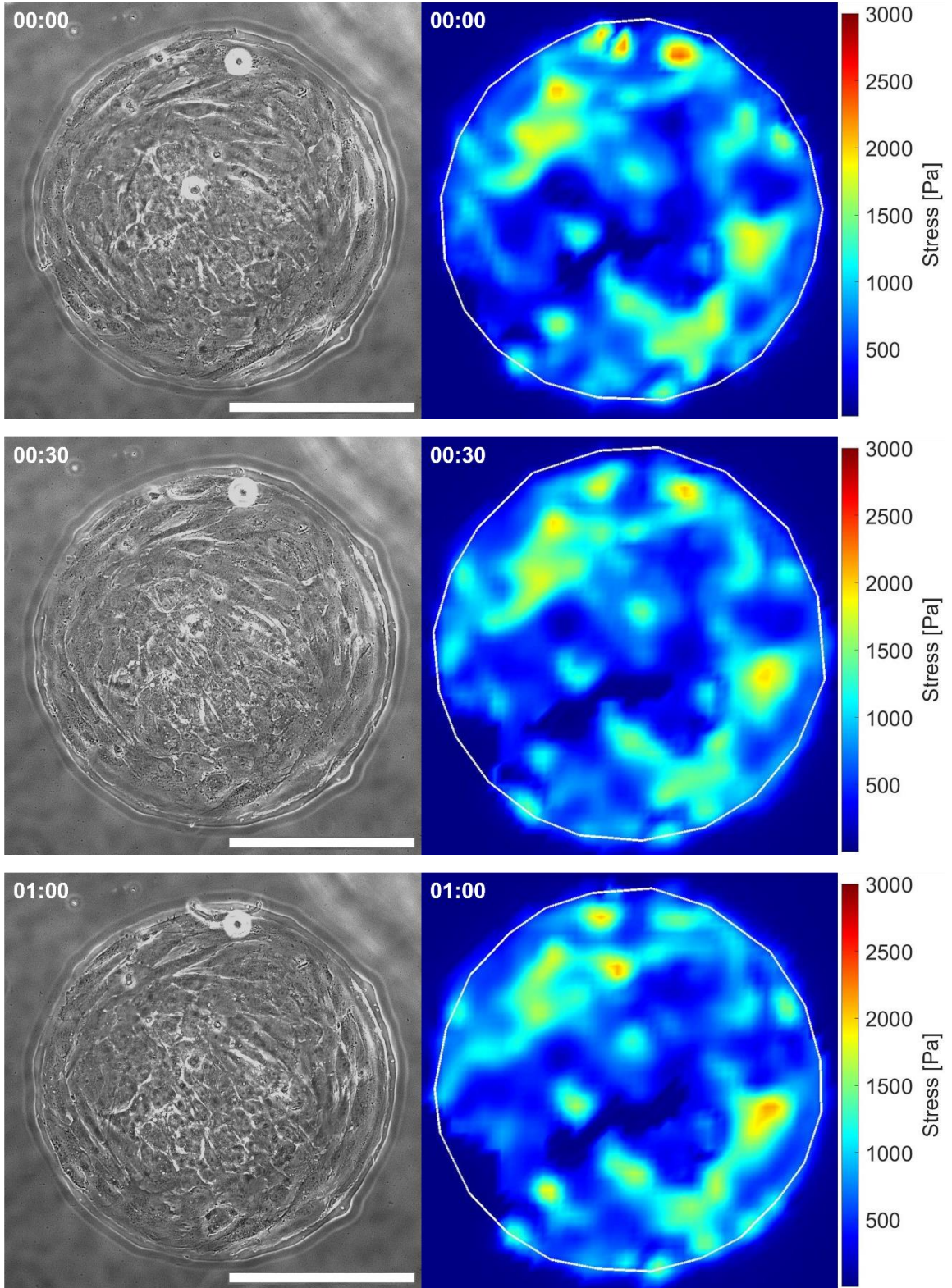
Chapter III: Multicellular Aligned Bands Disrupt Global Collective Cell Behavior



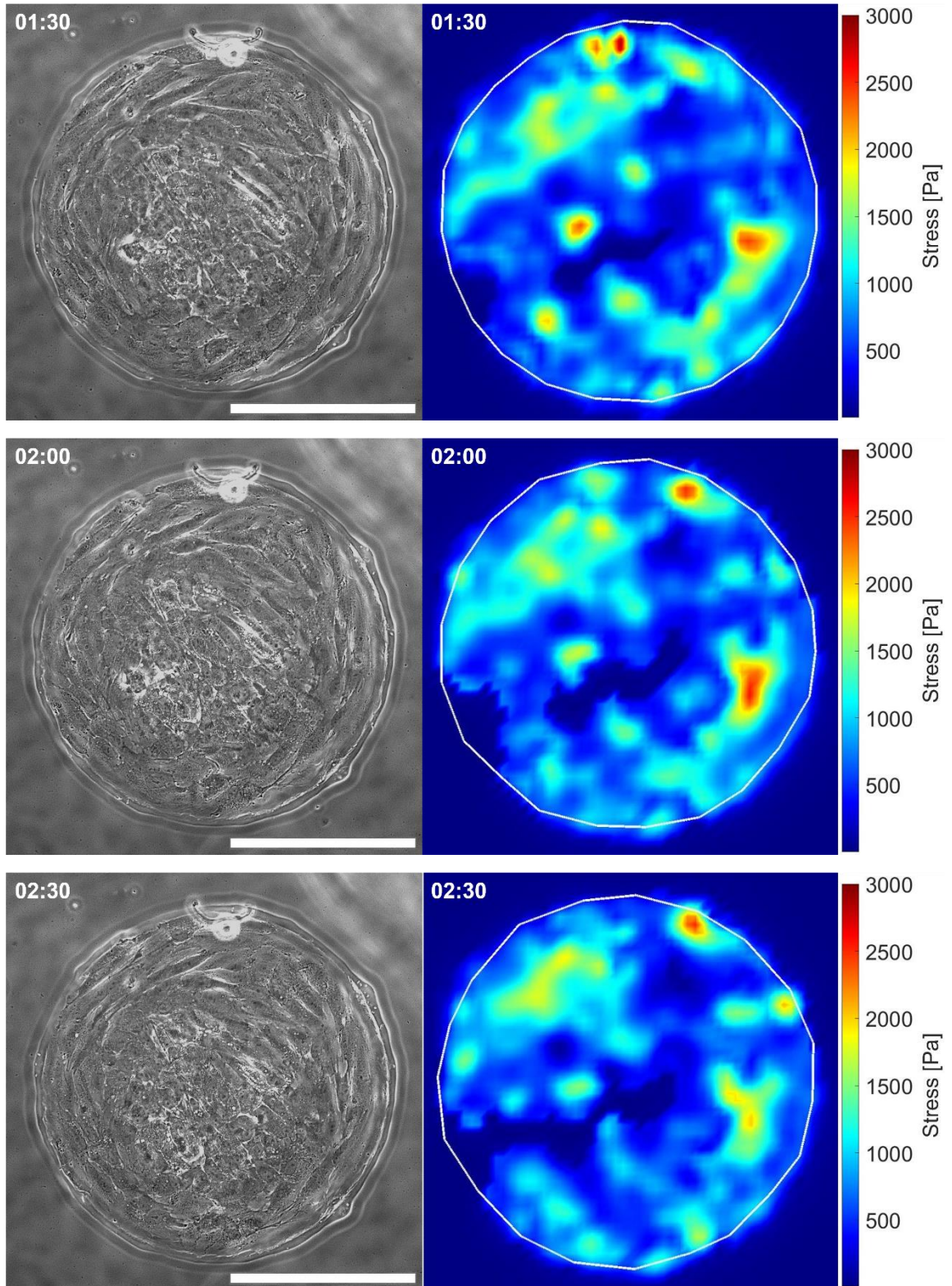


*Movie 1. Trace of the cells is shown. Each dot is the center of the rectangle containing the cell's area. The red dot on each trace corresponds to the last frame.*

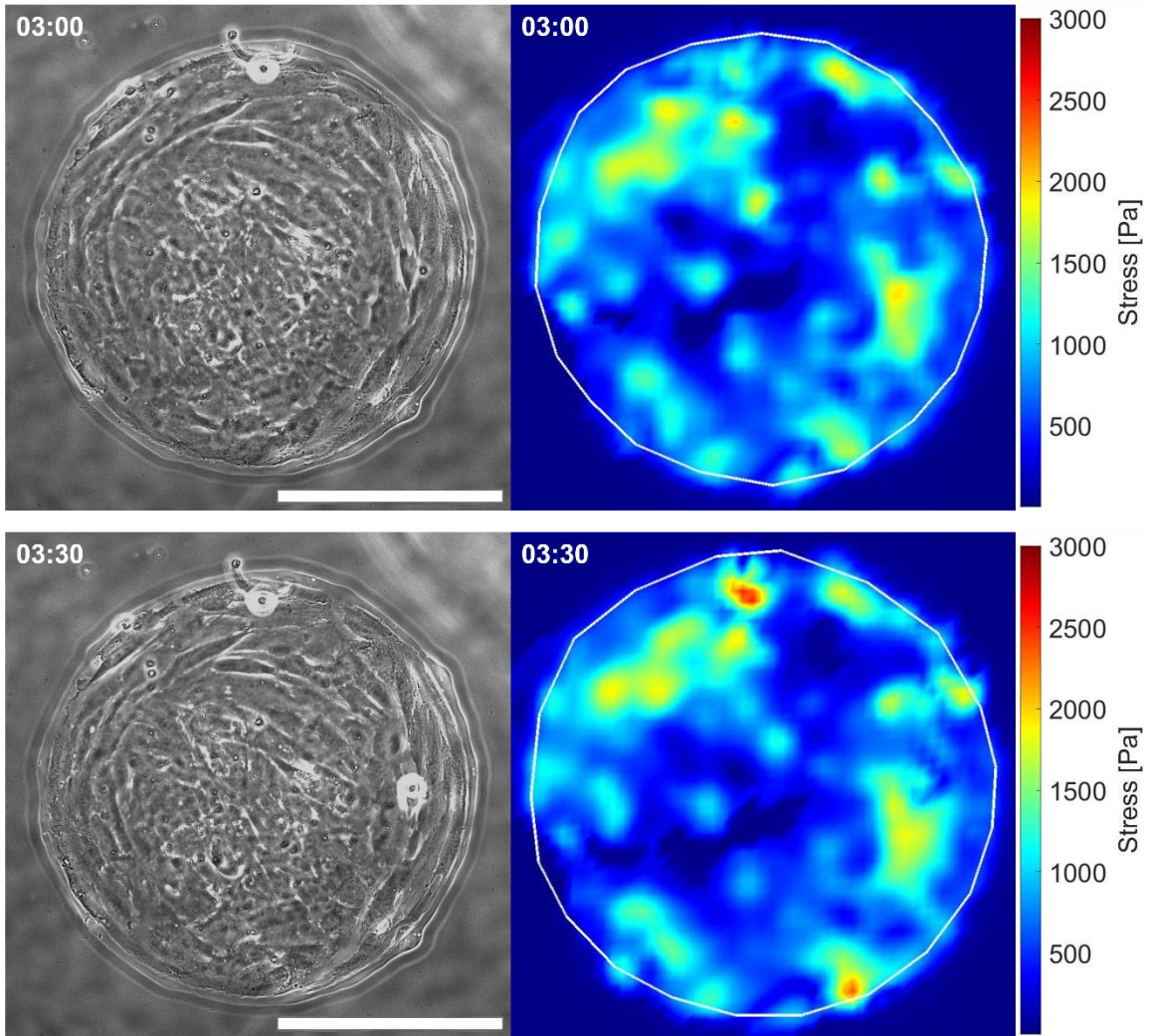
3.11.2 Movie 3

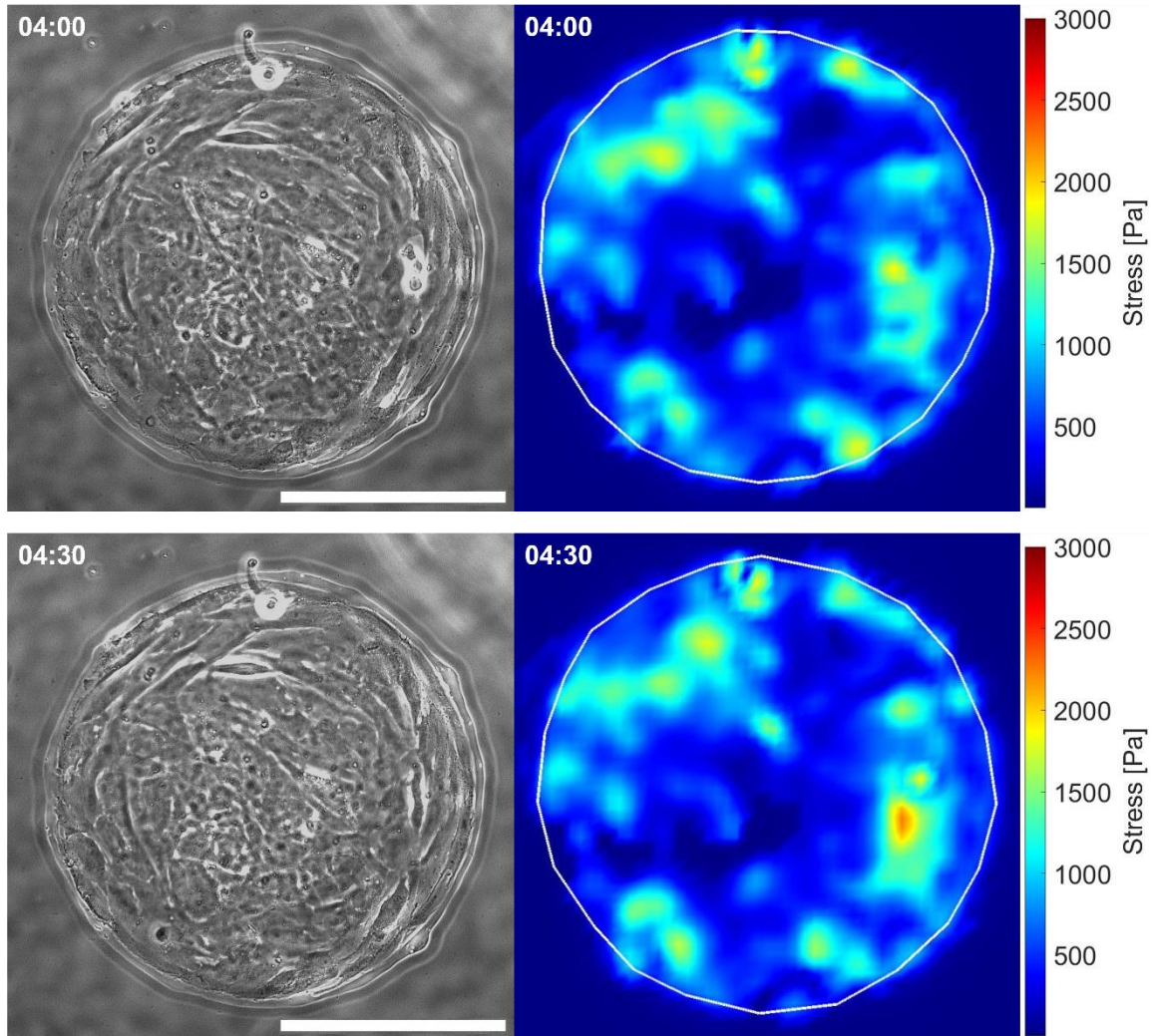


Chapter III: Multicellular Aligned Bands Disrupt Global Collective Cell Behavior



Chapter III: Multicellular Aligned Bands Disrupt Global Collective Cell Behavior





### 3.12 References

Aragona, M., T. Panciera, A. Manfrin, S. Giullitti, F. Michielin, N. Elvassore, S. Dupont and S. Piccolo (2013). "A Mechanical Checkpoint Controls Multicellular Growth through Yap/Taz Regulation by Actin-Processing Factors." *Cell* **154**(5): 1047-1059.

Atia, L., D. Bi, Y. Sharma, J. A. Mitchel, B. Gweon, S. Koehler, S. J. DeCamp, B. Lan, J. H. Kim, R. Hirsch, A. F. Pegoraro, K. H. Lee, J. R. Starr, D. A. Weitz, A. C. Martin, J. A. Park, J. P. Butler and J. J. Fredberg (2018). "Geometric Constraints During Epithelial Jamming." *Nature Physics* **14**: 613-620.

Berent, Z. T., I. Jain, G. H. Underhill and A. J. Wagoner Johnson (2022). "Simulated Confluence on Micropatterned Substrates Correlates Responses Regulating Cellular Differentiation." *Biotechnology and Bioengineering* **119**(6): 1641-1659.

Bogdanova, M., A. Zahirnyk, A. Malashicheva, K. Z. Enayati, T. A. Karlsen, M.-L. Kaljusto, J.-P. E. Kvitting, E. Dissen, G. J. Sullivan, A. Kostareva, K.-O. Stensl kken, A. Rutkovskiy and J.

### Chapter III: Multicellular Aligned Bands Disrupt Global Collective Cell Behavior

Vaage (2019). "Interstitial Cells in Calcified Aortic Valves Have Reduced Differentiation Potential and Stem Cell-Like Properties." Scientific Reports **9**(1): 12934.

Brown, R. A., R. Prajapati, D. A. McGrouther, I. V. Yannas and M. Eastwood (1998). "Tensional Homeostasis in Dermal Fibroblasts: Mechanical Responses to Mechanical Loading in Three-Dimensional Substrates." Journal of Cellular Physiology **175**(3): 323-332.

Calvo, F., N. Ege, A. Grande-Garcia, S. Hooper, R. P. Jenkins, S. I. Chaudhry, K. Harrington, P. Williamson, E. Moeendarbary, G. Charras and E. Sahai (2013). "Mechanotransduction and Yap-Dependent Matrix Remodelling Is Required for the Generation and Maintenance of Cancer-Associated Fibroblasts." Nature Cell Biology **15**(6): 637-646.

Camley, B. A. and W.-J. Rappel (2017). "Physical Models of Collective Cell Motility: From Cell to Tissue." Journal of physics D: Applied physics **50**(11): 113002.

Carlson, M. A., A. K. Prall, J. J. Gums, A. Lesiak and V. K. Shostrom (2009). "Biologic Variability of Human Foreskin Fibroblasts in 2d and 3d Culture: Implications for a Wound Healing Model." BMC Research Notes **2**(1): 229.

Chansard, A., N. Dubrulle, M. Poujol de Molliens, P. B. Falanga, T. Stephen, M. Hasan, G. van Zandbergen, N. Aulner, S. L. Shorte and B. David-Watine (2021). "Unveiling Interindividual Variability of Human Fibroblast Innate Immune Response Using Robust Cell-Based Protocols." Frontiers in Immunology **11**: 569331-569331.

Cirka, H., M. Monterosso, N. Diamantides, J. Favreau, Q. Wen and K. Billiar (2016). "Active Traction Force Response to Long-Term Cyclic Stretch Is Dependent on Cell Pre-Stress." Biophys J **110**(8): 1845-1857.

Cirka, H. A., J. Uribe, V. Liang, F. J. Schoen and K. L. Billiar (2017). "Reproducible in Vitro Model for Dystrophic Calcification of Cardiac Valvular Interstitial Cells: Insights into the Mechanisms of Calcific Aortic Valvular Disease." Lab Chip **17**(5): 814-829.

Codelia, V. A., G. Sun and K. D. Irvine (2014). "Regulation of Yap by Mechanical Strain through Jnk and Hippo Signaling." Current Biology **24**(17): 2012-2017.

Das, A., R. S. Fischer, D. Pan and C. M. Waterman (2016). "Yap Nuclear Localization in the Absence of Cell-Cell Contact Is Mediated by a Filamentous Actin-Dependent, Myosin Ii- and Phospho-Yap-Independent Pathway During Extracellular Matrix Mechanosensing." J Biol Chem **291**(12): 6096-6110.

Deglinerti, A., F. Etoc, M. C. Guerra, I. Martyn, J. Metzger, A. Ruzo, M. Simunovic, A. Yoney, A. H. Brivanlou, E. Siggia and A. Warmflash (2016). "Self-Organization of Human Embryonic Stem Cells on Micropatterns." Nature Protocols **11**(11): 2223-2232.

Doxzen, K., S. R. K. Vedula, M. C. Leong, H. Hirata, N. S. Gov, A. J. Kabla, B. Ladoux and C. T. Lim (2013). "Guidance of Collective Cell Migration by Substrate Geometry." Integrative Biology **5**(8): 1026-1035.

Duclos, G., C. Erenkämper, J.-F. Joanny and P. Silberzan (2017). "Topological Defects in Confined Populations of Spindle-Shaped Cells." Nature Physics **13**(1): 58-62.

### Chapter III: Multicellular Aligned Bands Disrupt Global Collective Cell Behavior

- Dupont, S., L. Morsut, M. Aragona, E. Enzo, S. Giulitti, M. Cordenonsi, F. Zanconato, J. Le Digabel, M. Forcato, S. Bicciato, N. Elvassore and S. Piccolo (2011). "Role of Yap/Taz in Mechanotransduction." Nature **474**(7350): 179-183.
- Dutta, S., S. Mana-Capelli, M. Paramasivam, I. Dasgupta, H. Cirka, K. Billiar and D. McCollum (2018). "Trip6 Inhibits Hippo Signaling in Response to Tension at Adherens Junctions." EMBO reports **19**(2): 337-350.
- Egerbacher, M., S. P. Arnoczky, O. Caballero, M. Lavagnino and K. L. Gardner (2008). "Loss of Homeostatic Tension Induces Apoptosis in Tendon Cells: An in Vitro Study." Clinical orthopaedics and related research **466**(7): 1562-1568.
- Fisher, C. I., J. Chen and W. D. Merryman (2012). "Calcific Nodule Morphogenesis by Heart Valve Interstitial Cells Is Strain Dependent." Biomechanics and modeling in mechanobiology **1**.
- Foolen, J., M. W. J. T. Janssen-van den Broek and F. P. T. Baaijens (2014). "Synergy between Rho Signaling and Matrix Density in Cyclic Stretch-Induced Stress Fiber Organization." Acta Biomaterialia **10**(5): 1876-1885.
- Garcia, S., E. Hannezo, J. Elgeti, J.-F. Joanny, P. Silberzan and S. Gov Nir (2015). "Physics of Active Jamming During Collective Cellular Motion in a Monolayer." Proceedings of the National Academy of Sciences **112**(50): 15314-15319.
- G eremie, L., E. Ilker, M. Bernheim-Dennery, C. Cavaniol, J.-L. Viovy, D. M. Vignjevic, J.-F. Joanny and S. Descroix (2022). "Evolution of a Confluent Gut Epithelium under on-Chip Cyclic Stretching." Physical Review Research **4**(2): 023032.
- Goldblatt, Z. E., H. Ashouri Choshali, H. A. Cirka, V. Liang, Q. Wen, D. McCollum, N. Rahbar and K. L. Billiar (2020). "Heterogeneity Profoundly Alters Emergent Stress Fields in Constrained Multicellular Systems." Biophysical Journal **118**(1): 15-25.
- Gould, R. A. and J. T. Butcher (2010). "Isolation of Valvular Endothelial Cells." Journal of Visualized Experiments(46): 2158.
- Greiner, A., H. Chen, J. Spatz and R. Kemkemer (2013). "Cyclic Tensile Strain Controls Cell Shape and Directs Actin Stress Fiber Formation and Focal Adhesion Alignment in Spreading Cells." PLoS One **8**: e77328.
- He, S., C. Liu, X. Li, S. Ma, B. Huo and B. Ji (2015). "Dissecting Collective Cell Behavior in Polarization and Alignment on Micropatterned Substrates." Biophysical Journal **109**(3): 489-500.
- Humphrey, J. D., E. R. Dufresne and M. A. Schwartz (2014). "Mechanotransduction and Extracellular Matrix Homeostasis." Nature reviews. Molecular cell biology **15**(12): 802-812.
- Jebeli, M., S. K. Lopez, Z. E. Goldblatt, D. McCollum, S. Mana-Capelli, Q. Wen and K. Billiar (2022). "Multicellular Aligned Bands Disrupt Global Collective Cell Behavior." Acta Biomaterialia.
- Jian, B., N. Narula, Q.-y. Li, E. R. Mohler and R. J. Levy (2003). "Progression of Aortic Valve Stenosis: Tgf-B1 Is Present in Calcified Aortic Valve Cusps and Promotes Aortic Valve Interstitial Cell Calcification Via Apoptosis." The Annals of thoracic surgery **75**(2): 457-465.

### Chapter III: Multicellular Aligned Bands Disrupt Global Collective Cell Behavior

- Kahl, C. R. and A. R. Means (2003). "Regulation of Cell Cycle Progression by Calcium/Calmodulin-Dependent Pathways." Endocr Rev **24**(6): 719-736.
- Kaunas, R., P. Nguyen, S. Usami and S. Chien (2005). "Cooperative Effects of Rho and Mechanical Stretch on Stress Fiber Organization." Proceedings of the National Academy of Sciences **102**(44): 15895-15900.
- Kloxin, A. M., J. A. Benton and K. S. Anseth (2010). "In Situ Elasticity Modulation with Dynamic Substrates to Direct Cell Phenotype." Biomaterials **31**(1): 1-8.
- Ladoux, B. and R.-M. Mège (2017). "Mechanobiology of Collective Cell Behaviours." Nature Reviews Molecular Cell Biology **18**(12): 743-757.
- Li, B., F. Li, H. X. Li, X. C. Xu, M. Szczodry, Z. C. Yang, J. S. Lin and J. H. C. Wang (2006). "Cellular Mechanical Stress Gradient Regulates Cell Proliferation and Differentiation Patterns." Molecular and Cellular Biomechanics **3**(4).
- Li, B., F. Li, K. M. Puskar and J. H. Wang (2009). "Spatial Patterning of Cell Proliferation and Differentiation Depends on Mechanical Stress Magnitude." Journal of biomechanics **42**(11): 1622-1627.
- Li, B. and Sean X. Sun (2014). "Coherent Motions in Confluent Cell Monolayer Sheets." Biophysical Journal **107**(7): 1532-1541.
- Lin, S.-Z., W.-Y. Zhang, D. Bi, B. Li and X.-Q. Feng (2021). "Energetics of Mesoscale Cell Turbulence in Two-Dimensional Monolayers." Communications Physics **4**(1): 21.
- Lin, Z., P. Zhou, A. von Gise, F. Gu, Q. Ma, J. Chen, H. Guo, P. R. R. van Gorp, D.-Z. Wang and W. T. Pu (2015). "Pi3kcb Links Hippo-Yap and Pi3k-Akt Signaling Pathways to Promote Cardiomyocyte Proliferation and Survival." Circulation research **116**(1): 35-45.
- Liu, C., S. He, X. Li, B. Huo and B. Ji (2016). "Mechanics of Cell Mechanosensing on Patterned Substrate." Journal of Applied Mechanics **83**(5): 051014.
- Liu, Y., K. He, Y. Hu, X. Guo, D. Wang, W. Shi, J. Li and J. Song (2017). "Yap Modulates Tgf-B1-Induced Simultaneous Apoptosis and Emt through Upregulation of the Egf Receptor." Scientific Reports **7**(1): 45523.
- Lynch, M. D. and F. M. Watt (2018). "Fibroblast Heterogeneity: Implications for Human Disease." The Journal of Clinical Investigation **128**(1): 26-35.
- Ma, H., A. R. Killaars, F. W. DelRio, C. Yang and K. S. Anseth (2017). "Myofibroblastic Activation of Valvular Interstitial Cells Is Modulated by Spatial Variations in Matrix Elasticity and Its Organization." Biomaterials **131**: 131-144.
- Maruthamuthu, V., B. Sabass, U. S. Schwarz and M. L. Gardel (2011). "Cell-Ecm Traction Force Modulates Endogenous Tension at Cell-Cell Contacts." Proc Natl Acad Sci U S A **108**(12): 4708-4713.

### Chapter III: Multicellular Aligned Bands Disrupt Global Collective Cell Behavior

- Mascharak, S., P. L. Benitez, A. C. Proctor, C. M. Madl, K. H. Hu, R. E. Dewi, M. J. Butte and S. C. Heilshorn (2017). "Yap-Dependent Mechanotransduction Is Required for Proliferation and Migration on Native-Like Substrate Topography." Biomaterials **115**: 155-166.
- Moussus, M., C. d. Loughian, D. Fuard, M. Courçon, D. Gulino-Debrac, H. Delanoë-Ayari and A. Nicolas (2014). "Intracellular Stresses in Patterned Cell Assemblies." Soft Matter **10**(14): 2414-2423.
- Nanavati, B. N., A. S. Yap and J. L. Teo (2020). "Symmetry Breaking and Epithelial Cell Extrusion." Cells **9**(6).
- Nelson, C. M., R. P. Jean, J. L. Tan, W. F. Liu, N. J. Sniadecki, A. A. Spector and C. S. Chen (2005). "Emergent Patterns of Growth Controlled by Multicellular Form and Mechanics." Proceedings of the National Academy of Sciences of the United States of America **102**(33): 11594-11599.
- Ng, M. R., A. Besser, J. S. Brugge and G. Danuser (2014). "Mapping the Dynamics of Force Transduction at Cell–Cell Junctions of Epithelial Clusters." eLife **3**: e03282.
- Paek, J., J. W. Song, E. Ban, Y. Morimitsu, C. O. Osuji, V. B. Shenoy and D. D. Huh (2021). "Soft Robotic Constrictor for in Vitro Modeling of Dynamic Tissue Compression." Scientific Reports **11**(1): 16478.
- Pérez-González, C., R. Alert, C. Blanch-Mercader, M. Gómez-González, T. Kolodziej, E. Bazellieres, J. Casademunt and X. Trepat (2019). "Active Wetting of Epithelial Tissues." Nat Phys **15**(1): 79-88.
- Reinhart-King, C. A., M. Dembo and D. A. Hammer (2005). "The Dynamics and Mechanics of Endothelial Cell Spreading." Biophysical Journal **89**(1): 676-689.
- Ristori, T., T. M. W. Notermans, J. Foolen, N. A. Kurniawan, C. V. C. Bouten, F. P. T. Baaijens and S. Loerakker (2018). "Modelling the Combined Effects of Collagen and Cyclic Strain on Cellular Orientation in Collagenous Tissues." Scientific Reports **8**(1): 8518.
- Schaumann, E. N., M. F. Staddon, M. L. Gardel and S. Banerjee (2018). "Force Localization Modes in Dynamic Epithelial Colonies." Molecular biology of the cell **29**(23): 2835-2847.
- Sears, C. and R. Kaunas (2016). "The Many Ways Adherent Cells Respond to Applied Stretch." Journal of biomechanics **49**(8): 1347-1354.
- Shao, Y., X. Tan, R. Novitski, M. Muqaddam, P. List, L. Williamson, J. Fu and A. P. Liu (2013). "Uniaxial Cell Stretching Device for Live-Cell Imaging of Mechanosensitive Cellular Functions." The Review of scientific instruments **84**(11): 114304-114304.
- Silver, B. B., A. E. Wolf, J. Lee, M.-F. Pang and C. M. Nelson (2020). "Epithelial Tissue Geometry Directs Emergence of Bioelectric Field and Pattern of Proliferation." Molecular biology of the cell **31**(16): 1691-1702.
- Streichan, S. J., C. R. Hoerner, T. Schneidt, D. Holzer and L. Hufnagel (2014). "Spatial Constraints Control Cell Proliferation in Tissues." Proceedings of the National Academy of Sciences of the United States of America **111**(15): 5586-5591.

### Chapter III: Multicellular Aligned Bands Disrupt Global Collective Cell Behavior

- Tondon, A. and R. Kaunas (2014). "The Direction of Stretch-Induced Cell and Stress Fiber Orientation Depends on Collagen Matrix Stress." PLoS One **9**(2): e89592.
- Tran, R., C. Moraes and C. Hoesli (2020). "Controlled Clustering Enhances Pdx1 and Nkx6.1 Expression in Pancreatic Endoderm Cells Derived from Pluripotent Stem Cells." Scientific Reports **10**: 1190.
- Trepat, X. and J. J. Fredberg (2011). "Plithotaxis and Emergent Dynamics in Collective Cellular Migration." Trends in Cell Biology **21**(11): 638-646.
- Trepat, X., M. R. Wasserman, T. E. Angelini, E. Millet, D. A. Weitz, J. P. Butler and J. J. Fredberg (2009). "Physical Forces During Collective Cell Migration." Nature Physics **5**(6): 426-430.
- Uroz, M., S. Wistorf, X. Serra-Picamal, V. Conte, M. Sales-Pardo, P. Roca-Cusachs, R. Guimerà and X. Trepat (2018). "Regulation of Cell Cycle Progression by Cell–Cell and Cell–Matrix Forces." Nature Cell Biology **20**(6): 646-654.
- Vig, D. K., A. E. Hamby and C. W. Wolgemuth (2017). "Cellular Contraction Can Drive Rapid Epithelial Flows." Biophysical Journal **113**(7): 1613-1622.
- Vishwakarma, M., B. Thurakkal, J. P. Spatz and T. Das (2020). "Dynamic Heterogeneity Influences the Leader–Follower Dynamics During Epithelial Wound Closure." Philosophical Transactions of the Royal Society B: Biological Sciences **375**(1807): 20190391.
- Voccoli, V., I. Tonazzini, G. Signore, M. Caleo and M. Cecchini (2014). "Role of Extracellular Calcium and Mitochondrial Oxygen Species in Psychosine-Induced Oligodendrocyte Cell Death." Cell Death and Disease **5**(11): e1529-e1529.
- Wada, K.-I., K. Itoga, T. Okano, S. Yonemura and H. Sasaki (2011). "Hippo Pathway Regulation by Cell Morphology and Stress Fibers." Development **138**(18): 3907-3914.
- Wang, H., S. M. Haeger, A. M. Kloxin, L. A. Leinwand and K. S. Anseth (2012). "Redirecting Valvular Myofibroblasts into Dormant Fibroblasts through Light-Mediated Reduction in Substrate Modulus." PLoS One **7**(7): e39969-e39969.
- Wang, J. H. C., P. Goldschmidt-Clermont, J. Wille and F. C. P. Yin (2001). "Specificity of Endothelial Cell Reorientation in Response to Cyclic Mechanical Stretching." Journal of biomechanics **34**(12): 1563-1572.
- Wyatt, T. P. J., A. R. Harris, M. Lam, Q. Cheng, J. Bellis, A. Dimitracopoulos, A. J. Kabla, G. T. Charras and B. Baum (2015). "Emergence of Homeostatic Epithelial Packing and Stress Dissipation through Divisions Oriented Along the Long Cell Axis." Proceedings of the National Academy of Sciences **112**(18): 5726-5731.
- Xie, T., S. R. St Pierre, N. Olanont, L. E. Brown, M. Wu and Y. Sun (2021). "Condensation Tendency and Planar Isotropic Actin Gradient Induce Radial Alignment in Confined Monolayers." eLife **10**: e60381.
- Xu, J., X. Xu, X. Li, S. He, D. Li and B. Ji (2022). "Cellular Mechanics of Wound Formation in Single Cell Layer under Cyclic Stretching." Biophysical Journal **121**(2): 288-299.

### Chapter III: Multicellular Aligned Bands Disrupt Global Collective Cell Behavior

Yip Cindy Ying, Y., J.-H. Chen, R. Zhao and A. Simmons Craig (2009). "Calcification by Valve Interstitial Cells Is Regulated by the Stiffness of the Extracellular Matrix." Arteriosclerosis, thrombosis, and vascular biology **29**(6): 936-942.

Zhang, H., H. A. Pasolli and E. Fuchs (2011). "Yes-Associated Protein (Yap) Transcriptional Coactivator Functions in Balancing Growth and Differentiation in Skin." Proceedings of the National Academy of Sciences of the United States of America **108**(6): 2270-2275.

## Chapter IV: Phosphatidylserine Correlates with in vitro Calcification of Valvular Interstitial Cells

### 4.1 Introduction

Calcific aortic valve disease (CAVD) is the second leading cause of heart surgery, impacting our aging population (Yutzey et al. 2014). In CAVD, the leaflets of the heart slowly become thick, stiff, and calcified. This process causes nodules to form on the valve and inhibits its normal function (Yutzey et al. 2014). The current treatments include surgical aortic valve replacement with a mechanical or bioprosthetic valve that can still calcify again and cause valve failure.

Apoptosis, programmed cell death, is the body's natural process of removing dead, abnormal, or diseased cells during development or aging and has been linked to dystrophic calcification, especially in the cardiovascular system (Gu et al. 2011, London et al. 2005, Nakahara et al. 2017, Otsuka et al. 2014, Proudfoot et al. 2000, Zazzeroni et al. 2018). Apoptotic bodies of dead cells and debris of vascular smooth muscle cells (VSMCs) react with other molecules in the body. They may provide a suitable environment for calcification, as calcium and phosphate accumulate at this nucleation site and form calcium crystals (Loscalzo 2006). Even though apoptosis is shown to be a precursor to calcification (Loscalzo 2006), yet, there is a gap in our knowledge about the possible mechanisms that correlate calcification to apoptosis.

During apoptosis, Phosphatidylserine (PtdSer) flips to the outside of the cell. This process allows the phagocytes to recognize and remove the apoptotic cells (Uchida et al. 1998). Phosphatidylserine (PtdSer) is a major phospholipid component of mammalian cell membranes that contributes to many regulatory processes of biological response, such as apoptosis (Uchida et al. 1998). Prior to apoptosis, PtdSer resides in the inner leaflet of the plasma membrane (Uchida et al. 1998) but is translocated to the outer leaflet during the early stages of apoptosis (Nagata et al. 2016). The translocation of PtdSer from the inside to the outside of the cell may have implications for calcification when not

cleared, as they naturally bind to negatively charged phospholipids in the membrane, such as PtdSer (Sinn et al. 2006). The interaction of PtdSer with calcium ions is essential for endocytosis and exocytosis and assist in the transport of small molecules across cell membranes (Boettcher et al. 2011, Li et al. 2018, Tarafdar et al. 2012, Varga et al. 2020).

Investigating the correlation of PtdSer with calcification in the already well-known correlation between apoptosis and calcification will help us better understand the initiation of calcification and the CAVD. We hypothesize that PtdSer exposure to the extracellular environment is one of the possible mechanisms linking apoptosis and calcification. To evaluate our hypothesis, we will utilize a 2D VICs model (Cirka et al. 2017) to inhibit apoptosis while adding PtdSer and measuring calcification changes. We expect to see an increase in calcification in cells with PtdSer addition. Further, as male cells are more prone to calcification (Porras et al. 2017), we will use both male and female cells to measure the impact of the sex.

## 4.2 Methods

### 4.2.1 Substrate preparation

Microcontact printed 400  $\mu\text{m}$  diameter circular protein islands were formed by coating plasma-treated and 70% EtOH pre-rinsed polydimethylsiloxane (PDMS) stamps with collagen and placing them onto untreated 22x22 mm square coverslips for 1 hr; a 50 g weight was lightly applied to create uniform pressure on the stamp. The collagen solution consisted of 25  $\mu\text{L}$  of 4 mg/mL collagen, 75  $\mu\text{L}$  of 0.1 M acetic acid, 900  $\mu\text{L}$  sodium acetate buffer, and sodium periodate. Before transfer, excess collagen was removed from the stamp using a combination of air drying and nitrogen stream.

Collagen was chosen following the VICs environment in aortic valve. Aortic valve has collagenous leaflets having three layers; fibrosa, spongiosa, and ventricularis (Rutkovskiy et al. 2017). Spongiosa is rich in proteoglycans while ventricularis is rich in elastin. But the formation of calcification is mainly observed in fibrosa layer, aortic side of the aortic valve, which is rich in collagen (Hsu et al. 2022, Rutkovskiy et al. 2017).

## Chapter IV: Phosphatidylserine is a Key Determinant of in vitro Calcification of Valvular Interstitial Cells

Circular collagen patterns were printed onto polyacrylamide (PA) gels by indirect microcontact printing (Cirka et al. 2017). Briefly, for each substrate, 50  $\mu\text{L}$  of PA solution (acrylamide:bisacrylamide (Biorad) of percentages of 7.5/0.24 for  $\sim 20$  kPa) were pipetted onto an activated coverslip. The coverslips were activated by soaking in 1.5% (aminopropyl) trimethoxysilane solution for 30 min, then in 0.5% glutaraldehyde overnight at 4  $^{\circ}\text{C}$  and thoroughly dried before use. After placement of PA solution on activated coverslips, an inactivated collagen microcontact printed coverslip was gently placed on top. Following 12 min of polymerization of the PA-gel, the coverslips were separated by a razor blade. The gels were treated with 2mL of antibiotic/antifungal cocktail in 1xPBS in the fridge overnight to prepare for cell seeding. A modulus of  $\sim 20$  kPa was chosen because it is in the range of reported stiffness values for healthy and diseased valves (Kloxin et al. 2010, Wang et al. 2012).

### 4.2.2 Cells and media

Aortic VICs were isolated from porcine hearts, from pigs 2-4 months old of different sexes, obtained from a local abattoir (Adam's Farm, Groton, MA) using previous protocols (Gould et al. 2010). Porcine VICs are primary fibroblastic cells and were chosen for their similarity to human VICs. VICs at passages 3-6 were seeded at 12,500 cells/ $\text{cm}^2$  (Cirka et al. 2017). The cells were cultured in DMEM supplemented with 10% FBS and 1% Antibiotic/Antifungal at 37  $^{\circ}\text{C}$  with 10%  $\text{CO}_2$ . Media were exchanged every 48 hr.

To investigate the effects of exogenous PtdSer, apoptosis was inhibited five days before seeding the cells by adding ZVAD-FMK with the final concentration of 20 $\mu\text{M}$  (Cirka et al. 2017). We kept the concentration of the ZVAD-FMK constant for the rest of the experiments. To study the effects of Phosphatidylserine (PtdSer) on calcification, the PtdSer solution was added at 5, 10, 15, 20  $\mu\text{M}$  (Sigma, St. Louis, MO, catalog number: P6641) on seeding and kept the concentration constant during the experiments. Varga et al. mention the 10  $\mu\text{M}$  concentration as safe for the cells as the higher concentrations of PtdSer might be toxic to the cells (Varga et al. 2020).

### 4.2.3 Immunohistochemistry and imaging

Individual aggregates were tracked for four days. Our previous work showed that collective behavior of the cells takes days to happen, utilizing a motorized stage and automated position tracking software (Zeiss Axiovision 4.8.2 SP1) on a BioTek Cytation Gen5 inverted microscope. They were imaged with phase contrast 10x. To track individual aggregates at specific locations, coordinates of each aggregate were saved in complementary software running the microscope to follow the same aggregates chosen on the first day of the experiment to eliminate heterogeneities that local collective behaviors cause (Jebeli et al. 2022). To observe apoptosis, samples were incubated for 30 min in standard media with CellEvent Caspase 3/7 (1:400, C10423, Invitrogen) before imaging.

To stain for calcification using Alizarin red S dye, on day 4, the samples were fixed by adding 4% paraformaldehyde (PFA) (USB Products) for 12 minutes at room temperature, 20 $\mu$ L Alizarin red S dye for 2 minutes at room temperature, and rinsing 5 times with diH<sub>2</sub>O to remove the excess stain (Cirka et al. 2017). A color camera immediately imaged the samples on a Cytation Generation5 microscope as no PBS was added to the sample before imaging.

To visualize the presence of the PtdSer in the cell membrane after adding the PtdSer exogenously, we utilize Annexin V (V13241, Invitrogen) per manufacturer instructions with modifications to fit the fluorescent microscopy. After a wash with PBS, we used 100  $\mu$ L of 1X annexin-binding buffer with Alexa Fluor 488 Annexin V (5:100) and Propidium Iodide (1:100) in the kit incubated for 15 min at room temperature. Then 400  $\mu$ L of 1X annexin buffer was added, and the samples were imaged in less than 30 minutes as the annexin bonding is unstable and the fluorescent signal vanishes fast, per manufacturer's instructions. To visualize PtdSer incorporation into the cell membrane, we utilized fluorescently tagged PtdSer (810198, Avanti Polar Lipids) at 10  $\mu$ M concentration.

#### 4.2.4 Uniform confluency was targeted for the aggregates to study

To count for the variability reported previously by our lab (Jebeli et al. 2022), we chose a uniform cellular distribution to have confluent aggregates,  $n = 969$  in 153 different dishes across cells from 7 different sources with 6 of them with known sexes, on day 4. We did not proceed further into hyperconfluency or self-detached levels to keep a controlled environment for the cells. We reported as the confluency progresses, the cellular interactions and the collective behavior is affected (Jebeli et al. 2022). An example of a confluent aggregate, apoptosis, and calcification is shown in Fig. 4-1.

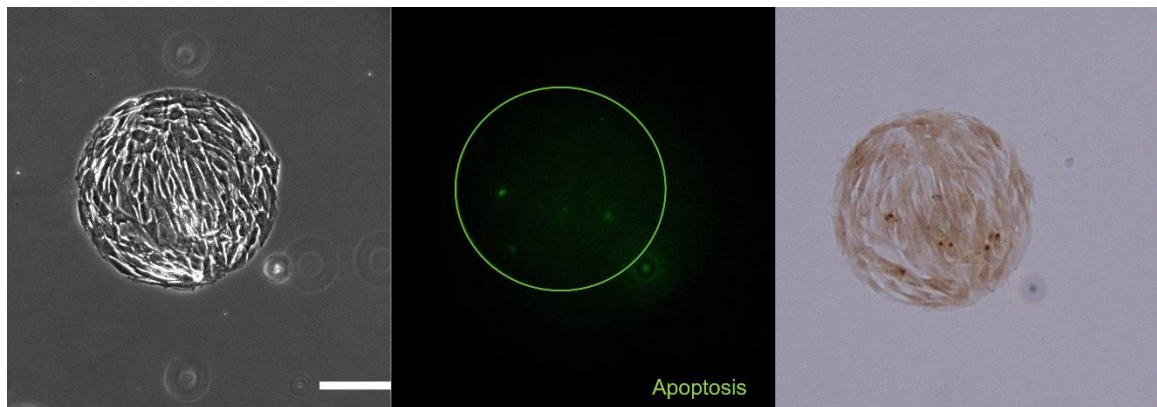


*Figure 4-1. Confluent aggregates were chosen to account for the variability previously observed in our model (Jebeli et al. 2022). An aggregate on day 4. From left to right, phase image, apoptosis (green), the green circle is the periphery of aggregate extracted from the phase image, and calcification after fixation (red).*

#### 4.2.5 Image Analysis in MATLAB

The images were analyzed for the percentage of area positive for calcification and apoptosis by a custom-written MATLAB code. In short, the outline of the aggregates was traced. Then, the phase and caspase images were aligned on top of each other, and the tracing using the phase images was used to exclude the noise signal outside the aggregates. The same tracking was performed for calcification images in the red channel of the BRG images. A threshold was defined to count the area percentage positive for

caspase or calcification, and each pixel higher than the threshold was counted as positive. Area percentage positive is the positive counted pixels per total pixels of each aggregate.

#### 4.2.6 Quantification of Annexin V tagged PtdSer

To evaluate the changes in PtdSer exposure on the cell membrane after the addition of exogenous PtdSer, 10  $\mu\text{M}$  of this solution was added to cells at the time of seeding. In a control group, no exogeneous PtdSer was added. 24 hrs post seeding, the cells were tagged with Annexin V and Propidium Iodide. The images were analyzed by ImageJ. First, the background noise was subtracted. Then using the analyze particle tool in the software, information on the size and location of particles of sizes 10 to 300 pixels (1.2 to 36.5  $\mu\text{m}^2$ ) were extracted. Smaller sizes would include the noise in the green channel and the larger sizes would overlap with the particles colocalizing with the propidium iodide signal which shows dead cells.

#### 4.2.7 Statistical analysis

The experiments were repeated at least two times; each data point corresponding to an experiment is a mean of aggregates in the same dish in that experiment. Data are presented as mean and standard deviation. Two-way ANOVA was performed to evaluate the effects of PtdSer addition and ZVAD. Three-way ANOVA was performed to evaluate the effects of PtdSer addition, ZVAD, and different sexes. Holm-Sidak (HSD) post-hoc test was used with two-way ANOVA performed on the effects of PtdSer addition and ZVAD. Analyses were completed using R, and a p-value of less than 0.05 was considered statistically significant, unless otherwise stated for p less than 0.1 to be significant.

P value is a determinant of how much probability exist for the main hypothesis, for example if the P value is 0.05, it means that there is 5% chance that the observed difference between means is arbitrary, or 95% chance that the difference is not due to errors. When using  $p < 0.1$  to be significant, it means that even with having a p value of 0.1, still there is 90% chance that the difference between means is not arbitrary and it is not due to errors.

## 4.3 Results

### 4.3.1 Calcification increases with the addition of PtdSer in inhibited apoptosis treatments as well as the not-treated cells

To evaluate the effect of PtdSer addition on calcification, we analyzed the images of aggregates in different treatment groups. We observed more calcification as the amount of PtdSer concentration was increased both with and without ZVAD treatments, Fig. 4-2. However, the increase is not statistically significant (p value of two-way ANOVA for different PtdSer concentrations 0.22, and for apoptosis inhibited cells vs. not treated ones 0.70). We observed an increase in apoptosis with an increase in PtdSer concentration while not inhibiting it.

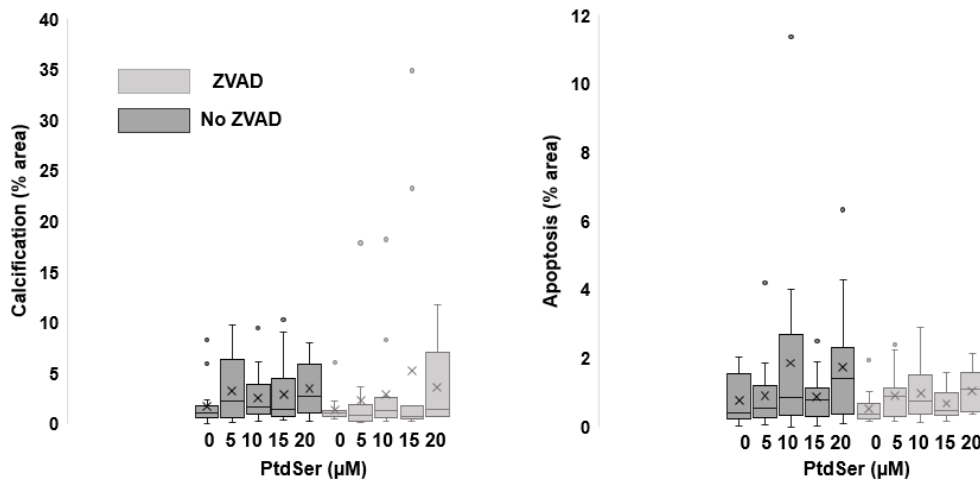
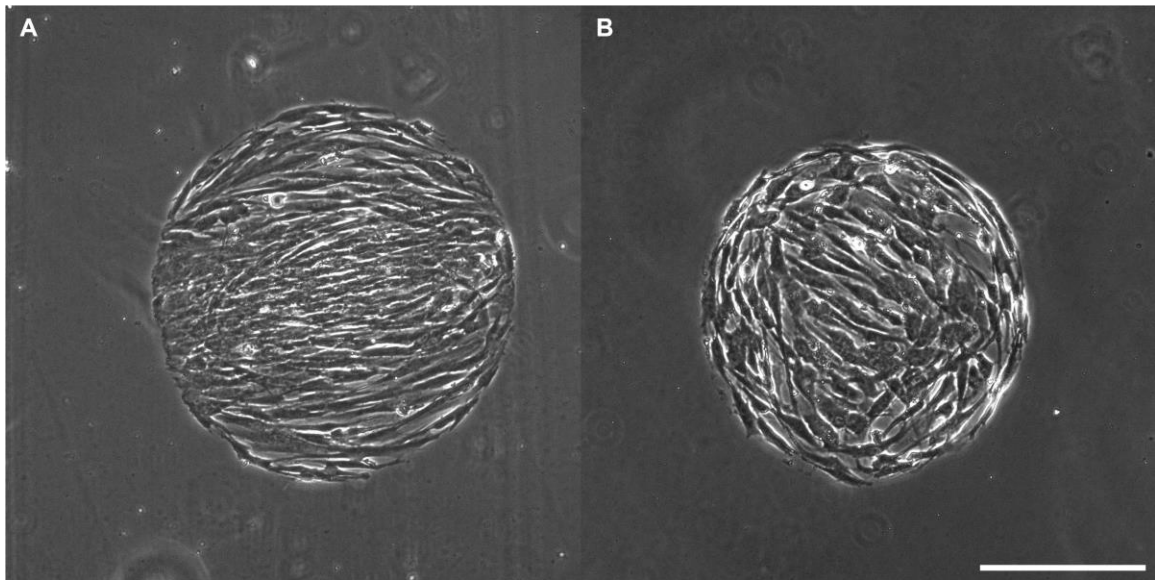


Figure 4-2. Increase in calcification with the addition of PtdSer, independent of apoptosis level ( $n = 969$  aggregates in 153 different replicates across 7 different cell source, 3 females, 3 males, one unknown sex). A) Increase in calcification with higher concentrations of exogenous PtdSer. B) Level of apoptosis in corresponding treatment groups. Apoptosis increases with a higher concentration of PtdSer when it is not inhibited. With inhibition of apoptosis, even in higher concentrations of PtdSer, there is no significant change in apoptosis.

### 4.3.2 Heterogeneity observed in reported data

To find a possible explanation for the variability observed in the presented results in Section 4.3.1, we inspected our results more closely. Following our obtained knowledge from research presented in Chapter 3 of this thesis, on the possible role of confluency on different biological markers, the results were refined to include aggregates closer to the confluent-hyperconfluent level, Fig. 4-3A, compared to aggregates closer to the pre-confluent-confluent level, Fig. 4-3B.



*Figure 4-3. Confluency, a possible player in the heterogeneity of the results. The cell source of the two aggregates is the same. A) An aggregate closer to the confluent-hyperconfluency level. The cells inside of the band are crowded and pushed together. B) An aggregate closer to pre-confluent-confluency level, even though the cells cover most of the aggregate area, there are slight surface areas from the substrate underneath visible.*

### 4.3.3 Limiting the confluency of the analyzed aggregates further removes heterogeneity in response to exogenous PtdSer

To remove more heterogeneity from our initial results, only the results of the aggregates that are closer to confluent-hyperconfluent were kept in the analysis, as the effects of confluency on different biological markers were discussed in our previous

## Chapter IV: Phosphatidylserine is a Key Determinant of in vitro Calcification of Valvular Interstitial Cells

research (Jebeli et al. 2022) also presented in chapter 3 of this thesis. In Fig 4-4, an increase in calcification is shown by the addition of PtdSer, even in treatments where apoptosis is inhibited.

A two-way ANOVA was performed to analyze the effect of the addition of PtdSer and apoptosis inhibition on calcification. This test revealed addition of PtdSer has a statistically significant effect on calcification ( $p = 0.07$  for  $p < 0.1$  to be significant,  $df = 2$ ,  $F$  value = 2.97), while there were no significant differences while inhibiting apoptosis compared to not inhibiting it ( $p = 0.31$ ). This test was performed on  $n = 372$  aggregates in 35 replicates from 7 different cell sources. A post-hoc Tukey HSD test showed that calcification in the treatments with 20  $\mu\text{M}$  PtdSer differs significantly from treatments with no PtdSer ( $p = 0.05$ ). The simulated power on effects of PtdSer is 56.6%.

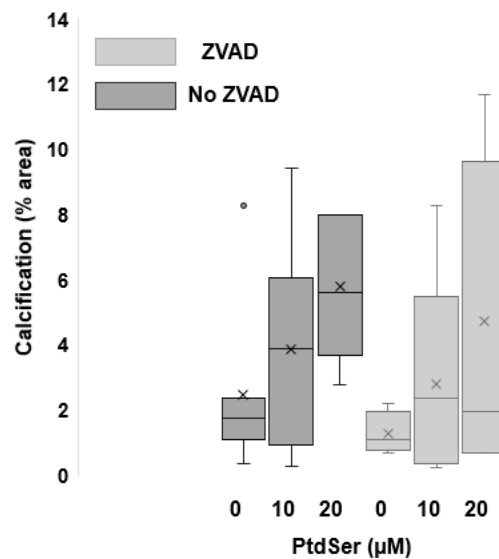


*Figure 4-4. Limiting the data to only confluent-hyperconfluent aggregates as in our initial analysis, confluency seemed to play a role in how the cells react to exogenous PtdSer. The filtered data ( $n = 372$  aggregates in 35 replicates from 7 different cell sources) in this graph shows less heterogeneity and an increase in calcification with the addition of PtdSer, even while apoptosis is inhibited.*

#### 4.3.4 Exogenous PtdSer enters as lipid vesicles into the media and incorporates into the cell membrane

To validate the presence of higher PtdSer in the cell membranes with the addition of exogenous PtdSer, we quantified the presence of PtdSer in the cell membrane. We observed a significant increase in PtdSer presence in cell membrane while there were exogenous PtdSer added ( $p = 0.08$  for  $p < 0.1$  significant), Fig. 4-5. We observed the incorporation of the exogenous PtdSer into the cell membrane, Supplemental Movie 4-1. As a control, we analyzed the area in the dishes with no cells and observed no signal of Annexin V.

Our calculations did not include the dead cell debris recognized by propidium iodide stain. The colocalization of the large particles of Annexin V positive areas and the propidium iodide verifies that those areas are apoptotic bodies, Fig. S. 4-1.

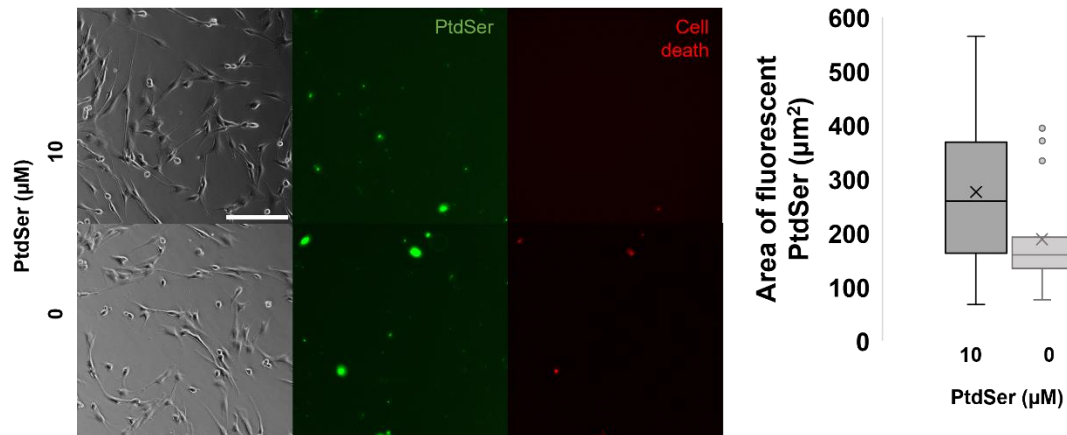


Figure 4-5. The amount of PtdSer exposure in the cell membrane is significantly increased with exogenous PtdSer ( $p = 0.076$ ,  $p < 0.1$  to be significant). The left panels are phase images; the middle is PtdSer as green stained with Annexin V; the right panels are cell death red-stained by propidium iodide. The large particles in the Annexin V channel are not included in evaluations as they are colocalized with propidium iodide positive areas, showing apoptotic bodies. Scale bar corresponds to  $200 \mu\text{m}$ .

### 4.3.5 Exogenous PtdSer affects female cells more than male cells

To study the role of sex in calcification resulting from exogenous PtdSer, we repeated our experimental design for 3 different female and male cells. A three-way ANOVA was performed to analyze the effect of the addition of PtdSer, apoptosis inhibition, and sex on calcification. This test revealed sex has a statistically significant effect on calcification ( $p = 0.07$  for  $p < 0.1$  to be significant,  $df = 1$ ,  $F$  value = 3.27). Also, the concentration of PtdSer significantly affects the calcification ( $p = 0.05$ ,  $df = 2$ ,  $F$  value = 3.13), Fig. 4-6. Also, ZVAD seems to have different effects on different sexes, as the effect of the interaction between ZVAD and sex on calcification is significant ( $p = 0.09$  for  $p < 0.1$  to be significant,  $df = 1$ ,  $F$  value = 2.87). A post-hoc Tukey HSD test showed that calcification in the treatments with 20  $\mu\text{M}$  PtdSer differs significantly ( $p = 0.05$ ) from treatments with no PtdSer. Also, calcification for the same concentrations in female cells ( $p = 0.07$ , for  $p < 0.1$  to be significant), and no PtdSer in male cells with 20  $\mu\text{M}$  PtdSer in female cells ( $p = 0.06$ ) are significantly different.

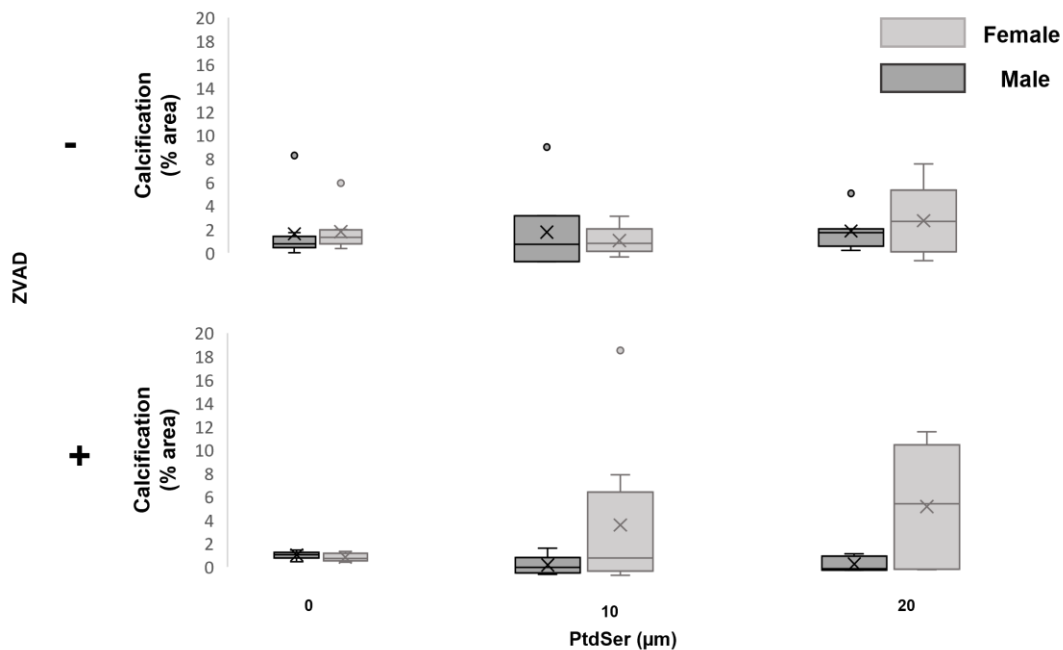


Figure 4-6. Male vs. Female. In ZVAD treated treatments, higher calcification is noticed with the addition of PtdSer in female cells.

## 4.4 Discussion

This research investigated the effect of the addition of PtdSer on the calcification of VICs. As PtdSer is exposed in the initial steps of apoptosis, to remove the effect of apoptosis, it was inhibited while different concentrations of PtdSer were experimentally added to 2D cellular aggregates. As we hypothesized, with addition of PtdSer, an increase in calcification was observed even while apoptosis was inhibited. While we expected no different effect of addition of PtdSer on different sexes, we noticed that female cells exhibited more calcification when apoptosis was inhibited, and PtdSer was added simultaneously.

The response of 2D VIC aggregates to experimentally adding PtdSer included variability. Initially, to obtain a controlled environment, we excluded the self-detached aggregates. With closer examination of the possible sources of such variability, confluency differences between aggregates were noticed. Following the knowledge acquired in Chapter 3 of this thesis, to further remove the observed variability reported in the initial results, they were limited to aggregates closer to the confluent-hyperconfluency level, which resulted in less variable results. However, confluency could be one of several reasons for the observed heterogeneity. The sex and age of the pigs could be other players. Two of the female pigs were two months old, while the other female and male pig were four months old. Also, the heart size of the younger pigs was smaller than the others. However, with limiting the aggregate confluency status alone, the results' variability was decreased substantially.

Numerous studies showed the correlation between apoptosis and calcification but did not investigate the link between these two biological phenomena. In this research, we showed that PtdSer enters the medium as vesicles, a hydrophobic lipid, and is incorporated into the cell membrane. The experimentally adding of PtdSer increased the amount of PtdSer exposure, shown by fluorescent Annexin V, to the extracellular matrix. The addition of PtdSer resulted in an increase in calcification even while apoptosis was inhibited. These results show that PtdSer could be one of the components linking apoptosis to calcification in *in vitro* VICs.

## Chapter IV: Phosphatidylserine is a Key Determinant of in vitro Calcification of Valvular Interstitial Cells

The correlation between PtdSer and calcification is studied mainly in research related to bone formation (Merolli et al. 2009) to show the presence of PtdSer as a necessary component of the initiation of mineralization. Also, in other forms of mineralization, such as in matrix vesicles, PtdSer is shown to be a vital component (Canet-Soulas et al. 2021).

PtdSer has a high binding affinity for  $\text{Ca}^{2+}$  (Boyan et al. 1989, Sinn et al. 2006).  $\text{Ca}^{2+}$  cations most probably bind to phosphate and carboxyl groups in the structure of PtdSer (Martín-Molina et al. 2012). This causational link has been investigated by the development of a PtdSer-enriched monolayer, showing PtdSer nucleated amorphous calcium phosphate that later proceeds to hydroxyapatite happened only in the presence of PtdSer (Cruz et al. 2020).

In the body, intracellular and extracellular calcifications are usually inhibited by physical separation and mineralization inhibitors, respectively (Canet-Soulas et al. 2021). However, during apoptosis,  $\text{Ca}^{2+}$  cations released from the endoplasmic reticulum (Boraldi et al. 2021) or extracellular  $\text{Ca}^{2+}$  can bind to negatively charged PtdSer exposed to the extracellular matrix (Canet-Soulas et al. 2021). While our results show that with inhibition of apoptosis and the addition of PtdSer, the calcification increases. We speculate the PtdSer exposed to the extracellular matrix is binding to extracellular  $\text{Ca}^{2+}$  cations, as we did not notice a significant increase in apoptosis, hence assuming no outflow of  $\text{Ca}^{2+}$  from the endoplasmic reticulum.

PtdSer may have effects on endocytosis (Hirama et al. 2017) and osteogenic differentiation of VICs (Xu et al. 2013). The increase in endocytosis might affect apoptosis, e.g., the observed increase in apoptosis with the addition of PtdSer while apoptosis was not inhibited. Following our observations, we anticipate the effects of a maximum of 20  $\mu\text{M}$  of PtdSer for four days in the media would not lead to osteogenic differentiation of VICs, as this differentiation was reported for higher concentration, e.g., 2.5 to 5 folds higher, and longer culture duration, i.e., 21 days compared to 4 days in this thesis (Xu et al. 2013).

Studies showed that male cells are more prone to calcification (Porrás et al. 2017), but they do not discuss the effects of exogenous materials on different sexes. We expected no different effects of PtdSer on different sexes; however, we noticed more

## Chapter IV: Phosphatidylserine is a Key Determinant of *in vitro* Calcification of Valvular Interstitial Cells

calcification in female cells than male cells with the same amount of PtdSer while apoptosis was inhibited. As we observed the PtdSer incorporation into the cell membrane when the cell was in motion, we speculate the female cells might have higher motility hence higher incorporation of PtdSer in their membrane. However, the postulated higher motility might have resulted from the younger age of the cell source.

Lifestyle choices might affect the calcification rates between males and females differently, such as obesity in men and smoking in women (Kim et al. 2021). Other than these risk factors, environmental players such as hormones could lead to the difference in calcification; for example, estrogen, the female sex hormone (Shames et al. 2013, Woodward et al. 2021).

Cues that might be involved in *in vitro* models, such as ours, are differences in gene expressions that could lead to differences in calcification. For example, gene expressions such as MAPK/ERK, a pathway involved in different calcification rates in male/female cells, could play a role in such observed differences (McCoy et al. 2012). Another example, elevated osteopontin gene expression that reduces osteogenic activity more in females compared to males (Schroeder et al. 2022).

We observed colocalization of apoptosis signal and calcification in several aggregates. We previously reported a dynamic environment inside the 2D aggregates (Jebeli et al. 2022) that made studying colocalization between apoptosis in earlier days with calcification on day 4 not feasible, as it takes 48 hours for calcification to develop (Cirka et al. 2017). The observed colocalization might be due to prolonged apoptosis, as apoptosis was initiated in the early stages of the experiment; while the cell was moving, calcium accumulated on top of it and showed both apoptosis and calcification markers at the end. Also, it has been reported that calcium nodules could show autofluorescence (Baugh et al. 2017), which could be an explanation for why such colocalization is observed in the aggregates in current research.

This study's results show that PtdSer correlates with observed calcification in *in vitro* VICs. This correlation indicates that PtdSer exposure could be the component relating apoptosis to calcification. As PtdSer exposure is one of the first steps of apoptosis,

unraveling its possible role in calcification in *in vitro* VIC model and in the correlation between apoptosis and calcification can lead to the development of therapeutic medicine to solely target PtdSer; however, its side effects should be considered as entirely inhibiting PtdSer may cause cancer.

## 4.5 Appendix 1: Additional Experiments to Examine Further the Mechanisms of PtdSer-Induced Calcification

### 4.5.1 Future work 1:

Our rationale is that the addition of PtdSer in low concentrations and short durations does not affect the phenotype of the VICs. In our current experiments in Chapter 4, the mechanisms of how the PtdSer affects the calcification is not investigated. One of the possible mechanisms is osteogenic differentiation of VICs after the experimentally addition of PtdSer; in this mechanism PtdSer does not directly initiates calcification and is involved in calcification through induction of osteogenesis. In this future work section, we propose experimental designs to evaluate such possible mechanism. We hypothesize that we will not observe osteoblast differentiation in VICs in our model, evaluated by 3 different markers.

As in the body, the VICs transition to other types when involved in the progression of CAVD, the changes of phenotypes with/without the addition of PtdSer should be evaluated to investigate the osteogenic activities. VICs' phenotypes are from the same cell population but different in ultrastructural and immunohistochemical properties (Gevaert et al. 2014) and with different cellular and molecular functions (Liu et al. 2007). During the process of phenotype transition, many proteins and enzymes are involved, such as Osteonectin, Osteocalcin, and Alkaline Phosphatase; Osteonectin and Osteocalcin are proteins secreted by osteoblasts, during differentiation and later mineralization (Ozdemir et al. 2016). Osteonectin influences the osteoblast differentiation as well as osteoclast activity, by influencing bone matrix assembly (Rosset et al. 2016), while osteocalcin which is produced exclusively by osteoblasts is an inhibitor of bone mineralization (Zoch et al. 2016). Alkaline Phosphatase is an enzyme, a byproduct of

## Chapter IV: Phosphatidylserine is a Key Determinant of in vitro Calcification of Valvular Interstitial Cells

osteoblast differentiation (Lee et al. 2017) that acts as a catalyst and provides inorganic phosphate to facilitate mineralization (Szulc et al. 2021, Vimalraj 2020).

With staining for Osteonectin and Osteocalcin, if any considerable amount found, the timeline of the differentiation will be assessed. Osteonectin is mainly an early marker of mineralization whereas Osteocalcin is the marker of late phases of mineralization (Thorwarth et al. 2005). Alkaline Phosphatase is also an early marker of osteoblast differentiation (Lee et al. 2017).

These evaluations provide information on the possible mechanisms that connect PtdSer and calcification. If a significant increase in Osteonectin, when PtdSer is added compared to the treatment without the addition of PtdSer, is observed, it could be due to initiation of osteoblast differentiation. If a significant increase in Osteoclast, when PtdSer is added compared to the treatment without the addition of PtdSer, is observed, it shows the presence of osteoblasts as this protein is secreted exclusively by osteoblasts, and it shows late stages of osteoblast differentiation. Also, in our 2D model, as liver is not present to secrete Alkaline Phosphatase, a significant increase in this marker, shows the early osteoblast differentiation. If there are late stages markers present, it could be articulated that most of the observed calcification in Chapter 4 of this thesis are due to osteogenic activities. However, if the early markers of osteoblast differentiation are observed, not majority of calcification can be contributed to the osteoblast differentiation.

However, with the concentration used in this research (maximum of 20  $\mu\text{M}$  and maximum of 4 days) compared to another study that reports a significant amount of osteogenic marker due to the addition of PtdSer on higher concentrations and longer duration of culture (Xu et al. 2013), we anticipate no significant changes in the osteogenic markers.

As described in aim 1, 2-D 400  $\mu\text{m}$  in diameter aggregates of VICs will be prepared on 20 kPa stiffness substrate. This experiment will be performed under static conditions, and with PtdSer concentration at 0  $\mu\text{M}$ , 10  $\mu\text{M}$ , and 20  $\mu\text{M}$ .

### Experimental design:

## Chapter IV: Phosphatidylserine is a Key Determinant of in vitro Calcification of Valvular Interstitial Cells

Indirect microcontact printing: We will use our 2D model for developing aggregates, as in Chapter 3. We will have our treatment groups of aggregates in with PtdSer concentration at 0  $\mu$ M, 10  $\mu$ M, and 20  $\mu$ M.

Cell isolation and culture: VICs from at least two different sources (passages 3-7) will be seeded on substrates. The same cell sources should be used for all different treatment groups.

Immunostaining: The media for samples will be changed every 48 h post-seeding and the concentration of PtdSer will be kept constant during 4 days of experiment. To measure osteoblast-related biomarkers, to point out if the calcification is dystrophic or osteogenic, Osteonectin (1:100, PA5-78178, Invitrogen) and Osteocalcin (1:100, PA5-96529, Invitrogen) will be quantified by fluorescent microscopy. Also, the live stain for alkaline phosphatase (1:500, A14353, Invitrogen) will be utilized to indicate osteoblastic differentiation (Lee et al. 2017).

Data analysis: The custom MALTLAB code developed in Billiar's lab will be used to analyze the aggregates and different markers. In detail, the aggregates of the same treatment group will be in the same folder and numbered. The code will open the images one by one. The user must trace the aggregate's edges to their best ability. In this step, the centroid of the aggregate is calculated to later transfer all the aggregates to the center of the image and on top of each other to average the value of different signals.

On each image, the background noise is subtracted from the image, so there is no need to prepare the images for this code. Different channels, such as Phase and different fluorescent channels will be stored in different matrices to be analyzed separately.

The periphery of each aggregate will be divided into a number of rings (will be defined in the code). On each ring a percentage of positive area for each signal, by visiting the image pixel by pixel, will be calculated. These numbers will be averaged on each ring, over the number of aggregates in the same treatment group. On the last step, the distribution of the desired signal will be plotted by distance from the center. Refer to the proliferation signal's radial distribution in chapter 3 of this thesis.

## Chapter IV: Phosphatidylserine is a Key Determinant of in vitro Calcification of Valvular Interstitial Cells

Statistics: Significant differences between different treatment groups will be analyzed using one-way ANOVA and post-hoc testing (Tukey's HSD). This experiment will have 3 groups with three different concentrations of PtdSer. As the percentage of the positive area for each signal will be analyzed, the same as the analysis on Chapter 4 for calcification, we used the same mean and variances for different treatment groups to make an estimation on sample size. To obtain power analysis of 80%, repeat each treatment for each cell source for four times with 3-10 confluent-hyperconfluent aggregates, a total of 8 replicates for each treatment group ( $\alpha = 0.05$ , mean of the same treatment groups from Chapter 4 experiments, with equal variance (the mean of variances of experiments on Chapter 4)).

Expected outcomes: We expect to observe no significant changes in osteoblastic protein expression, as we hypothesize that low concentrations of maximum 20  $\mu\text{M}$  and for duration of 4 days used in this thesis will not induce VICs to express osteogenic proteins compared to the concentration and duration used in other studies; e.g., for concentrations of 2.5 to 5 folds higher, and longer culture duration, 21 days, osteogenic activity was found where in lower concentration and shorter durations, 3 days, no significant difference in osteogenic markers such as Alkaline Phosphate was observed (Xu et al. 2013). We predict the majority of calcification in VIC aggregates will be dystrophic calcification and with minimal expression of osteogenic markers. With these results, it could be articulated that PtdSer does not affect calcification through osteogenic differentiation of VICs.

Potential pitfalls and alternative approaches: If the fluorescent staining of the Alkaline Phosphatase activity is not successful, chemical staining of this enzyme will be considered (Yip Cindy Ying et al. 2009). For the chemical stain, imaging will be performed under light microscopy compared to the original proposed fluorescent microscopy. The chemical staining of Alkaline Phosphatase activity is not in the initial experimental design of the current proposed experimental design following the challenges and limitation of chemical staining of Alizarin Red S mentioned in limitation section of this thesis and its associated variabilities.

### 4.5.2 Future work 2:

Our rationale is that as in previous studies the changes in calcification in cellular models has been contributed to PtdSer presence and the binding of calcium to the phosphate head of PtdSer. Because of the observed variability in our model in Chapter 4, we limited the data only to confluent and hyperconfluent aggregates, and noticed an increase in calcification with the addition of PtdSer. However, the effects of the addition of other phospholipids existing in the cell membrane on calcification should be measured to test if the calcification is due to PtdSer specifically rather than other phospholipids in the cell membrane. We hypothesize that with addition of Phosphatidylcholine we will observe no significant changes in calcification of VICs in our model.

Phosphatidylcholine, the principal phospholipids in animals, is critical in regulating the physical aspects of cell membrane (Kanno et al. 2007), and in maintenance of cell cycle (Tercé et al. 1994). The structure of Phosphatidylcholine is very similar to the PtdSer, except the Serine head in PtdSer is replaced with Choline head group (Che et al. 2018).

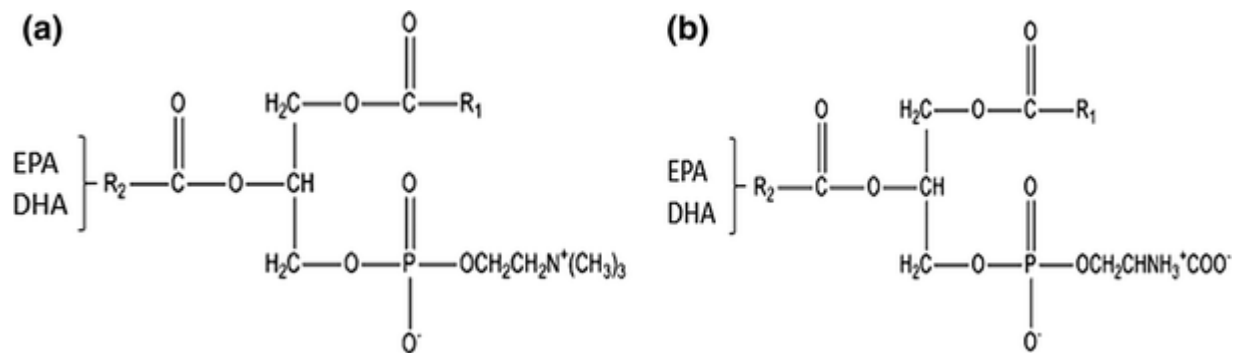


Figure 7. Different structures of phosphatidylcholine and phosphatidylserine. a) Phosphatidylcholine with choline head-group attached to phosphate head vs b) Phosphatidylserine with a serine head-group attached to phosphate head. From (Che et al. 2018), permission to reuse in this thesis is obtained from Springer Nature, under license number 5410310873016.

Phosphatidylcholine addition is mainly investigated for its effects on cell cycle (Tseu et al. 2002, Werlein et al. 2015). In calcification studies, it is shown that its oxidized hydrolysis form in high concentrations (up to 100  $\mu$ M) and long durations (up to 21 days) could result in osteogenic gene expression (Vickers et al. 2010) that could result in calcification.

## Chapter IV: Phosphatidylserine is a Key Determinant of in vitro Calcification of Valvular Interstitial Cells

### Experimental design:

Indirect microcontact printing: We will use our 2D model for developing aggregates, as in Chapter 3. We will have our treatment groups of aggregates with three concentrations of Phosphatidylcholine at 0  $\mu\text{M}$ , 10  $\mu\text{M}$ , and 20  $\mu\text{M}$  (Nishiyama-Naruke et al. 2000, Vickers et al. 2010).

Cell isolation and culture: VICs from at least two different sources (passages 3-7) will be seeded on substrates. The same cell sources should be used for all different treatment groups.

Immunostaining: Samples will be examined 24 h post-seeding to pick the aggregates with uniform distribution of cells to prevent variability in the signals on day 4. On day 4, Calcium deposits will be detected by Alizarin Red S solution (Yip et al. 2009).

Data analysis: The same custom MATLAB code (of the future work 1 and Chapter 4) will be used for analyzing the images and different signals. The aggregates that are in confluent and hyperconfluent levels will be included in these analyses to remove the observed variability in calcification. More details regarding the removal of the observed variability are provided in Chapter 4.

Statistics: Significant differences between different treatment groups will be analyzed with one-way ANOVA and post-hoc testing (Tukey's HSD). This experiment will have 3 groups, with three different concentrations of Phosphatidylcholine. To obtain power analysis of 80%, repeat each treatment for each cell source for four times with 3-10 confluent-hyperconfluent aggregates ( $\alpha = 0.05$ , mean of the same treatment groups from Chapter 4 experiments, with equal variance (the mean of variances of experiments on Chapter 4)).

Expected outcomes: We expect no significant increase in calcification, we anticipate the increase in calcification is limited to PtdSer. Previously, it has been shown the mineralization happening only in presence of PtdSer in monolayers (Cruz et al. 2020).

Potential pitfalls and alternative approaches: Any limitation related to experiments of PtdSer, could be applied here. Such as storing the lipid in glass

containers, handling it with glass syringe, and storing it in well-closed containers to prevent the vaporization of the solvent.

## 4.6 Supplemental material

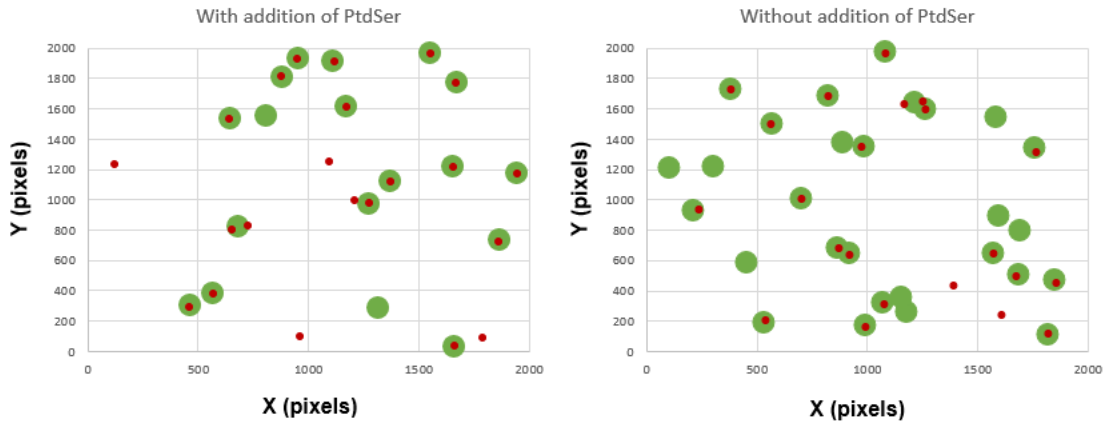


*Figure S.4-1. Colocalization of large particles in Annexin V and Propidium iodide ( $n = 3$  of each treatment) shows that the large particles appearing in the Annexin V channel are mainly dead cells in the Propidium Iodide channel (89% of large particles in Annexin V are colocalized with the propidium iodide with addition of PtdSer, and 75% without addition of PtdSer). This analysis provides evidence of not including large particles in our analysis of the amount of Annexin V present in different samples.*

## 4.7 References

- Baugh, L. M., Z. Liu, K. P. Quinn, S. Osseiran, C. L. Evans, G. S. Huggins, P. W. Hinds, L. D. Black, 3rd and I. Georgakoudi (2017). "Non-Destructive Two-Photon Excited Fluorescence Imaging Identifies Early Nodules in Calcific Aortic-Valve Disease." Nat Biomed Eng **1**(11): 914-924.
- Boettcher, J. M., R. L. Davis-Harrison, M. C. Clay, A. J. Nieuwkoop, Y. Z. Ohkubo, E. Tajkhorshid, J. H. Morrissey and C. M. Rienstra (2011). "Atomic View of Calcium-Induced Clustering of Phosphatidylserine in Mixed Lipid Bilayers." Biochemistry **50**(12): 2264-2273.
- Boraldi, F., F. D. Lofaro and D. Quaglino (2021). "Apoptosis in the Extrasosseous Calcification Process." Cells **10**(1).
- Boyan, B. D., Z. Schwartz, L. D. Swain and A. Khare (1989). "Role of Lipids in Calcification of Cartilage." the Anatomical Record **224**(2): 211-219.
- Canet-Soulas, E., L. Bessueille, L. Mechtouff and D. Magne (2021). "The Elusive Origin of Atherosclerotic Plaque Calcification." Frontiers in Cell and Developmental Biology **9**.

## Chapter IV: Phosphatidylserine is a Key Determinant of in vitro Calcification of Valvular Interstitial Cells

- Che, H., X. Fu, L. Zhang, X. Gao, M. Wen, L. Du, C. Xue, J. Xu and Y. Wang (2018). "Neuroprotective Effects of N-3 Polyunsaturated Fatty Acid-Enriched Phosphatidylserine against Oxidative Damage in Pc12 Cells." Cellular and Molecular Neurobiology **38**(3): 657-668.
- Cirka, H. A., J. Uribe, V. Liang, F. J. Schoen and K. L. Billiar (2017). "Reproducible in Vitro Model for Dystrophic Calcification of Cardiac Valvular Interstitial Cells: Insights into the Mechanisms of Calcific Aortic Valvular Disease." Lab Chip **17**(5): 814-829.
- Cruz, M. A. E., C. R. Ferreira, C. B. Tovani, F. A. de Oliveira, M. Bolean, L. Caseli, S. Mebarek, J. L. Millán, R. Buchet, M. Bottini, P. Ciancaglini and A. Paula Ramos (2020). "Phosphatidylserine Controls Calcium Phosphate Nucleation and Growth on Lipid Monolayers: A Physicochemical Understanding of Matrix Vesicle-Driven Biomineralization." J Struct Biol **212**(2): 107607.
- Gevaert, T., E. Vanstreels, D. Daelemans, J. Franken, F. Van Der Aa, T. Roskams and D. De Ridder (2014). "Identification of Different Phenotypes of Interstitial Cells in the Upper and Deep Lamina Propria of the Human Bladder Dome." J Urol **192**(5): 1555-1563.
- Gould, R. A. and J. T. Butcher (2010). "Isolation of Valvular Endothelial Cells." Journal of Visualized Experiments(46): 2158.
- Gu, X. and K. S. Masters (2011). "Role of the Rho Pathway in Regulating Valvular Interstitial Cell Phenotype and Nodule Formation." American Journal of Physiology-Heart and Circulatory Physiology **300**(2): H448-H458.
- Hirama, T., S. M. Lu, J. G. Kay, M. Maekawa, M. M. Kozlov, S. Grinstein and G. D. Fairn (2017). "Membrane Curvature Induced by Proximity of Anionic Phospholipids Can Initiate Endocytosis." Nature Communications **8**(1): 1393.
- Hsu, C.-P. D., A. Tchir, A. Mirza, D. Chaparro, R. E. Herrera, J. D. Hutcheson and S. Ramaswamy (2022) "Valve Endothelial Cell Exposure to High Levels of Flow Oscillations Exacerbates Valve Interstitial Cell Calcification." Bioengineering **9** DOI: 10.3390/bioengineering9080393.
- Jebeli, M., S. K. Lopez, Z. E. Goldblatt, D. McCollum, S. Mana-Capelli, Q. Wen and K. Billiar (2022). "Multicellular Aligned Bands Disrupt Global Collective Cell Behavior." Acta Biomaterialia.
- Kanno, K., M. K. Wu, E. F. Scapa, S. L. Roderick and D. E. Cohen (2007). "Structure and Function of Phosphatidylcholine Transfer Protein (Pc-Tp)/Stard2." Biochim Biophys Acta **1771**(6): 654-662.
- Kim, B. S., N. Chan, G. Hsu, A. N. Makaryus, M. Chopra, S. L. Cohen and J. N. Makaryus (2021). "Sex Differences in Coronary Arterial Calcification in Symptomatic Patients." The American journal of cardiology **149**: 16-20.
- Kloxin, A. M., J. A. Benton and K. S. Anseth (2010). "In Situ Elasticity Modulation with Dynamic Substrates to Direct Cell Phenotype." Biomaterials **31**(1): 1-8.

## Chapter IV: Phosphatidylserine is a Key Determinant of in vitro Calcification of Valvular Interstitial Cells

Lee, J. M., M. G. Kim, J. H. Byun, G. C. Kim, J. H. Ro, D. S. Hwang, B. B. Choi, G. C. Park and U. K. Kim (2017). "The Effect of Biomechanical Stimulation on Osteoblast Differentiation of Human Jaw Periosteum-Derived Stem Cells." Maxillofac Plast Reconstr Surg **39**(1): 7.

Li, R., S. Chiguru, L. Li, D. Kim, R. Velmurugan, D. Kim, S. C. Devanaboyina, H. Tian, A. Schroit, R. P. Mason, R. J. Ober and E. S. Ward (2018). "Targeting Phosphatidylserine with Calcium-Dependent Protein-Drug Conjugates for the Treatment of Cancer." Molecular Cancer Therapeutics **17**(1): 169-182.

Liu, A. C., V. R. Joag and A. I. Gotlieb (2007). "The Emerging Role of Valve Interstitial Cell Phenotypes in Regulating Heart Valve Pathobiology." The American journal of pathology **171**(5): 1407-1418.

London, G. M., S. J. Marchais, A. P. Guérin and F. Métivier (2005). "Arteriosclerosis, Vascular Calcifications and Cardiovascular Disease in Uremia." Current opinion in nephrology and hypertension **14**(6): 525-531.

Loscalzo, J. (2006). "Vascular Calcification: Pathobiological Mechanisms and Clinical Implications." Circulation research : journal of the American Heart Association. **99**(10): 1044-1059.

Martín-Molina, A., C. Rodríguez-Beas and J. Faraudo (2012). "Effect of Calcium and Magnesium on Phosphatidylserine Membranes: Experiments and All-Atomic Simulations." Biophys J **102**(9): 2095-2103.

McCoy, C. M., D. Q. Nicholas and K. S. Masters (2012). "Sex-Related Differences in Gene Expression by Porcine Aortic Valvular Interstitial Cells." PLoS One **7**(7): e39980.

Merolli, A. and M. Santin (2009). "Role of Phosphatidyl-Serine in Bone Repair and Its Technological Exploitation." Molecules **14**(12): 5367-5381.

Nagata, S., J. Suzuki, K. Segawa and T. Fujii (2016). "Exposure of Phosphatidylserine on the Cell Surface." Cell Death Differ **23**(6): 952-961.

Nakahara, T., M. R. Dweck, N. Narula, D. Pisapia, J. Narula and H. W. Strauss (2017). "Coronary Artery Calcification: From Mechanism to Molecular Imaging." JACC Cardiovascular Imaging **10**(5): 582-593.

Nishiyama-Naruke, A. and R. Curi (2000). "Phosphatidylcholine Participates in the Interaction between Macrophages and Lymphocytes." American Journal of Physiology-Cell Physiology **278**(3): C554-C560.

Otsuka, F., K. Sakakura, K. Yahagi, M. Joner and R. Virmani (2014). "Has Our Understanding of Calcification in Human Coronary Atherosclerosis Progressed?" Arteriosclerosis, thrombosis, and vascular biology **34**(4): 724-736.

Ozdemir, B., B. Kurtis, G. Tuter, B. Senguven and B. Yildirim (2016). "Osteocalcin and Osteonectin Expression after Double Application of Platelet-Rich Plasma in Rabbits." J Istanbul Univ Fac Dent **50**(2): 1-9.

## Chapter IV: Phosphatidylserine is a Key Determinant of in vitro Calcification of Valvular Interstitial Cells

Porras, A. M., C. M. McCoy and K. S. Masters (2017). "Calcific Aortic Valve Disease: A Battle of the Sexes." Circ Res **120**(4): 604-606.

Proudfoot, D., J. N. Skepper, L. Hegyi, M. R. Bennett, C. M. Shanahan and P. L. Weissberg (2000). "Apoptosis Regulates Human Vascular Calcification in Vitro." Circulation research **87**(11): 1055-1062.

Rosset, E. M. and A. D. Bradshaw (2016). "Sparc/Osteonectin in Mineralized Tissue." Matrix Biol **52-54**: 78-87.

Rutkovskiy, A., A. Malashicheva, G. Sullivan, M. Bogdanova, A. Kostareva, K.-O. Stensløkken, A. Fiene and J. Vaage (2017). "Valve Interstitial Cells: The Key to Understanding the Pathophysiology of Heart Valve Calcification." Journal of the American Heart Association **6**(9): e006339.

Schroeder, M. E., D. Batan, A. Gonzalez Rodriguez, K. F. Speckl, D. K. Peters, B. E. Kirkpatrick, G. K. Hach, C. J. Walker, J. C. Grim, B. A. Aguado, R. M. Weiss and K. S. Anseth (2022). "Osteopontin Activity Modulates Sex-Specific Calcification in Engineered Valve Tissue Mimics." Bioengineering & Translational Medicine **n/a**(n/a): e10358.

Shames, S. and L. D. Gillam (2013). "Sex Differences in Aortic Valve Calcification." Circulation: Cardiovascular Imaging **6**(1): 8-10.

Sinn, C. G., M. Antonietti and R. Dimova (2006). "Binding of Calcium to Phosphatidylcholine–Phosphatidylserine Membranes." Colloids and Surfaces A: Physicochemical and Engineering Aspects **282-283**: 410-419.

Szulc, P., D. C. Bauer and R. Eastell (2021). Chapter 65 - Biochemical Markers of Bone Turnover in Osteoporosis. Marcus and Feldman's Osteoporosis (Fifth Edition). D. W. Dempster, J. A. Cauley, M. L. Bouxsein and F. Cosman, Academic Press: 1545-1588.

Tarafdar, P. K., H. Chakraborty, S. M. Dennison and B. R. Lentz (2012). "Phosphatidylserine Inhibits and Calcium Promotes Model Membrane Fusion." Biophys J **103**(9): 1880-1889.

Tercé, F., H. Brun and D. E. Vance (1994). "Requirement of Phosphatidylcholine for Normal Progression through the Cell Cycle in C3h/10t1/2 Fibroblasts." J Lipid Res **35**(12): 2130-2142.

Thorwarth, M., S. Rupprecht, S. Falk, E. Felszeghy, J. Wiltfang and K. A. Schlegel (2005). "Expression of Bone Matrix Proteins During De Novo Bone Formation Using a Bovine Collagen and Platelet-Rich Plasma (Prp)--an Immunohistochemical Analysis." Biomaterials **26**(15): 2575-2584.

Tseu, I., R. Ridsdale, J. Liu, J. Wang and M. Post (2002). "Cell Cycle Regulation of Pulmonary Phosphatidylcholine Synthesis." Am J Respir Cell Mol Biol **26**(4): 506-515.

Uchida, K., K. Emoto, D. L. Daleke, K. Inoue and M. Umeda (1998). "Induction of Apoptosis by Phosphatidylserine." The Journal of Biochemistry **123**(6): 1073-1078.

Varga, K., Z. J. Jiang and L. W. Gong (2020). "Phosphatidylserine Is Critical for Vesicle Fission During Clathrin-Mediated Endocytosis." Journal of Neurochemistry **152**(1): 48-60.

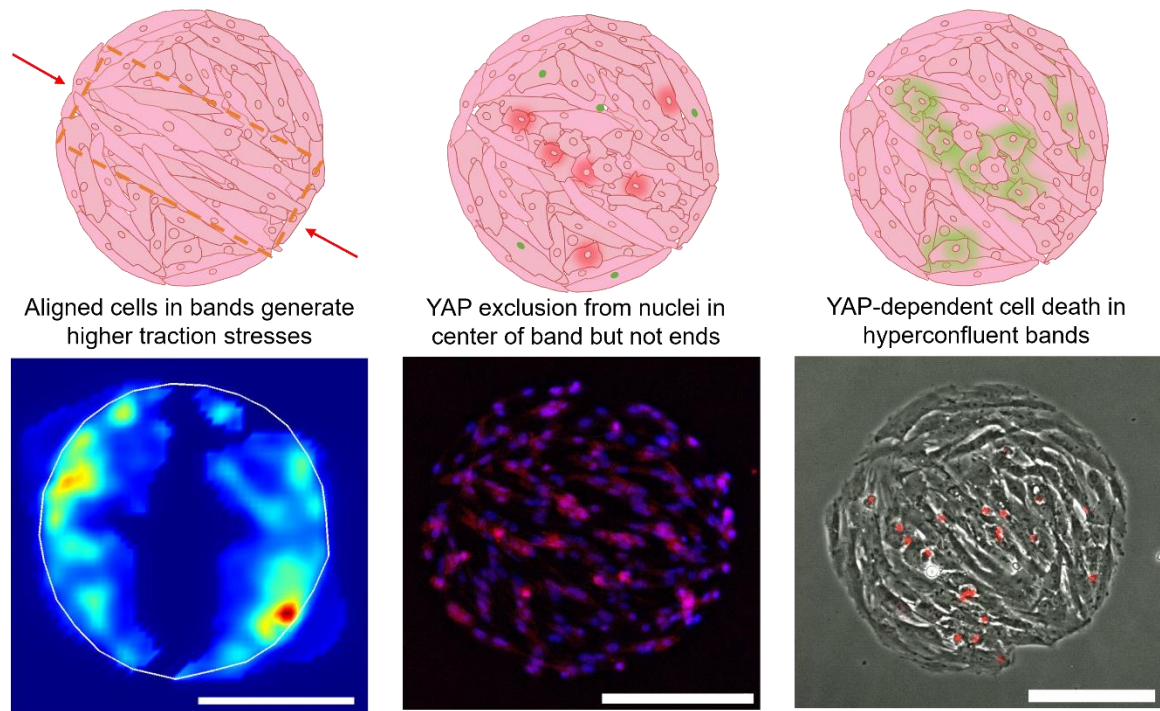
## Chapter IV: Phosphatidylserine is a Key Determinant of in vitro Calcification of Valvular Interstitial Cells

- Vickers, K. C., F. Castro-Chavez and J. D. Morrisett (2010). "Lyso-Phosphatidylcholine Induces Osteogenic Gene Expression and Phenotype in Vascular Smooth Muscle Cells." *Atherosclerosis* **211**(1): 122-129.
- Vimalraj, S. (2020). "Alkaline Phosphatase: Structure, Expression and Its Function in Bone Mineralization." *Gene* **754**: 144855.
- Wang, H., S. M. Haeger, A. M. Kloxin, L. A. Leinwand and K. S. Anseth (2012). "Redirecting Valvular Myofibroblasts into Dormant Fibroblasts through Light-Mediated Reduction in Substrate Modulus." *PLoS One* **7**(7): e39969-e39969.
- Werlein, A., A. Peters, R. Ngoune, K. Winkler and G. Pütz (2015). "Interference of Phosphatidylcholines with in-Vitro Cell Proliferation — No Flock without Black Sheep." *Biochimica et Biophysica Acta (BBA) - Biomembranes* **1848**(7): 1599-1608.
- Woodward, H. J., D. Zhu, P. W. F. Hadoke and V. E. MacRae (2021). "Regulatory Role of Sex Hormones in Cardiovascular Calcification." *International journal of molecular sciences* **22**(9).
- Xu, C., Z. Zheng, L. Fang, N. Zhao, Z. Lin, T. Liang, Z. Zhai and J. Zhou (2013). "Phosphatidylserine Enhances Osteogenic Differentiation in Human Mesenchymal Stem Cells Via Erk Signal Pathways." *Materials Science and Engineering: C* **33**(3): 1783-1788.
- Yip Cindy Ying, Y., J.-H. Chen, R. Zhao and A. Simmons Craig (2009). "Calcification by Valve Interstitial Cells Is Regulated by the Stiffness of the Extracellular Matrix." *Arteriosclerosis, thrombosis, and vascular biology* **29**(6): 936-942.
- Yip, C. Y. Y., J.-h. Chen, R. Zhao and C. A. Simmons (2009). "Calcification by Valve Interstitial Cells Is Regulated by the Stiffness of the Extracellular Matrix." *Arteriosclerosis, Thrombosis, and Vascular Biology* **29**(6): 936-942.
- Yutzey, K. E., L. L. Demer, S. C. Body, G. S. Huggins, D. A. Towler, C. M. Giachelli, M. A. Hofmann-Bowman, D. P. Mortlock, M. B. Rogers, M. M. Sadeghi and E. Aikawa (2014). "Calcific Aortic Valve Disease: A Consensus Summary from the Alliance of Investigators on Calcific Aortic Valve Disease." *Arteriosclerosis, thrombosis, and vascular biology* **34**(11): 2387-2393.
- Zazzeroni, L., G. Faggioli and G. Pasquinelli (2018). "Mechanisms of Arterial Calcification: The Role of Matrix Vesicles." *European Journal of Vascular and Endovascular Surgery* **55**(3): 425-432.
- Zoch, M. L., T. L. Clemens and R. C. Riddle (2016). "New Insights into the Biology of Osteocalcin." *Bone* **82**: 42-49.

## Chapter V: Conclusions, Limitations, and Future Work

### 5.1 Conclusions

This dissertation examines the evolution of collective behavior of the cells inside multicellular printed aggregates and its effect on apoptosis, and the correlation of PtdSer, which is naturally exposed to the extracellular environment during apoptosis, with calcification. Two aims helped us to explore these research areas. The first aim focused on investigating the effects of collective behavior of the cells on observed variability in different signals such as apoptosis in multicellular printed aggregates, Figure below.



The second aim is to experimentally change the concentration of PtdSer in our 2D aggregates to identify its effects on the calcification in *in vitro* VIC model. Studying the collective behavior of VICs provided us with insight into the development of apoptosis that is correlated with calcification in the aortic valve, as determination of the effects of PtdSer on calcification in *in vitro* VIC models would assist us in better understanding the

nature of calcification as well as similar diseases such as atherosclerosis. The results from this research could be transferred to other cell types, especially fibroblasts.

### 5.1.1 Conclusions: Aim 1

In Aim 1, we investigated the evolution of collective behavior in multicellular aggregates. We tracked individual aggregates as the development of local collective behaviors are multiday multicell occurrences. We observed novel collective behavior of banding in VICs, which has not been reported previously; it appears the banding could be the reason behind the heterogeneity we recorded in our previous studies. Additionally, we studied velocity, proliferation, and traction forces cells apply collectively to the substrate, which showed us the motion of cells under the influence of collective behaviors, proliferation throughout the surface of the aggregate, and not limited to the edge. Non-uniform traction stresses on edge with high stresses at the endpoints of the bands. We also observed different markers such as apoptosis, YAP exclusion from nuclei, and non-spread shape of the cells, related to low-stress environments in the middle of bands. These findings may seem contradictory, but it looks like even though there are higher traction forces at the endpoints of the bands, due to the higher number of cells in the middle of the bands, the cells in those regions are experiencing low stresses, i.e., high traction stresses overall but low stress per cell.

Additionally, we investigated the relative importance of stretch compared to collective behaviors. Surprisingly, in contrast to previous studies, we found the cells reorienting towards the stretch direction, which could be to maintain their homeostatic stress level (Hayakawa et al. 2000, Hsu et al. 2010, Wang et al. 2001) following our observations of low-stress markers in the middle of the bands.

Our results show that the fibroblasts have strong local collective behaviors that influence the cells' global collective behavior that computational models anticipate. VICs at a sparse level form local collective banding behavior, then more cells join and realign with the bands making them highly contractile. Even though the cells collectively apply high traction forces, the individual cells in the middle of the bands are experiencing low

stresses. In this aim, we uncovered a novel collective behavior of the VICs, thus leading to heterogeneities in different markers such as apoptosis.

This heterogeneity and the novel behavior recognized in VICs could assist us in better understanding the events leading to calcification of the aortic valve, as the significant cells involved are VICs, and nodule formation has been reported in CAVD. Not only does the band formation and self-detachment affect the apoptosis of VICs, but they might also play a role in the nodule formation later developing into calcific nodules. Knowing the behavior of the cells in proximity to other cells would assist us in better investigating, modeling, and simulating the behavior of the cells in the body and how it leads to diseases like CAVD.

### 5.1.2 Conclusions: Aim 2

In Aim 2, we presented experimental evidence indicating the correlation of PtdSer with calcification in VICs. Utilizing our 400  $\mu\text{m}$  multicellular aggregates, we measured the changes in calcification with the experimental addition of PtdSer. Numerous studies provide evidence of the correlation between apoptosis and calcification (Cirka et al. 2017, Fujita et al. 2014, Gu et al. 2011, Kockx Mark et al. 1998, London et al. 2005, Nakahara et al. 2017, Otsuka et al. 2014, Proudfoot et al. 2000, Zazzeroni et al. 2018), so we also inhibited apoptosis while manually adding different concentrations of PtdSer. To observe the mechanisms of the PtdSer incorporation into the cell membrane, we utilized fluorescent PtdSer and imaged the samples for 24 hours. Additionally, we evaluated the changes of PtdSer exposed to an extracellular matrix environment with Annexin V. We observed a significant increase in calcification with the increase in added PtdSer, even in samples with inhibited apoptosis. As we observed the incorporation of PtdSer into the cell membrane, which may cause the increase in nucleation sites for calcium to bind, PtdSer, resulted in an increase in observed calcification. Previous studies have shown a strong correlation between apoptosis and calcification (Proudfoot et al. 2000); however, they did not investigate which part of the apoptosis cascade plays a role. In this aim, we provided evidence on the possible role of PtdSer, which is exposed at the beginning of apoptosis, in calcification of VICs.

It is known that Statin, a medicine used for lowering cholesterol levels in the blood, helps with CAVD as well (Mohler et al. 2007), but the mechanism is unknown. Statin, in addition to reducing the production of LDL cholesterol, made of Phosphatidylcholine (a phospholipid) by the liver, lowers the level of LDL already existing in the blood (Pinal-Fernandez et al. 2018). We think the effect of Statin on phosphatidylcholine might be projectable on PtdSer as well, and this effect might be how it helps with CAVD. The knowledge obtained from this research could help further investigate the role of PtdSer that could lead to the development of therapeutics that can solely target the PtdSer.

However, the side effects of solely targeting PtdSer should be considered as it is involved in the production of cancerous cells (with no PtdSer showing), in the phagocytosis of the apoptotic bodies (when there is PtdSer exposed to the extracellular matrix macrophages start phagocytosing), or in the brain and memory activity. One way to prevent the side effects on the whole body could be by delivering the medicine through a catheter to the aortic valve.

## 5.2 Experimental limitations and next steps

There were several limitations in completing aims 1 and 2 that could assist in eliminating the deficiencies of the experiments. These limitations did not take away from the overall findings that we discovered concerning the collective behaviors that affect the response of the cells and the effect of PtdSer in calcification. The next step should shed light on some of those limitations and employ improvements in experimental procedures.

### 5.2.1 Study limitations: Aim 1

For dynamic loading, we attached PA gels on silicone stretchable wells. While detaching the coverslip from the surface of the PA gel, as the underneath was a soft surface (silicone), the outcoming surface of the gel was affected. In some substrates, the surface was non-uniform, which caused issues with focusing on aggregates during imaging with microscopes. In detail, some parts of the aggregate were in focus as the other parts were blurry due to uneven gel underneath.

In the same dynamic experiment, we aimed to stain F-actin before and after the applied loading to investigate the reorientation of the cells. As we wanted to study the same aggregates before and after dynamic cyclic loading, we could not have used a stain compatible with fixing the cells. Even though we could perform such an investigation in the live F-actin stain, the F-actin signal in the live culture was weak, and not all the cells in the same aggregate were stained.

To study the YAP-deactivation, we stained the cells for YAP and quantified the deactivation with image analysis. For this purpose, the YAP and nuclei signals are processed to measure their colocalization. However, we could not use automatic image analysis tools as there were cells in the banded and hyperconfluent areas that lay on top of each other, and one cell's extracellular YAP might have been on top of the different cell's nuclei, causing an error in automatic image analysis. Additionally, not all the YAP were excluded from the nuclei; we observed nucleated cytosolic YAP in several cells.

To gather more data on the mechanical state of the cells inside the bands, we needed to know the forces they apply to the substrate and each other. Even though we used different markers such as apoptosis, YAP, etc., or measured the forces cells apply to the substrate to show the mechanical state of the cells, it would have been stronger if we were able to measure the forces cells apply to each other.

Even though measurements of the cell-cell forces were not feasible, studying the forces cells apply to the substrate collectively before and after the implication of dynamic cyclic loading would help us understand the changes in the mechanical state of the cells inside of bands after the reorientation. However, this experiment was not feasible with our current instruments, as the slightest change in the location of the aggregate would cause errors in the resulting computed traction forces. Also, for the dynamic loading, we used the small wells of 8x8 mm of CellScale device, that direct printing method is not achieved yet. For using coverslip with microbeads on them, we had to use the direct microcontact printing, and we have not developed a reproducible method to use the indirect printing method with the coverslip covered in microbeads that are used in transferring fluorescent beads to the surface of the gel.

### 5.2.2 Study limitations: Aim 2

It would have been stronger to study the correlation between apoptosis and calcification if we could measure the exact colocalization of apoptotic bodies with calcific nodules. Unfortunately, this analysis was not achievable due to the movement of the VICs inside the aggregates; even in hyperconfluency they move together and do not stay in the same location inside the aggregate.

We observed a lot of heterogeneity in the resulting calcification. We suspect this heterogeneity is a result of heterogeneity in confluency of the aggregates, the variability in ARS staining, aggregate size variability, or PtdSer pipetting.

As discussed in aim 1, the cells' collective behavior and the aggregate's confluency state cause heterogeneity in different signals. We think the confluency state of the aggregate affects the amount of calcification in different treatment groups.

We measure the calcification with ARS and image, analyzing the area that shows signals higher than a threshold. However, the method is variable as it could differ even when a single operator stains the samples. We believe this variability is affecting the results as well.

When calculating the area of calcification, we divide the area higher than the threshold by the area of aggregates. As we calculate the average area of aggregates in different treatments individually, the percentage of positivity even in cases where the amount of positive area is the same but with varying sizes of aggregate would result in a higher percentage of the area is positive for the calcification in smaller aggregate.

PtdSer is lipid and hydrophobic, with a higher viscosity than regular media used in cell culture. Also, the amount needed to be added to the media for 5  $\mu\text{M}$  concentration was very small. Keeping it accurate with our current pipettes was problematic and may cause variabilities. The hydrophobic nature of this lipid prevented us from making a higher concentration and then diluting it to a lower concentration to solve the issue with pipetting as it does not dissolve in the media completely. Also, the higher viscosity could have affected the amount of PtdSer transferred into the pipette.

Additionally, the PtdSer is dissolved in chloroform:methanol. This volatile solution evaporates quickly, which may have caused some variability in the concentration of PtdSer. However, we tried to prevent such an event by keeping the solution in the glass container it was originally shipped in and concealing the syringe's entrance with parafilm. We extracted the amount we needed for each experiment using a needle.

### 5.3 Long-term future work for the field

The data presented in this dissertation have provided evidence on collective behaviors of VICs that affect different markers such as apoptosis, which correlate with calcification. When the cells start aligning and making multicellular bands, more cells are recruited to the bands leading to hyperconfluency. The hyperconfluency affects the cells' mechanical state, leading to heterogeneities in different markers and apoptosis. Later apoptosis, more specifically PtdSer exposure at the beginning of apoptosis, appears to have a role in the initiation of calcification. In addition to the conditions introduced in this thesis, there are additional markers, experiments, and conditions that have yet to be tested. Future work will strengthen our current understanding of the role of PtdSer and the collective behavior of VICs that lead to calcification.

#### 5.3.1 Future work: Aim 1

Due to limited resources for the experimental experiments, it would be beneficial to use computational modeling to predict and simulate cellular behavior in 2D aggregates. To model the collective behavior investigated in this project, uniform cellular area and distribution would not capture the complete picture. We anticipate considering cellular numbers inside the bands, and perhaps a muscle-like shape formed by cells for the bands would result in a better simulation of the heterogeneity involved.

To further evaluate the changes in the mechanical state of the cells inside the bands, evaluating the stress markers such as apoptosis in the bands after employing dynamic cyclic loading would shed light on the changes occurring in the mechanical state of the cells with cellular reorientation. Additionally, TFM could be measured utilizing

PA-gel with solved microbeads inside the gel. It should be noticed that the beads in the lower parts of the gel other than its surface may cause errors in the computations.

To better understand the causes of the banding behavior, ECM secreted by the cells could be evaluated after the band is formed. It might be the ECM secreted by multiple cells elongated in the middle of the aggregate that recruits other cells to align and join the band. However, we believe this might not be the sole reason, as we observed no hyperconfluency in calcium-free media. The alignment of these proteins to outline the banded region could be imaged using polarized microscopy (Koike-Tani et al. 2015). Another way to evaluate the effects of the proteins left behind by the cells in making the bands is by trypsinizing current banded cells and seeding new cells. Then if the new cells are aligned in the same direction as the previous band, it could be evidence of the effect of proteins secreted by cells in making the alignment. However, it should be considered that this new aligned band might result from a defect of higher collagen concentration on the endpoints of the presumable band.

To verify the collagen remnant after aggregates self-detach from the endpoints of the bands, the collagen could be stained using antibodies. Also, new cells could be seeded into the dish to observe if any cells would attach to the ripped part of the aggregate, demonstrating the collagen existence. However, in this method, the nodulated cells might die and cause more heterogeneity in the aggregate images. The current self-detached aggregates could be trypsinized, and a new set of cells could be seeded. Using this method, the operator should be sure of tracking the same aggregate as failure in it may cause errors in conclusions from observed newly formed aggregates. To prevent self-detachment of the cells, matrix binding could be increased using fibronectins or covalently binding proteins to the surface of the gel.

To better demonstrate the effect of cell-cell interaction on the band formation, cadherin could be blocked or knocked out instead of using EDTA to deplete calcium. Using this method, there would be no effect on the proliferation of the cells, and we might observe hyperconfluency even without any cell-cell interaction.

### 5.3.2 Future work: Aim 2

In addition to future works mentioned in the appendix for Chapter 4, the following future works could assist us to better understand the calcification of VICs. Also, for clinical practices, the effects of Statin on phosphatidylserine could be measured, as it affects the phosphatidylcholine.

To better remove the variabilities due to heterogeneity in confluency of the cells and variability in using ARS, a bilayer of PtdSer with QCM-D sensors could be used. The QCM-D sensors provide information on the mass and thickness of the bilayer. With this method, there is a uniform bilayer of PtdSer, and once there is any material attached to the bilayer, other sensors could record it.

With observed variability in effects of exogenous PtdSer on female and male cells in current research, the possible causes should be assessed using the current knowledge of different pathways involved in calcification in male vs. female cells, such as MAPK/ERK (McCoy et al. 2012).

3D models of cells compared to 2D models mimic the cells' natural environment more closely. In the future, 3D modeling of VICs to study calcification would provide knowledge on how the VICs behave collectively in a 3D environment and how it results in calcification. Another step would be the implication of dynamic loading in 3D or 2D models and study its effect on calcification.

To model the events in the body, it would be advantageous to employ macrophages to remove the apoptotic bodies and measure their effects on calcification. Macrophages mostly remove apoptotic cells in their entirety. The process of apoptotic cell removal by macrophages is termed efferocytosis (Cory 2018). Macrophages, “big eater” in Greek, are large cells, approximately 21  $\mu\text{m}$  in diameter (Krombach et al. 1997), and have the ability to phagocytose large targets ( $>0.5 \mu\text{m}$  in diameter) (Maderna et al. 2003). Macrophages mostly remove apoptotic cells in their entirety (Parnaik et al. 2000, Wood et al. 2000) and can engulf intact cells (Tóth et al. 2009).

Clearance of apoptotic cells reduces inflammatory responses in other diseases. Apoptosis is a vital part of healthy tissues' growth, homeostasis, and maintenance (Poon et al. 2014). Clearing of cell remnants happens rapidly, so apoptotic cells are not found, even in tissues with high apoptosis rates. Inefficiency in clearing apoptotic cells by macrophages can lead to inflammatory and autoimmune diseases (Poon et al. 2014).

Secondary necrosis happens when apoptotic cells that are left uncleared lose their membrane integrity and lyse (Poon et al. 2014). Exposure of the intracellular molecules signal inflammation responses in tissues (Poon et al. 2014). Targeting the clearance of apoptotic cells has become a popular approach to dealing with a wide range of diseases, from autoimmunity to cancer.

Examples of employing macrophages to achieve different goals could be the removal of excess apoptotic cells to prevent them from undergoing secondary necrosis and initiate an inflammatory response, such as in lung inflammation, or adding macrophages for an anti-inflammatory response of clearance of the apoptotic cells in their early stages apoptosis, such as in rheumatoid arthritis (Poon et al. 2014). Similar to these diseases, the clearance of apoptotic cells before their secondary necrosis stage may have an impact on calcification.

## 5.4 References

Cirka, H. A., J. Uribe, V. Liang, F. J. Schoen and K. L. Billiar (2017). "Reproducible in Vitro Model for Dystrophic Calcification of Cardiac Valvular Interstitial Cells: Insights into the Mechanisms of Calcific Aortic Valvular Disease." Lab Chip **17**(5): 814-829.

Cory, S. (2018). "Phosphatidylserine Hide-and-Seek." Proceedings of the National Academy of Sciences **115**(48): 12092-12094.

Fujita, H., M. Yamamoto, T. Ogino, H. Kobuchi, N. Ohmoto, E. Aoyama, T. Oka, T. Nakanishi, K. Inoue and J. Sasaki (2014). "Necrotic and Apoptotic Cells Serve as Nuclei for Calcification on Osteoblastic Differentiation of Human Mesenchymal Stem Cells in Vitro." Cell Biochemistry and Function **32**(1): 77-86.

Gu, X. and K. S. Masters (2011). "Role of the Rho Pathway in Regulating Valvular Interstitial Cell Phenotype and Nodule Formation." American Journal of Physiology-Heart and Circulatory Physiology **300**(2): H448-H458.

## Chapter V: Conclusions, Limitations, and Future Work

- Hayakawa, K., A. Hosokawa, K. Yabusaki and T. Obinata (2000). "Orientation of Smooth Muscle-Derived A10 Cells in Culture by Cyclic Stretching: Relationship between Stress Fiber Rearrangement and Cell Reorientation." Zoolog Sci **17**(5): 617-624.
- Hsu, H.-J., C.-F. Lee, A. Locke, S. Q. Vanderzyl and R. Kaunas (2010). "Stretch-Induced Stress Fiber Remodeling and the Activations of Jnk and Erk Depend on Mechanical Strain Rate, but Not Fak." PLoS One **5**(8): e12470.
- Kockx Mark, M., R. Y. De Meyer Guido, J. Muhring, W. Jacob, H. Bult and G. Herman Arnold (1998). "Apoptosis and Related Proteins in Different Stages of Human Atherosclerotic Plaques." Circulation **97**(23): 2307-2315.
- Koike-Tani, M., T. Tani, S. B. Mehta, A. Verma and R. Oldenbourg (2015). "Polarized Light Microscopy in Reproductive and Developmental Biology." Molecular Reproduction and Development **82**(7-8): 548-562.
- Krombach, F., S. Münzing, A. M. Allmeling, J. T. Gerlach, J. Behr and M. Dörger (1997). "Cell Size of Alveolar Macrophages: An Interspecies Comparison." Environmental health perspectives **105 Suppl 5**(Suppl 5): 1261-1263.
- London, G. M., S. J. Marchais, A. P. Guérin and F. Métivier (2005). "Arteriosclerosis, Vascular Calcifications and Cardiovascular Disease in Uremia." Current opinion in nephrology and hypertension **14**(6): 525-531.
- Maderna, P. and C. Godson (2003). "Phagocytosis of Apoptotic Cells and the Resolution of Inflammation." Biochimica et Biophysica Acta (BBA) - Molecular Basis of Disease **1639**(3): 141-151.
- McCoy, C. M., D. Q. Nicholas and K. S. Masters (2012). "Sex-Related Differences in Gene Expression by Porcine Aortic Valvular Interstitial Cells." PLoS One **7**(7): e39980.
- Mohler, E. R., 3rd, H. Wang, E. Medenilla and C. Scott (2007). "Effect of Statin Treatment on Aortic Valve and Coronary Artery Calcification." The Journal of heart valve disease **16**(4): 378-386.
- Nakahara, T., M. R. Dweck, N. Narula, D. Pisapia, J. Narula and H. W. Strauss (2017). "Coronary Artery Calcification: From Mechanism to Molecular Imaging." JACC Cardiovascular Imaging **10**(5): 582-593.
- Otsuka, F., K. Sakakura, K. Yahagi, M. Joner and R. Virmani (2014). "Has Our Understanding of Calcification in Human Coronary Atherosclerosis Progressed?" Arteriosclerosis, thrombosis, and vascular biology **34**(4): 724-736.
- Parnaik, R., M. C. Raff and J. Scholes (2000). "Differences between the Clearance of Apoptotic Cells by Professional and Non-Professional Phagocytes." Current Biology **10**(14): 857-860.
- Pinal-Fernandez, I., M. Casal-Dominguez and A. L. Mammen (2018). "Statins: Pros and Cons." Med Clin (Barc) **150**(10): 398-402.
- Poon, I. K., C. D. Lucas, A. G. Rossi and K. S. Ravichandran (2014). "Apoptotic Cell Clearance: Basic Biology and Therapeutic Potential." Nature Reviews Immunology **14**(3): 166-180.

## Chapter V: Conclusions, Limitations, and Future Work

Proudfoot, D., J. N. Skepper, L. Hegyi, M. R. Bennett, C. M. Shanahan and P. L. Weissberg (2000). "Apoptosis Regulates Human Vascular Calcification in Vitro." Circulation research **87**(11): 1055-1062.

Tóth, B., E. Garabuczi, Z. Sarang, G. Vereb, G. Vámosi, D. Aeschlimann, B. Blaskó, B. Bécsi, F. Erdodi, A. Lacy-Hulbert, A. Zhang, L. Falasca, R. Birge, Z. Balajthy, G. Melino, L. Fésüs and Z. Szondy (2009). "Transglutaminase 2 Is Needed for the Formation of an Efficient Phagocyte Portal in Macrophages Engulfing Apoptotic Cells." Journal of Immunology **182**: 2084-2092.

Wang, J. H. C., P. Goldschmidt-Clermont, J. Wille and F. C. P. Yin (2001). "Specificity of Endothelial Cell Reorientation in Response to Cyclic Mechanical Stretching." Journal of biomechanics **34**(12): 1563-1572.

Wood, W., M. Turmaine, R. Weber, V. Camp, R. A. Maki, S. R. McKercher and P. Martin (2000). "Mesenchymal Cells Engulf and Clear Apoptotic Footplate Cells in Macrophageless Pu.1 Null Mouse Embryos." Development **127**(24): 5245.

Zazzeroni, L., G. Faggioli and G. Pasquinelli (2018). "Mechanisms of Arterial Calcification: The Role of Matrix Vesicles." European Journal of Vascular and Endovascular Surgery **55**(3): 425-432.